Institut für Erd-und Umweltwissenschaften
Hydrologie - Klimatologie

Large-scale floodplain sediment dynamics in the Mekong Delta: present state and future prospects

Cumulative dissertation
zur Erlangung des akademischen Grades
"doctor rerum naturalium"
(Dr. rer. nat.)
in der Wissenschaftsdisziplin "Hydrologie"

eingereicht an der

Mathematisch-Naturwissenschaftlichen Fakultät

der Universität Potsdam

von Nguyen Van Manh

Potsdam, August 13, 2014

Published online at the
Institutional Repository of the University of Potsdam:
URN urn:nbn:de:kobv:517-opus-72512
http://nbn-resolving.de/urn:nbn:de:kobv:517-opus-72512

Acknowledgment

The present study was conducted in sections 5.4 Hydrology of the Helmholtz Centre Potsdam, GFZ, German Research Centre for Geosciences. Financial support from the German Ministry of Education and Research BMBF and the Vietnamese Ministry of Science and Technology is gratefully acknowledged, which has been provided within the project WISDOM – Water related Information System for a Sustainable Development of the Mekong Delta. GFZ Potsdam and University of Potsdam are greatly appreciated for the funding in the last year of the PhD duration.

I would like to express the deepest gratitude to my supervisors, Dr. Heiko Apel and Prof. Bruno Merz for the constant guidances, bright ideas, and constructive revises with encouragement throughout the study period. Both of you also received sincere thanks from my family in Vietnam.

I'm grateful to Dr. Nguyen Viet Dung and Dr. Nguyen Nghia Hung for the cooperation in the work, the help and support in the fieldwork, data collection as well as the helpful comments and feedbacks during my study progress.

Special thanks go to Stefan Luedtke, Do Thi Chinh and my friends in the WISDOM project who were going with me on the long roads of a Ph.D, exchange ideas, experiences the fieldwork in the Mekong Delta, travelling together...

My gratitude to GFZ section 5.4 for the good working atmosphere. I would especially like to thank Heiko Thoss, Knut Günther, Roumiana Zimmer and Astrid Krahn for supporting and helping me in any kind of requests.
I would like to acknowledge Dr. Vo Khac Tri, Dr. Trinh Thi Long and Dr. Lam Hung Son, Dr. Matti Kummu, who provided the valuable data for the model setup and model calibrations.

Finally, to my family, con rất biết ơn bố mẹ hai bên đã động viên, hỗ trợ, giúp đỡ vợ chồng con vô điều kiện trong thời gian vừa qua, những gì con có thể làm được đều có công sức của bố mẹ. Cảm ơn tình yêu của anh đã luôn bên anh trong những ngày tháng cô đơn này, bố xin lỗi hai mẹ con vì đam mê hư danh mà để cho hai mẹ con phải vất vả và buồn tủi.

Potsdam, August 13, 2014

Nguyen Van Manh

Author's declaration

I certify that the work contains no material which has been accepted for the award of any other degree, in any university or other tertiary institution and, to the best of my knowledge and belief, contains no material previously published or written by another person, except where due reference has been made in the text.

Nguyen Van Manh

Contents

List of Figures

List of Tables

Abstract

The Mekong Delta (MD) sustains the livelihood and food security of millions of people in Vietnam and Cambodia. It is known as the "rice bowl" of South East Asia and has one of the world's most productive fisheries. Sediment dynamics play a major role for the high productivity of agriculture and fishery on the delta. However, the MD is threatened by climate change, sea level rise and unsustainable development activities in the Mekong Basin. But despite its importance and the expected threats the understanding of the present and future sediment dynamics in the MD is very limited. This is a consequence of its large extent, the intricate system of rivers, channels and floodplains and the scarcity of observations. Thus this thesis aimed at (1) the quantification of suspended sediment dynamics and associated sediment-nutrient deposition in floodplains of the MD, and (2) assessed the impacts of likely future boundary changes on the sediment dynamics in the MD. The applied methodology combines field experiments and numerical simulation to quantify and predict the sediment dynamics in the entire delta in a spatially explicit manner.

The experimental part consists of a comprehensive procedure to monitor quantity and spatial variability of sediment and associated nutrient deposition for large and complex river floodplains, including an uncertainty analysis. The measurement campaign applied 450 sediment mat traps in 19 floodplains over the MD for a complete flood season. The data also supports quantification of nutrient deposition in floodplains based on laboratory analysis of nutrient fractions of trapped sedimentation. The main findings are that the distribution of grain size and nutrient fractions of suspended sediment are homogeneous over the Vietnamese floodplains. But the sediment deposition within and between ring dike floodplains shows very high spatial variability due to a high level of human inference. The experimental findings provide the essential data for setting up and calibration of a large-scale sediment transport model for the MD.

For the simulation studies a large-scale hydrodynamic model was developed in order to quantify large-scale floodplain sediment dynamics. The complex river-channel-floodplain system of the MD is described by a quasi-2D model linking a hydrodynamic and a cohesive sediment transport model. The floodplains are described as quasi-2D presentations linked to rivers and channels modeled in 1D by using control structures. The model setup, based on the experimental findings, ignored erosion and re-suspension processes due to a very high degree of human interference during the flood season. A two-stage calibration with six objective functions was developed in order to calibrate both the hydrodynamic and sediment transport modules. The objective functions include hydraulic and sediment transport parameters in main rivers, channels and floodplains. The model results show, for the first time, the tempo-spatial distribution of sediment and associated nutrient deposition rates in the whole MD. The patterns of sediment transport and deposition are quantified for different sub-systems. The main factors influencing spatial sediment dynamics are the network of rivers, channels and dike-rings, sluice gate operations, magnitude of the floods and tidal influences. The

superposition of these factors leads to high spatial variability of the sediment transport and deposition, in particular in the Vietnamese floodplains. Depending on the flood magnitude, annual sediment loads reaching the coast vary from 48% to 60% of the sediment load at Kratie, the upper boundary of the MD. Deposited sediment varies from 19% to 23% of the annual load at Kratie in Cambodian floodplains, and from 1% to 6% in the compartmented and diked floodplains in Vietnam. Annual deposited nutrients (N, P, K), which are associated to the sediment deposition, provide on average more than 50% of mineral fertilizers typically applied for rice crops in non-flooded ring dike compartments in Vietnam. This large-scale quantification provides a basis for estimating the benefits of the annual Mekong floods for agriculture and fishery, assessing the impacts of future changes on the delta system, and further studies on coastal deposition/erosion.

For the estimation of future prospects a sensitivity-based approach is applied to assess the response of floodplain hydraulics and sediment dynamics to the changes in the delta boundaries including hydropower development, climate change in the Mekong River Basin and effective sea level rise. The developed sediment model is used to simulate the mean sediment transport and sediment deposition in the whole delta system for the baseline (2000-2010) and future (2050-2060) periods. For each driver we derive a plausible range of future changes and discretize it into five levels, resulting in altogether 216 possible factor combinations. Our results thus cover all plausible future pathways of sediment dynamics in the delta based on current knowledge. The uncertainty of the range of the resulting impacts can be decreased in case more information on these drivers becomes available. Our results indicate that the hydropower development dominates the changes in sediment dynamics of the Mekong Delta, while sea level rise has the smallest effect. The floodplains of Vietnamese Mekong Delta are much more sensitive to the changes compared to the other subsystems of the delta. In terms of median changes of the three combined drivers, the inundation extent is predicted to increase slightly, but the overall floodplain sedimentation would be reduced by approximately 40%, while the sediment load to the Sea would diminish to half of the current rates. These findings provide new and valuable information on the possible impacts of future development on the delta, and indicate the most vulnerable areas. Thus, the presented results are a significant contribution to the ongoing international discussion on the hydropower development in the Mekong basin and its impact on the Mekong delta.

Zusammenfassung

Das Mekong Delta bildet die Existenzgrundlage und Nahrungsquelle für mehrere Millionen Menschen in Vietnam und Kambodscha. Die Sedimentdynamik spielt in diesem Zusammenhang eine große Rolle für die Landwirtschaft und Fischerei im Delta. Klimawandel und zweifelhaft nachhaltige Entwicklungen im Mekong Einzugsgebiet können jedoch diese essentielle Grundlage gefährden. Trotz der hohen Bedeutung des Sedimenthaushaltes für das Delta ist jedoch das Wissen um die räumliche und zeitliche Dynamik der Sedimentdynamik und insbesondere der Sedimentation auf den Überflutungsflächen sehr begrenzt. Dies liegt zum einen an der hohen Komplexität des Deltas mit unzähligen Kanälen, Deichen und hydraulischen Strukturen, zum anderen an dem Mangel an Beobachtungsdaten. Die vorliegende Arbeit zielte daher auf a) die Schaffung einer quantitativen Datenbasis zur Sedimentation auf den Überflutungsflächen, b) auf eine modellbasierte Abschätzung der Sedimentation im gesamten Mekong Delta, und c) auf die Abschätzung des Einflusses relevanter Änderungen in den Randbedingungen auf die zukünftige Sedimentdynamik.

Im experimentellen Teil der Arbeit wurde die Sedimentation auf den Überflutungsflächen im vietnamesischen Teil des Deltas mittels Sedimentfallen, die über weite Bereiche des Deltas verteilt wurden, quantitativ inklusive einer Unsicherheitsabschätzung bestimmt. Die Ergebnisse zeigten, dass die Sedimentation räumlich sehr stark variiert, verursacht durch die Komplexität und Diversität des hydraulischen Systems und insbesondere die menschliche Steuerung der hydraulischen Bauten. Die experimentellen Daten geben einen ersten Einblick in die räumliche Variabilität der Sedimentation im Mekong Delta, und bilden die Basis für die Kalibrierung des hydraulischen Modells im nächsten Schritt. Zusätzlich konnten auch die Nährstoffanteile im Sediment bestimmt werden, wodurch eine Basis zur Abschätzung des Nutzens der Sedimente für die Landwirtschaft gelegt wurde.

Die Sedimentdynamik wurde mittels eines quasi-2D hydraulischen Modells, das mit einer Sedimenttransportroutine für kohäsive Sedimente gekoppelt wurde, simuliert. Hierbei wurden die hydraulische und die Sedimenttransportroutine unabhängig voneinander mit mehreren Optimierungsfunktionen und Stations-, Feld- und Fernerkundungsdaten kalibriert. Durch die Modellergebnisse konnte zum ersten Mal die räumliche und zeitliche Variabilität des Sedimenttansports und der Sedimentation quantifiziert werden. Diese großskalige Quantifizierung bildet zudem die Basis für eine ökonomische Nutzensabschätzung der Sedimente für die Landwirtschaft und Fischerei.

Mittels des entwickelten und kalibrierten Modells konnten auch zukünftige Entwicklungen abgeschätzt werden. Hierzu wurde ein Verfahren basierend auf einem Sensitivitätsansatz implementiert, mittels dessen die Auswirkungen des Baus von Staudämmen im Mekong Einzugsgebiet, des Klimawandels auf den Abfluss und Sedimenttransport aus dem Mekong Einzugsgebiet und des effektiven Meeresspiegelanstiegs auf die Sedimentdynamik im Delta einzeln in verschiedenen Ausprägungsstufen als auch kombiniert quantifiziert werden konnte. Durch diese Kombinationen können alle möglichen zukünftigen Entwicklungen basierend auf dem jetzigen Kenntnisstand betrachtet werden. Von den betrachteten Faktoren hat der Bau von Staudämmen den größten Einfluss auf die Sedimentdynamik im Delta, insbesondere auf den vietnamesischen Teil des Deltas. Der Klimawandel hat das Potential diese Änderungen partiell zu dämpfen, aber auch zu verstärken. Die Änderungen im Meeresspiegel haben den geringsten Effekt, beschränken sich in den Auswirkungen auf den Vietnamesischen Teil und modulieren im Wesentlichen die Auswirkungen des Klimawandels. Diese Ergebnisse liefern somit neue quantitative Erkenntnisse zur möglichen zukünftigen Sedimentdynamik im Mekong Delta, identifiziert die verwundbarsten Regionen und trägt dadurch zur internationalen kontroversen Diskussion über die Auswirkungen des Staudammbaus im Mekong bei.

Chapter 1 General introduction

1.1 The Mekong Delta

The Mekong Delta (MD) is a very complex delta system and one of the most productive agro-aquaculture region in the world (Baran [2010]). The MD stretches from the station Kratie in the Mekong River in Cambodia to the coast in Vietnam (Fig. 1.1). The total area excluding the Tonle Sap Basin is approximately 63,000 km^2, divided into 39,500 km^2 in Vietnam and 23,500 km^2 in Cambodia. The upstream Mekong Basin (MB) consists of six countries with a total land area of 795,000 km^2 stretching from the eastern watershed of the Tibetan Plateau to the Mekong Delta over a length of 4900 km. The annual flood pulse caused by tropical monsoons in July to October is the key hydrological characteristic of the Mekong River. The start of the annual flood in the delta is defined when the river discharge exceeds the mean annual discharge of 13,600 $m^3.s^{-1}$ at Kratie, and is featured by a single flood hydrograph (MRC [2007]). The long-term average of annual flood volume is 330 km^3 and the mean annual flood duration is 137 *days* (MRC [2011a]). The estimated annual sediment load of the Mekong varies between 50 and 160 *million tons* (Lu et al. [2014]: 50÷ 91 *million tons*; Milliman and Farnsworth [2011]: 110 *million tons*; Walling [2008]: 160 *million tons*), and about 50% of this load is contributed by the upper part of the basin in China (Roberts [2001], Walling [2008]). The annual dissolved sediment load was estimated to 60 *million tons* by Milliman and Farnsworth [2011].

The typical flood characteristics in the MD are: (1) buffering of the flood pulse by the Tonle Sap Lake, (2) a secondary flood pulse besides the river pulse caused by large-scale overbank flow over the Cambodian floodplains to the Vietnamese Mekong Delta (VMD), (3) large-scale, annually inundated areas ($> 20,000$ km^2), (4) extended inundation periods ($3 \div 4$ months), and (5) strong human interference in the hydraulic regime and suspended sediment transport, particularly in the VMD.

The MD includes four subsystems characterized by specific hydraulic regimes: Cambodian Mekong Delta, Tonle Sap, Vietnamese Mekong Delta and coastal area (Fig. 1.1).

The Cambodian Mekong Delta (CMD) consists of all rivers and floodplains in Cambodia excluding the Tonle Sap. These floodplains with a total area of around 11,000 km^2 show mostly a low level of human interferences. During flood seasons floodplains are inundated by overbank flow from the Mekong and Bassac River causing large-scale inundation in that area. The overbank flooding is not stagnant, but continues to flow to the VMD.

The Tonle Sap includes Tonle Sap Lake (TSL) and Tonle Sap River. The flow into the TSL during the rising and high stage of flood hydrograph at Kratie is reversed during the falling stage and next dry season, hence the TSL retains flood water and sediment during the flood season.

The coastal area subsystem extends from downstream of the My Thuan gauging station

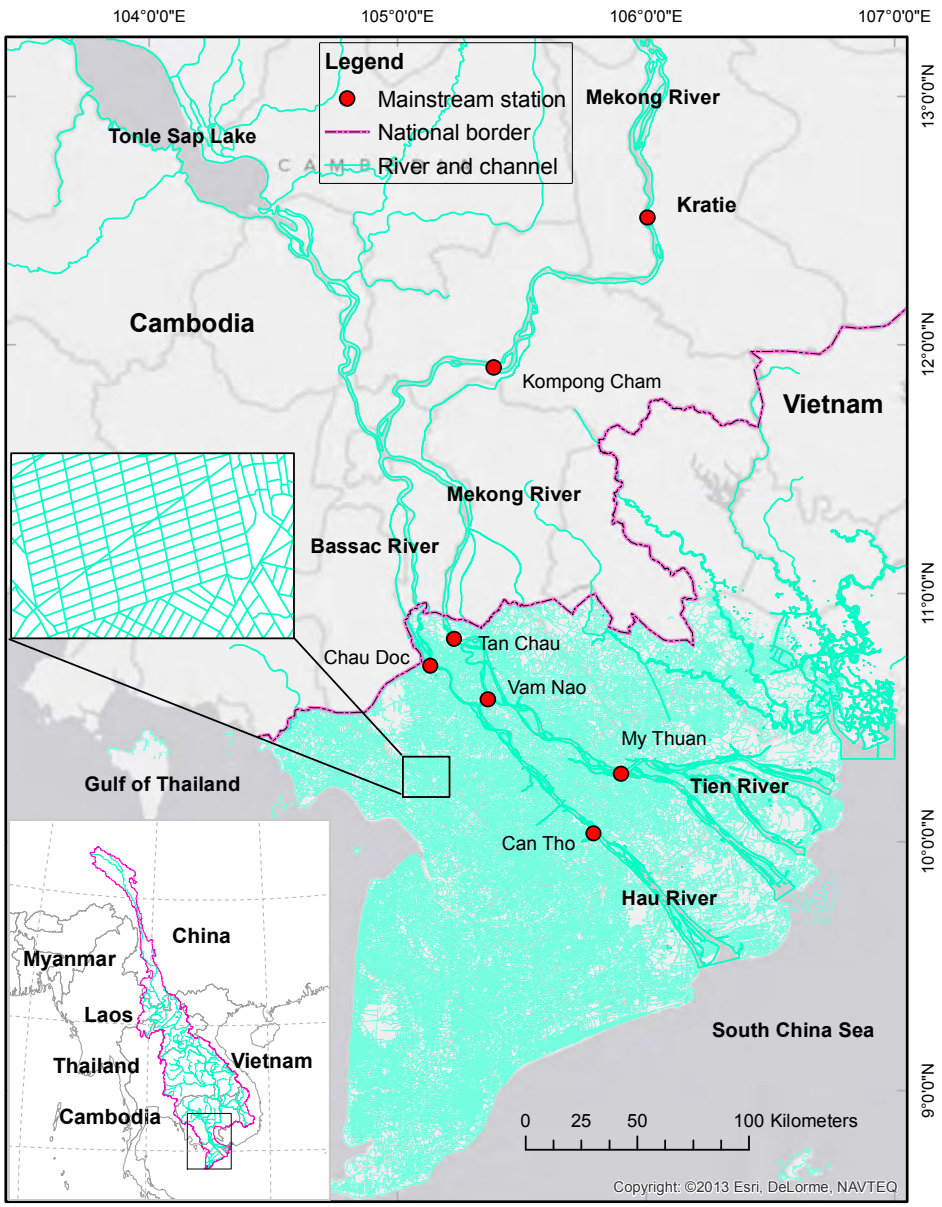

Figure 1.1: Map of the Mekong Delta from Kratie in Cambodia to the coast in Vietnam. It includes river and channel network and mainstream hydrological stations.

in the Mekong (Tien) River and downstream of Can Tho station in the Bassac (Hau) River to the sea. In this area tidal backwater effects occur throughout the year. Two tidal regimes exist, a diurnal tide in the Gulf of Thailand and semidiurnal tide in the South China Sea. The magnitude of the semidiurnal tide is significantly higher than the diurnal tide.

The Vietnamese Mekong Delta (VMD) stretches from gauging stations Tan Chau and Chau Doc to stations My Thuan and Can Tho at the Tien River and Hau River, respectively, with an area of about 19,500 km^2. The VMD is a highly complex river delta created by anthropogenic interference encompassing numerous channels, dikes, sluices gates and pumps. The total length of the channel network is about 91,000 km, resulting in a dike system that is approximately twice as long. 75% of the $\cong$ 10 *million* people in the VMD live in rural areas (GSO [2012]), whereas the rural residential areas are preferably distributed along the dike lines (Fig. 1.2). Most of the transportation during the flood season happens on the waterways, especially in high flood events. The main channels are connected to the Tien and

the Hau River (Fig. 1.2). Secondary channels distribute water from the main channels to floodplains and smaller channels. Thus the floodplains are dissected into numerous, mostly rectangular compartments that are typically enclosed by dike rings of different heights (Fig. 1.1).

The floodplains are almost completely altered and managed, as most of the VMD floodplains are used for agricultural production. The compartment areas range from 50 to 500 ha. They are linked to channels through sluice gates. The operation of these gates depends on flood magnitudes, ring dike heights and crop patterns. Ring dike are classified as low or high dike compartments. In high dike compartments the dike height is designed according to the maximum water level of the record flood in the year 2000. They are equipped with sluice gates and often with additional pumps. The flooding of these compartments is completely controlled under non-extreme flood events. The total length of the high dike compartments increased rapidly in the past ten years. Remote sensing data show that the triple crop area, an indicator of high dike rings and complete flood control, is concentrated in the middle and the western parts of the VMD (Leinenkugel et al. [2013]). In low dike compartments the flood can be controlled during the rising and falling stages of the flood season only. Overbank flow occurs during high stage of the annual floods. The heights of low dike compartments vary depending on the experience and capacity of famers. In a normal flood year, residual ponding water in these compartments is pumped out at the end of November for the dry season crop. In years of extreme or damaging floods, the water volume may exceed the pumping capacity and the dry season crop is not sown, as e.g. in 2011.

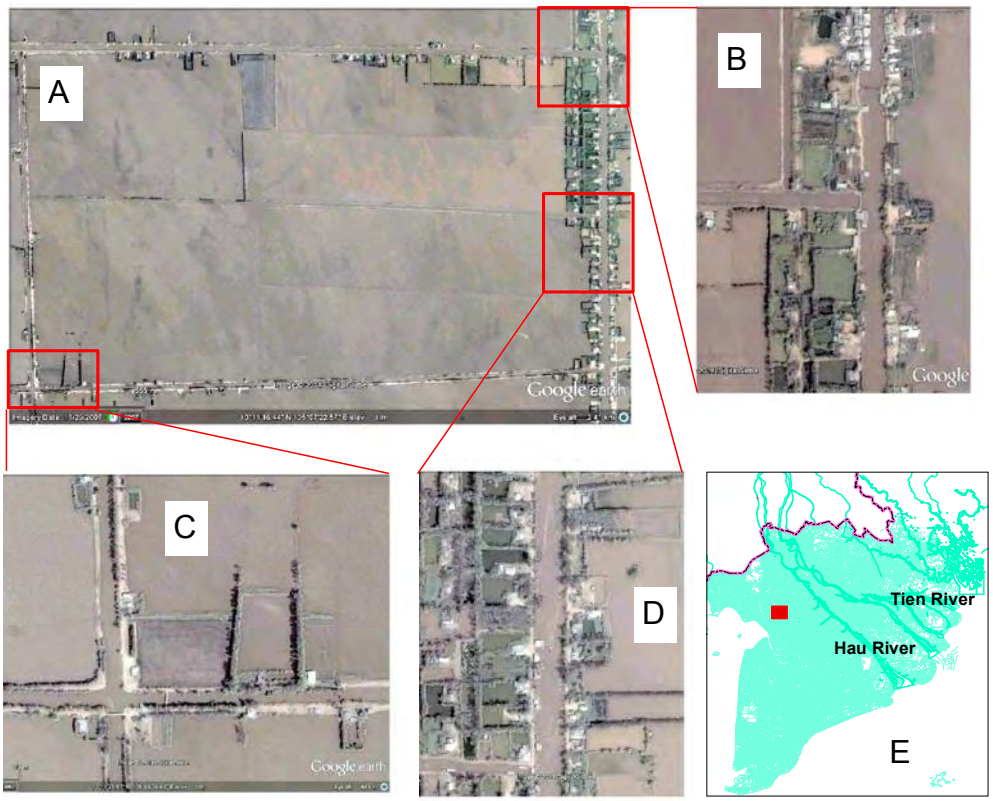

Figure 1.2: A typical floodplain in the VMD during flood season. [A] dike ring compartment with residences distributes along the ring-dikes, [B] and [C] zoom in the residential area in the dikes, [D] waterway transport in channel, [E] location of the floodplains in the VMD.

1.2 Motivation and objectives

The **motivation** of this work stems from the lack of knowledge on sediment dynamics in the Mekong Delta, where the understanding and quantification of the sediment and associated nutrient transport and deposition are crucial for the economy and ecology. Floodplains in the Mekong Delta are the residential and livelihood area of more than 10 *million* people in Vietnamese floodplains and several *million* people in Cambodian. Agriculture and aquaculture are the two main economic sectors, and the production depends on the annual Mekong flood regime. The large flood pulse with high sediment and associated nutrient loads is the core factor for the high agricultural productivity and high aqueous biodiversity and productivity of the fishery sector (Baran [2013]). The inland fisheries contribute 12%÷ 16% to GDP in Cambodian, and 7% in Vietnam (Baran [2010]). Moreover, the sedimentation in floodplains is a natural fertilizer with high economic value. Currently, the VMD is the heart of the rice production in SE-Asia, promoting Vietnam to the second largest rice exporter worldwide. The agricultural production in the VMD is strongly influenced by annual flooding patterns and floodplain sedimentation determining in combination with the dike system the cultivated crops and the amounts of required mineral fertilizers and pesticides.

Thus, the flood control is an ongoing debate in the VMD, where the benefits and disadvantages of the high dike system is discussed versus the traditional low dike system. The fully controlled floodplains with high dikes allow three crops per year, but due to limited inundation duration hardly any sediment and thus nutrients are trapped. The partially controlled floodplains of the low dike system allow just two crops per year, but they trap much higher sediments during the flood period. A knowledge and research gap in this debate is the lack of quantitative information of sediment-nutrient deposition on the floodplains, resp. in low dike and high dike systems. This study targets to fill this gap.

Regarding large-scale sediment transport and deposition in the whole MD, only one study has been published using a combination of 1D, 2D and 3D hydrodynamic models (MRCS/WUP-FIN [2007]). However, the study was limited to the Plain of Reeds (PoR, the north-eastern part of the Vietnamese MD), and considered only the main rivers and channels. It also lacked quantitative measurement data of floodplain deposition for calibrating the model. On the plot scale, a few experimental studies targeting specific aspects exist. These include fine sediment dynamics in the Mekong estuaries (Wolanski et al. [1996]) and in the Tonle Sap (MRC/DMS [2009]), fine sediment transport and deposition in the Long Xuyen Quadrangle (Thuyen et al. [2000]), sediment deposition and erosion in floodplains (Hung et al. [2014a], Hung et al. [2014b]), and sediment-nutrient deposition in floodplains (Vien et al. [2011]). These studies focused either on a small area or short duration, and none of them provides a quantification of the spatial distribution of sediment transport and deposition for the whole MD.

Moreover, the Mekong Delta is under threat, because the low-lying, flat floodplains of the MD are at high risk under global warming and human activities. In the Mekong basin the exploitation of the hydropower potential for the economic development has been increased rapidly in the recent 20 years. Land use change (Hoanh [2010]), damming (Keskinen et al. [2012], Räsänen et al. [2012], Lauri et al. [2012], Piman et al. [2013]) and climate change

(Eastham et al. [2008]; Hoanh [2010]; Västilä et al. [2010]; Kingston et al. [2011]; Lauri et al. [2012]) are altering the hydrology of the basin and thus the flow to the delta. The Mekong Delta itself is sinking due a combination of natural effects, human activities and climate change induced sea level rise (Ericson et al. [2006], Syvitski et al. [2009], Syvitski and Higgins [2012]). The estimated annual deltaic subsidence is 6 $mm.y^{-1}$ including eustatic sea level rise (Syvitski et al. [2009]). How the combination of these changes affects the sediment dynamics and floodplain sedimentation and thus the livelihood of the people in the MD has not been studied yet in a spatially explicit manner.

Thus, the general **objective** of this study is the quantification of the spatial distribution of sediment and related nutrients deposition in the floodplains in the whole Mekong Delta, and the prediction of spatial variability of the sedimentation under changing the MD boundary conditions. Following this overarching objective three specific objectives are defined:

1. Building an experimental data set of observations of sediment properties and floodplain sedimentation including spatial variability and physical-chemical characteristics in the whole MD, and quantifying uncertainty degrees of the achieved data set. This information combined with a literature review serves as the basis for the development of a sediment transport model, providing data for model calibration and quantification of the nutrients deposited with sediments in dike ring floodplains in VMD.

2. Quantifying large-scale sediment dynamics in the MD including the temporal-spatial distribution in the MD sub-systems from Kratie to the coast and sediment-nutrient deposition in floodplains. Development of a spatially distributed model of sediment transport which is able to simulate the present state and future prospects of the sediment dynamics in the whole MD.

3. Assessing the impacts of changing boundary conditions on sediment dynamics in floodplains using the sediment transport model. The changing boundary conditions consist of hydropower dam development trapping sediment and altering river flow, climate change altering the river flow and suspended sediments, and effective sea level rise including deltaic subsidence.

1.3 The organization of the dissertation

This dissertation consists of five chapters including three manuscripts, of which two are published and one is submitted to peer-reviewed ISI journals, the general introduction, and general discussion. The manuscripts are reformatted to match the format of a cumulative dissertation.

1. The first manuscript is entitled “Sedimentation monitoring including uncertainty analysis in complex floodplains: a case study in the Mekong Delta”. This manuscript developed a new approach to quantify sediment deposition in complex floodplains including an uncertainty estimation. The approach consists of a specific sediment trap design, strategic sampling scheme and analysis procedures for uncertainty analysis. The laboratory analysis for the collected data provided the sedimentation rate in different

spatial units, nutrients fractions and grain size distribution of sediment all over the regularly inundated VMD. An analysis was performed to derive the deposition uncertainty at each monitoring location, considering the uncertainty due to the collection of deposited sediment during the inundation phase. A Monte Carlo method was applied to propagate the uncertainties from these two sources. The measured data provided a first insight into the spatial and temporal dynamics of floodplain sediment deposition, from which nutrient deposition rates were derived. The information obtained by this study provides the basis for the development of a sediment transport model, as well as data for model calibration.

2. The second manuscript focused on "Large-scale suspended sediment transport and sediment deposition in the Mekong Delta". This paper proposes a comprehensive approach for large-scale sediment transport modelling of the MD. A quasi-2D presentation of diked VMD floodplains is implemented in the model linking floodplains to the channels and rivers by hydraulic structures. For model parameterization the study domain was classified into 11 parameter zones. A sensitivity analysis was performed to detect the sensitivity of each parameter in each zone of the model. Sensitivity parameters were included in the calibration while insensitive were fixed based on literature values. A two-stage calibration scheme with six objective functions was developed in order to properly simulate the hydraulic regime and the sediment dynamics in the temporal-spatial domain. The model setup ignores re-suspension processes and, thus, focuses on the net new annual sediment transport from Mekong River Basin (MRB) to the MD without local remobilization. This particular model setup enables the assessment of impacts of changing boundary conditions on floodplain sedimentation.

3. The last manuscript of the dissertation is entitled "Future sediment dynamics in the Mekong Delta: impacts of hydropower development, climate change and sea level rise". The study utilizes a sensitivity-based approach to assess the response of floodplain hydrology and sediment dynamics under hydropower development, climate change in the Mekong River Basin (MRB) and sea level rise. The developed quasi-2D suspended sediment model is used to simulate the sediment transport and sediment deposition in the whole delta system for the baseline (2000-2010) and future (2050-2060) periods. For each driver a plausible range of boundary changes was derived and discretized into five levels, resulting in altogether 216 possible combinations of boundary changes. These combinations cover all plausible future pathways of sediment dynamics in the Mekong Delta based on current knowledge on the change drivers.

Chapter 2 Sedimentation monitoring including uncertainty analysis in complex floodplains: A case study in the Mekong Delta

Abstract

Quantity and quality of sediment deposition in complex floodplains are affected by many processes which are typically highly spatially and temporally variable and hard to quantify exactly. The main processes in this context are suspended sediment transport dynamics in rivers, floodplain channel interactions, and internal floodplain processes. In consequence, any point measurement of sedimentation in floodplains contains a high degree of uncertainty, both stemming from measurement errors and from the lack of representativeness for a larger area. However, uncertainty analyses are not performed in publications on floodplain sedimentation data up to now. Therefore the presented work illustrates a field sampling strategy aiming at the monitoring of floodplain deposition and spatial variability on a large scale and at the quantification of uncertainties associated to sediment deposition data. The study was performed in the Mekong Delta, being an example for a large and complex floodplain with a high degree of anthropogenic disturbances. We present a procedure for the quantification of the uncertainty associated to the data, based on the design of the monitoring campaign, sampling procedures, and floodplain characteristics. Sediment traps were distributed strategically over the floodplain in clusters of three mat traps representing one monitoring point. The uncertainty originating from collection of the traps from still ponding water is quantified by lab experiments. The overall uncertainty of the deposition samples and the associated nutrient content is quantified in a Monte Carlo simulation and illustrated by uncertainty bounds. For the study area the results show a very high variability of the annual floodplain deposition ($2.2 \div 60\ kg.m^{-2}$) with uncertainty bounds ranging from -61% to +129% relative to overall mean deposition of 11.4 $kg.m^{-2}$. No correlations in the spatial distribution of sedimentation in the floodplains could be found. This is caused by the highly complex channel and dike system and the high number of hydraulic structures. Also, no differences in deposition between floodplain compartments protected with high and low dikes could be detected. However, it can be shown that within single floodplain compartments the spatial deposition variability depends on the dike levels and operation and location of hydraulic structures.

2.1 Introduction

Sediment deposition in floodplains in river deltas is controlled by sediment delivery from the upstream catchment, but also by characteristics of the particular delta. The delivery from the catchment, i.e. the suspended sediment transport, is controlled by climate, geography, soil types, land cover, and dam construction and operation. For the Mekong the impact of

reservoir construction and operation in the Chinese part (Lancang) has been studied by Lu and Siew [2006], Fu and He [2007], Fu et al. [2007], Kummu and Varis [2007], Kummu et al. [2010], Walling [2008] Gupta et al. [2012], Liu and He [2012], Liu et al. [2013], all showing that the dams reduced the sediment delivery from the Lancang after closure of the dams. The spatial variability of floodplain sedimentation is typically very high, due to the variability of the factors influencing supplied sediment and the actual deposition and erosion in the delta. In addition to the natural variability both sediment supply from the upstream catchment as well as the deposition in the delta show a high degree of anthropogenic influence in many regions of the world (Ericson et al. [2006], Syvitski and Saito [2007], Syvitski et al. [2009], Syvitski and Higgins [2012]).

In the Vietnamese part of the Mekong Delta (VMD), this interference is extraordinarily high. The VMD is known as the "rice bowl" of South East Asia. Almost the complete delta is used for agricultural production and dissected by a dense channel network compartmenting the floodplains into compartments. The compartments are enclosed by dikes for crop (low dikes) and flood (high dikes) protection. The question of increasing the number and length of the high dikes is under debate, because it enables cropping of a third crop per year during the flood period by blocking the floodplain inundation completely. This reduces the input of sediment and thus natural fertilizers, requiring a higher input of artificial mineral fertilizers and other agro-chemicals. However, the importance of natural floodplain sedimentation for agriculture, but also for the fishing industry and the ecosystem has been stressed by the Mekong River Commission (MRC [2010a]). In addition to these ecological and economical facets, floodplain sedimentation is also vital for counterbalancing deltaic subsidence. The subsidence is caused by natural compaction, but also anthropogenic causes as over-exploitation of ground water and urbanization (Syvitski et al. [2009], Syvitski and Higgins [2012], Wang et al. [2011]). These facts underline the importance of a good understanding and quantification of floodplain sedimentation.

Almost all of the floodplains in the VMD are compartmented by dike rings, and in case of high level dike rings the floodplain inundation is typically controlled by operation of sluice gates and pumps (Hung et al. [2012]). This interplay of different controlling factors suggests a high spatial variability of floodplain sedimentation (Hung et al. [2014a]). This expected spatial variability constricts the value of single point measurements. Considering also the known errors in sediment deposition measurements, it becomes clear that a) a representative monitoring of floodplain sedimentation for a large delta is a difficult task in general, and b) there is a clear need for a thorough estimation of the uncertainties of sedimentation data. The latter aspect facilitates a proper use and interpretation of the data and improves the credibility of the derived results and recommendations. The uncertainty analysis should identify the possible epistemic (lack of knowledge) and aleatory (natural variability) uncertainty sources and try to quantify them.

A number of studies monitoring sedimentation on floodplains are published, often using mat traps to quantify the accumulative sediment deposition during flood events (Asselman and Middelkoop [1995], Steiger et al. [2001], Steiger et al. [2003], Middelkoop [2005], Büttner et al. [2006], Baborowski et al. [2007], Hung et al. [2014b]). But to the knowledge of the authors

used multiple traps to quantify the deposition at a single point (Asselman and Middelkoop [1995], Steiger et al. [2001], Middelkoop [2005], Baborowski et al. [2007]). However, none of the studies quantified the uncertainties, neither epistemic sampling uncertainty, nor aleatory uncertainty related to spatial variability. There are publications on uncertainty analysis in sediment research (Salas and Shin [1999], Navratil et al. [2011], Shamsudin et al. [2012]). However, these studies focus on other aspects such as reservoir sedimentation, urban retention pond or suspended sediment mobilization and transport in small mountainous catchments.

This study presents a monitoring scheme aiming at the quantification of spatial variability of sediment and associated nutrient floodplain deposition in the VMD, as well as a strategy to quantify the uncertainty of the sediment sampling scheme. The study is the first large scale monitoring of floodplain sedimentation in the VMD. In addition, it also provides uncertainty estimates for the monitoring results for the first time, thus indicating the trustworthiness of sediment trap data. The uncertainty analysis procedure is adopted from the procedures developed by Apel et al. [2004], Apel et al. [2006], Apel et al. [2008] in the context of flood risk assessment. The derived data can contribute to the debate on the economic value of floodplain deposition in terms of nutrients, which is a hot topic in the VMD. There is a trend to totally blocking floodplain inundation in favor of three cropping periods per year, that have to be sustained by increasing input of mineral fertilizers (Ve [2009]). In addition, the results can also serve as a quantitative basis for the discussion of the importance of floodplain deposition to counterbalance the subsidence of the Delta.

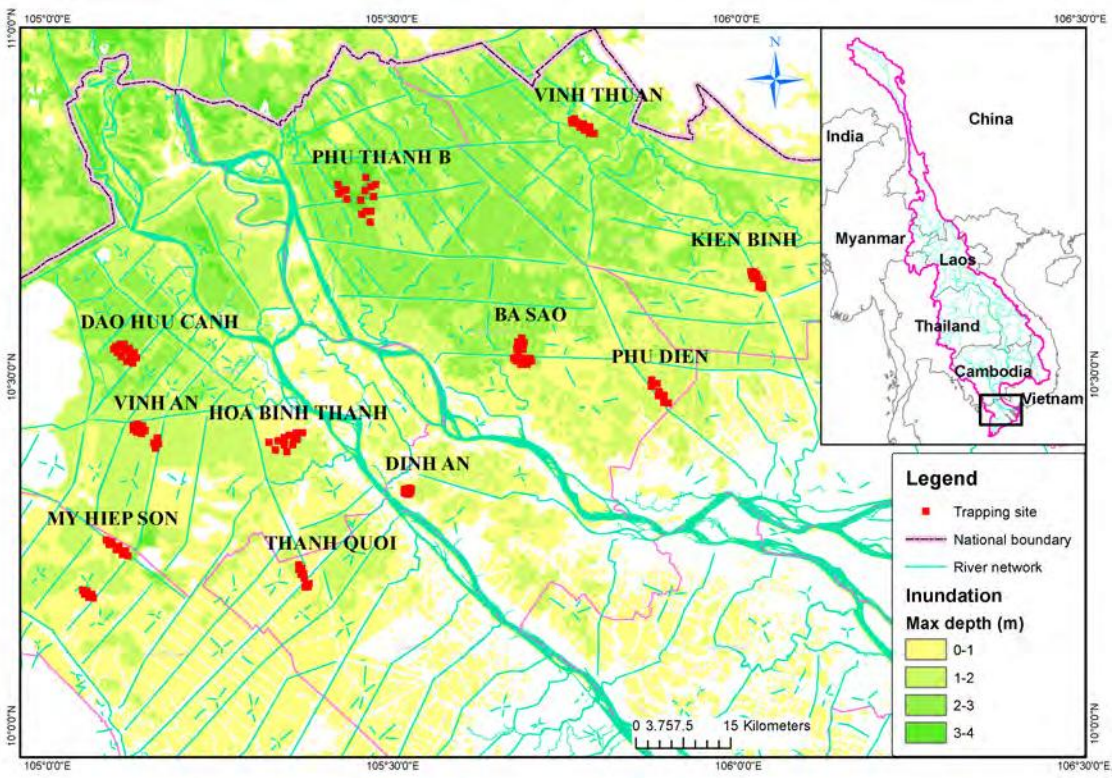

Figure 2.1: The study area in the MD in Vietnam: the main map shows the mean of maximum observed inundation depths over 2000÷2010 period, and the 11 selected sites including 19 compartments of either high dike or low dike systems. The map top right shows the entire Mekong River Basin with the Mekong delta marked by a gray box.

2.2 Study area and site selection

The Mekong Delta begins near Phnom Penh in Cambodia where the largest tributary, the Bassac River, branches away from the Mekong River. Both branches formed the huge fertile flat plain in southern Vietnam, the Vietnamese part of the Mekong Delta (VMD). It is known as the most complex channel network in the world and it is the habitat of more than 10 *million* people. The annual inundated floodplain area in the Mekong Delta within the Vietnamese territory is around 19.500 km^2 (Hung et al. [2012]) with a channel network of in total 91.000 km length (MARD [2012]), (Fig. 2.1).

The annual flood lasts from July or August to the end of November or mid-December. The main inundated areas are located in the northern part of the VMD, which are differentiated into the Plan of Reeds east of the Mekong (Tien in Vietnamese) branch, the Long Xuyen Quadrangle west of the Bassac (Hau in Vietnamese) branch, and the area between the Tien and Hau rivers. A number of secondary channels connected to either the Tien or Hau River facilitate widespread distribution of the flood water to the floodplains.

Deposited sediments play a very important role for the agricultural development in the MD. The annual suspended sediment load into the MD is about 160 *million tons* based on Walling [2008] and 110÷150 *million tons* based on Milliman and Farnsworth [2011]. In addition, Milliman and Farnsworth [2011] provided the number of 60 *million tons* of total dissolved solids per year. Approximately 80% of Mekong delivered sediment is trapped within the delta area (Xue et al. [2010]). The annual loads of total nitrogen (TN) and total phosphorous (TP) at the river mouths of the MD were estimated to be 2.7 $10^4 tNy^{-1}$ and 9 $10^3 tPy^{-1}$ (1987÷1999) (Yoshimura et al. [2009]).

Flood control is a hot issue in the VMD, low dike protection vs. high dike protection is under hot debate. However quantitative studies about floodplain sedimentation and associated nutrient deposition do not exist. Thus also an estimation of the economic benefits of the floodplain inundation and natural fertilizer input by sediments vs. higher flood protection and control is missing at present. In general terms, assumed higher suspended sediments and sedimentation on floodplains with low dikes does not only supply more natural fertilizer for agriculture, but also increase the output of wild catch fishery on floodplains over the flood season. On the other side, a high dike system enables growth of a third rice crop per year, but requires more artificial mineral fertilizers.

The agricultural system is adapted to the annual floods. Traditionally two crops are grown around the flood period utilizing the sediments and flood waters for irrigation and as nutrient source. Recently, a third crop was introduced in the shallow inundated areas of the delta, where the flood protection systems are well developed and floodplain inundation can be controlled completely under normal flood conditions. The spatial extent of the three crop system depends on the flood magnitude and economic factors. The presented study aims to provide a first quantitative data base for the estimation of the economic benefit the natural fertilizer input via flood sediments. This may serve as a basis for a cost-benefit analysis for the construction of high dike systems of triple crops area.

The study area is the entire regularly inundated floodplain in the VMD. The inundated flood-

plains vary year by year depending on the flood magnitude and the seasonal cropping pattern in the floodplains. These are controlled by the hydraulic structures, which operation is based on communal agreements. The main difference of flood characteristics in MD to other parts of the world is that the flood event is always longer than 3 months, setting it apart not only in the spatial, but also the temporal inundation extent compared to typical inundation durations from a few days to two weeks in smaller basins. Normally, the inundation duration extends from 4 to 5 months with single or double peak hydrographs. The sedimentation rate in floodplains generally depends on the following factors:

(1) Flood magnitude and duration;
(2) Distance to main rivers and associated suspended sediment concentration;
(3) Floodplain topography;
(4) Tidal regimes;
(5) Dikes, hydraulic structures and their operation and
(6) Human activities (fishing...).

The floodplains in the VMD are intensively used, even during floods. Typically a portion of the flood water is retained in the floodplain compartments and used for paddy cultivation. Depending on the flood magnitude and duration and the dike elevations, the farmers start to pump the water from the floodplains at some point in December in order to enable growing of two crops between flood seasons (Hung et al. [2012]). In most cases paddy rice is grown after the flood period, thus the farmers retain ponding water on the floodplains in the range of 20÷40 cm.

During the inundation the floodplains are used for fishing, which is traditionally done with nets. This disturbs the deposition and erosion processes, but has also impacts on the sediment monitoring as it puts the sediment traps at risk of being destroyed. This adds additional uncertainty to the monitored sediment deposition, both by loss of traps as well as by re-suspension and relocation processes. Thus the sediment trapping and uncertainty analysis require appropriate trap design, trap installation, trap collection, and methods to quantify the uncertainties stemming from these processes.

The selected sampling sites must be representative for the different inundation regions, inundation depths and flood protection levels. The criteria for site selections sorted by descending priority are as follows:

1. The selected sites have to be distributed on the main floodplains in the VMD, including the Plan of Reeds, Long Xuyen quadrangle and the area between Tien River and Hau River.

2. The selection is based on the flood depths in "high stage" in floodplains (Hung et al. [2012]): greater than 2 meter depth, from 1 meter to 2 meter depth and below 1 meter depth. The flood depths can be determined by intersection of inundation maps of different years derived from radar satellite images (Dung et al. [2011a]) and the digital elevation model (SRTM).

3. The sites should encompass full flood control compartments (termed "high dike" in Vietnam), as well as partial flood control compartment ("low dike"). For more infor-

mation on the dike system (see Hung et al. [2012]).

4. The sites should be suitable for monitoring of a long flooding period.

Although each site should ideally include a low dike and a high dike, this criteria could not be met everywhere. High dike compartments do not exist everywhere, so that some sites contain low dike compartments only. Finally, 11 sites were selected containing 19 compartments (cf. Fig. 2.1, Table 2.1) with overall 11 low dike and 8 high dike compartments.

Table 2.1: Sediment trap installation and collection in 19 compartments, and distance from the sites to main rivers.

No	Compartment	Collected traps	Installed traps	Percent	Distance to river
1	Vinh Thuan 1	9	15	60%	50 km
2	Vinh Thuan 2	20	27	74%	50 km
3	Kien Binh 1	15	15	100%	70 km
4	Kien Binh 2	27	27	100%	71 km
5	Phu Thanh B1	14	15	93%	12 km
6	Phu Thanh B2	10	15	67%	8 km
7	Phu Thanh B3	4	15	27%	10 km
8	Ba Sao 1	2	24	8%	15 km
9	Ba Sao 2	1	30	3%	15 km
10	Phu Dien	1	24	4%	40 km
11	Dinh An	2	24	8%	5 km
12	Hoa Binh Thanh	6	36	17%	7 km
13	Vinh An 1	2	15	13%	20 km
14	Vinh An 2	1	27	4%	21 km
15	Dao Huu Canh	20	42	48%	15 km
16	My Hiep Son 1	17	24	71%	47 km
17	My Hiep Son 2	17	33	52%	40 km
18	Thanh Quoi 1	1	24	4%	18 km
19	Thanh Quoi 2	2	15	13%	18 km
	Total	171	447	38%	

2.3 Methodology

2.3.1 Sediment trap design

Sedimentation is mostly monitored by sediment traps, as shown by a number of recent studies (Steiger et al. [2001], Steiger et al. [2003], Middelkoop [2005], Büttner et al. [2006], Baborowski et al. [2007], Hung et al. [2014b]). Sediment traps can provide cumulative samples for different physical and chemical analyses. Flexible sediment traps are an adequate method for sampling sediment deposited by flowing water in floodplains and are in recent studies preferred to flat devices with a smoother surface, because they can represent the natural ground surface more appropriately (Steiger et al. [2003]). We followed this recommendation and used flexible traps built from artificial grass with a rectangular dimension of 30 cm by 30 cm and 1.5 cm long tufts. To be able to retrieve the traps from still ponding water with minimum sediment loss, the traps were designed with eight strings (60 cm long) attached to the corners and the middle of the sides. The traps were tested to withstand upward pulling by the strings with more than 60 $kg.m^{-2}$ sediment load, which is well above the maximum documented

deposition of 20 $kg.m^{-2}.y^{-1}$ in VMD (Hung et al. [2014b]). When the traps are pulled up by the strings, they form a bowl-shape retaining most of the sediment (Fig. 2.3). However, the retrieval cannot be loss free, and it has to be expected, that the higher the deposition volume, the higher is the loss, as the overflow over the sides of the bowl is likely to carry more sediment compared to small deposition volumes. The loss due to retrieval is quantified by lab experiments presented in Section 2.3.1. The traps were fixed to the ground by bamboo stakes instead of steel pins, in order to avoid injuries of the farmers when they accidentally step on them in their fields.

2.3.2 Sampling scheme

Measurement of sedimentation using clusters of traps has been performed to indicate differences in sediment accumulation over short distances Asselman and Middelkoop [1995], and to calculate average deposition rates (Steiger et al. [2001], Middelkoop [2005], Baborowski et al. [2007]). In order to increase the representativeness of a *single trap* for the sedimentation processes due to very high variability of local hydraulic regimes in compartments (Hung et al. [2012]), clusters of 3 traps were installed for every monitoring point in the presented study. The number of 3 traps for each cluster is a compromise between overall number of samples that could be handled with the available resources (Fig. 2.2) and the need for getting a quantitative insight into the sampling uncertainty at each sampling point By this repeated sampling the variability at a given location can be estimated. This variability stems from the different floodplain processes, both natural and anthropogenic, influencing the deposition. The traps of each cluster were positioned in an equiangular triangle of 2 m side length (Fig. 2.2). Each cluster was marked with flags on high poles to indicate the fishing farmers the trap location.

The farmers retain ponding water on the floodplains for the second/third crop of a year after the flood, which has consequences for the sediment monitoring. First of all, the time for trap deployment and collection is limited, as there are just a few *days* between the crops and the inundation where the land is not used. The traps have to be placed and collected in these short time windows, otherwise the farmers will either remove the traps, or the positioning is not possible because the floodplains are already inundated. Besides this logistical obstacle, there is also the problem that the traps have to be collected with water still ponding on the fields. This obviously introduces measurement errors, which need to be taken into account (Section 2.3.1). In order to quantify the spatial variability of deposition within a compartment, each compartment was equipped with several monitoring point clusters, each consisting of three traps. The monitoring points are arranged perpendicular and parallel to the expected flow direction in the compartment.

A total number of 149 trap clusters (447 traps) were deployed at the monitoring sites for the measurement campaign starting in late July 2011 and lasting until mid-December 2011. The maximum and minimum number of points (trap clusters) in a compartment were 14 and 5, respectively, while the biggest and the smallest monitored compartments are 858 hectares and 52 hectares, respectively. The distance from the sites to main rivers range from 5 km in Dinh An compartment up to 71 km in Kien Binh 2 compartment (Table 2.1). The traps were retrieved just after the flood season and before cropping activities in the fields started.

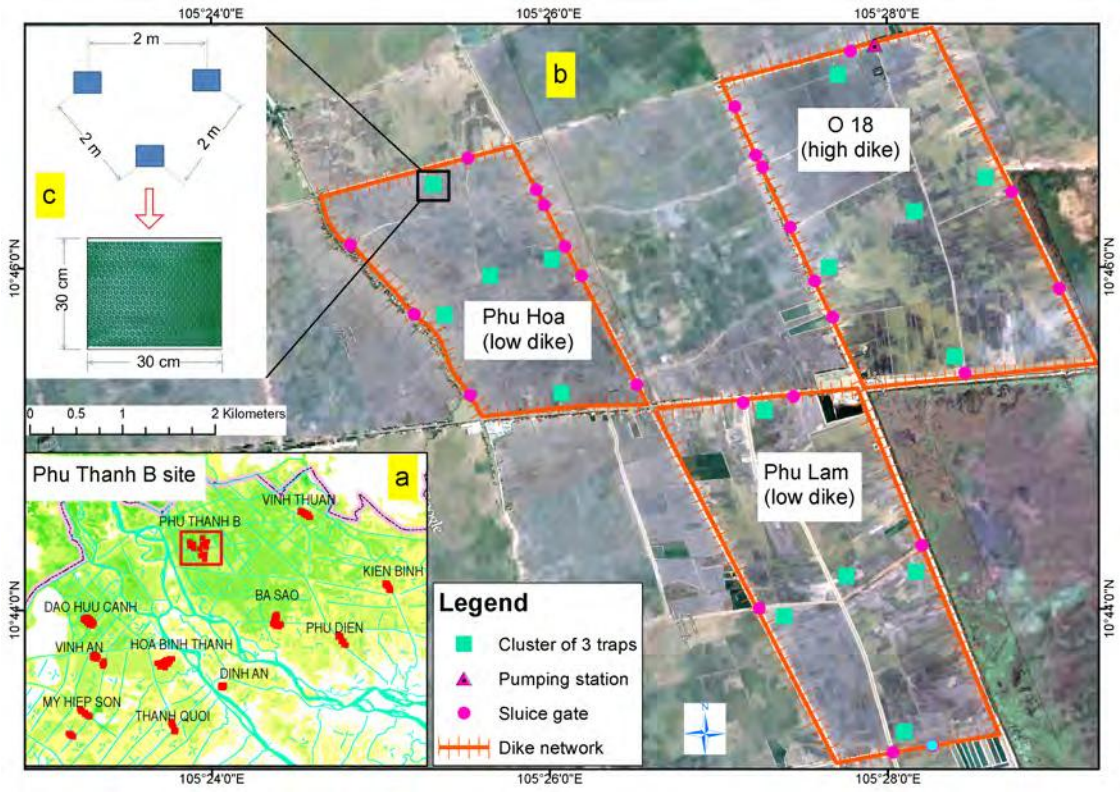

Figure 2.2: Map illustrating the typical setup of the sediment traps in a site: map (a) shows all selected sites. The main map (b) describes the sediment trap installation in the study site of Phu Thanh B, the map (c) shows a cluster of 3 traps, the distances between the traps and the dimension of a trap.

2.3.3 Uncertainty analysis

Uncertainty associated to trap collection in ponding water

Trap removal from ponding water will always produce less (or equal at best) sediment mass compared to dry trap collection. Sediments can only be lost, not gained by trap removal from ponding water, as water flowing from the trap will carry parts of the deposited sediment when the trap is pulled out of the water. In order to quantify this loss, experiments were conducted in a small reservoir, where traps with known and equal dry weights are immersed. After complete mixing and following settlement of the now suspended sediment, one trap is pulled out of the water by the strings. Following the removal of one trap, the water is carefully removed from the reservoir until the remaining trap can be removed without pulling it through water. The sediment masses in the traps are determined by weighing after drying of the removed samples yielding sediment masses of wet and dry collection conditions. The tests were performed with 32 different initial sediment masses equivalent to reported annual deposition masses of $0.07 \div 21\ kg.m^{-2}.y^{-1}$, as referenced in Hung et al. [2014b]. The results of this test are shown in Fig. 2.4, where the constraint that the wet collection mass must be lower than the dry collection is represented by the truncation line.

The regression model with constraint:

$$y = 0.0561\ x^2 + 0.6659\ x + 0.9141 \tag{2.1}$$

Figure 2.3: The sediment trap design, strength and balance test. Left: a fixed trap on the ground, right: bowl-shape trap when pulled up.

$$y \geq x \tag{2.2}$$

In which x: Wet retrieval sediment mass $[kg.m^{-2}]$, y: Dry retrieval sediment mass $[kg.m^{-2}]$ The 95% *Confidence Interval* (CI) of the regression, also shown in Fig. 2.4, shows the uncertainty stemming from the parameter estimation and is computed as $CI = para \pm \tau\sqrt{S}$, in which *para* denotes the estimated parameters, t depends on the confidence level, and is computed using the inverse of Student's τ cumulative distribution function, and S is a vector of the diagonal elements from the estimated covariance matrix of the coefficient estimates (Mendenhall et al. [2009]).

The exponential regression models describing the data can also be justified by the trap removal procedure. When a trap is removed by pulling it upward with the strings, the mat forms a bowl-like shape. When there is only little sediment in the trap and the trap is removed carefully, only little sediment is re-suspended by the outflowing water. However, the higher deposition masses are, the closer the deposited sediment is to the brim of the "removal bowl", thus causing higher losses by the outflowing water or even direct losses in extreme cases. The uncertainty of the model is captured by confidence intervals (Apel et al. [2004]). In the following this sampling uncertainty is called "wet-dry correction model". This uncertainty source represents an epistemic uncertainty source according to Merz and Thieken [2005].

Deposition uncertainty

The second uncertainty source of the sampling scheme is the deposition sampling uncertainty, i.e. the representativeness of a sediment trap measurement for the actual deposition at the sampling point. The layout in clusters of three traps aimed at the quantification of this uncertainty. For every cluster the mean and standard deviation were taken as a measure for the deposition uncertainty. In case the clusters are damaged or partially lost, a *single trap* had to be used to represent to deposition at the given location. In order to use these traps in the given uncertainty estimation framework instead of discarding them, we have to assume that the mean of these "*single trap* clusters" is represented by the measured deposition value. As this assumption is also uncertain, we "penalize" these samples with a higher degree of uncertainty (i.e. wider confidence intervals) compared to the three trap clusters. Details on

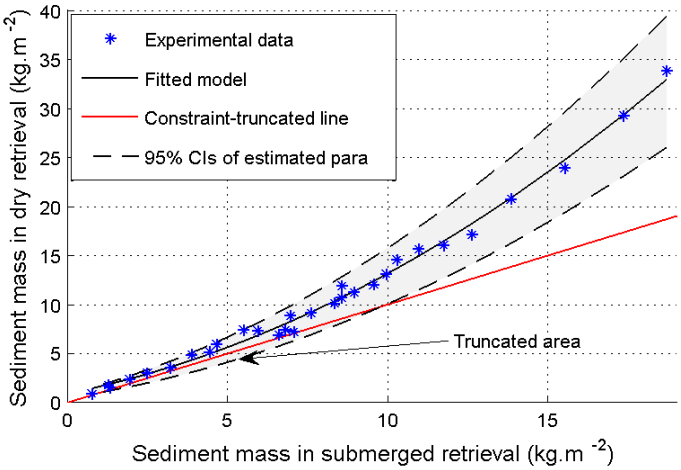

Figure 2.4: Experimental results of trap retrieval from ponding water and under dry condition. The stars are the experimental data, the black solid line is the regression model, while the dashed lines indicate the 95% confidence bounds of the regression derived from the parameter uncertainty. The truncated domain is the area below the constrain line in red.

this are given in Sect. "Sediment mass" below. At this point we have to emphasize that we assume normality in the distribution of the cluster trap deposition, and that the sample mean and standard deviation calculated from the trap results represent the moments of the distribution. Of course, the statistical significance of these moments is very limited due to the small sample size. However, given the constraints in practically feasible sample numbers and sample analysis, thee derived statistical moments from the trap samples provide essential information for the uncertainty analysis. It has also to be noted that obtaining statistically significant sample sizes for the determination of the distribution of deposition masses within a trap cluster would require a much higher number of traps per cluster. This is, however, not practicable in an experimental study on this large scale. But even in a small scale study the required number of traps per cluster (approx. ≥ 30) would face the problem that the required space for this experimental setup is too large to actually depict the local deposition uncertainty, because natural spatial variability of deposition might already come into play. Thus we regard the information derived from the 3-sample clusters as an important step towards a quantification of sediment deposition uncertainty, as already this small sample size indicates a large variability. And generally speaking, we argue in line with Pappenberger and Beven [2006] that it is better to acknowledge the uncertainties in data and models, even by subjective assumptions, than to neglect the uncertainties completely and present data as deterministic and precise, while they are clearly not.

Monte Carlo analysis

The overall uncertainty stemming from the uncertainty in deposition monitoring and wet trap removal is quantified in a Monte Carlo (MC) framework. For every sampling location, the uncertainty from both sources is combined by a randomized sampling of wet deposition and subsequent wet-dry sample mass correction. As mentioned above, we assume normality for the uncertainty distribution of the sampling uncertainty, but also for the wet-dry correction. The moments of the uncertainty distribution of the wet-dry correction model parameters are derived from the uncertainty bounds of the regression parameters shown in Fig. 2.4.

The MC uncertainty analysis was performed for deposition mass, nutrient fractions (TN, TP, TK, TOC), grain size fractions (Sand, Silt, Clay) and pH. The uncertainty of the deposition mass was calculated for every monitoring point. This uncertainty was further propagated to nutrient masses by combining the deposition uncertainty with the uncertainty of the nutrient

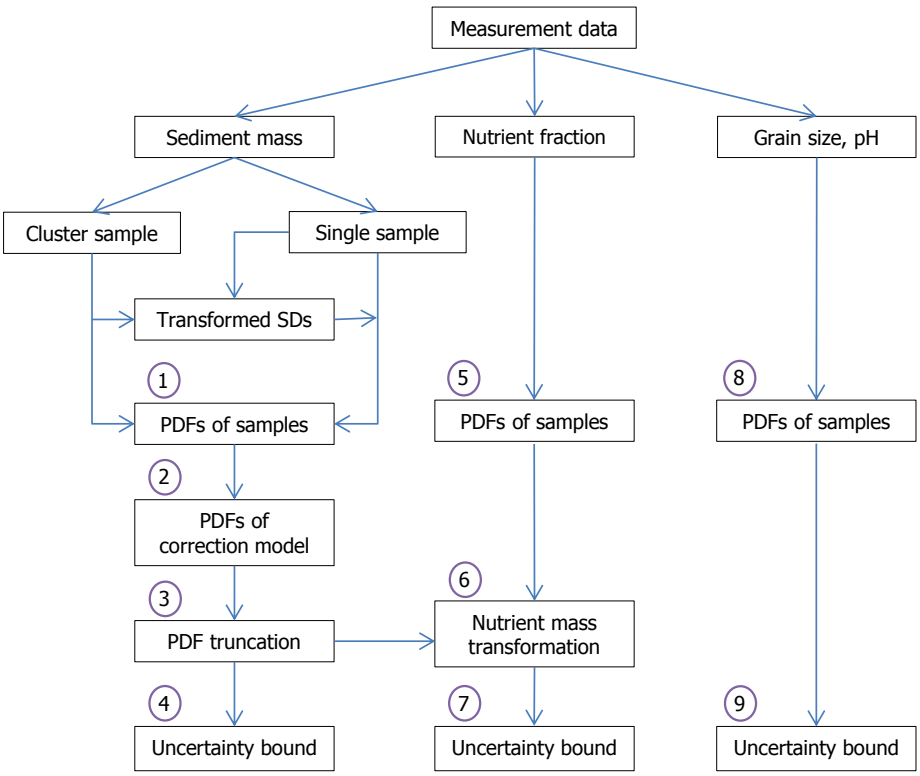

Figure 2.5: Uncertainty analysis workflows for sediment mass, nutrient fractions and grain size, pH..

fractions. The grain size fraction and pH do not depend on the deposition mass, as the very small CV values indicate, thus the spatial units of their uncertainty analysis are the compartments. According to the different spatial units, the uncertainty analysis consists of three workflows (shown in Fig. 2.5): uncertainty analysis for sediment mass, nutrient fractions, and finally grain size fractions and pH. The sediment mass workflow contains 2 branches: *cluster traps* (two/three traps) and *single traps*. Details are given below. For every parameter 5000 MC runs were performed.

a. Sediment mass

The uncertainty analysis of the sediment mass is performed in 4 steps:

Step 1: Derivation of PDFs for wet collected deposition mass for *cluster traps* and *single traps*

Cluster traps: derive the PDFs are based on the mean and SD of each trap cluster

Single traps: In order to include these values in the uncertainty analysis assumptions about the real mean and standard deviation have to be taken. First we assume that the measured value can be used as an approximation of the real cluster mean. SDs are derived from the linear correlation of the mean values to the SDs of the *cluster traps*. Fig. 2.6 shows a scatter plot of the cluster means vs. the cluster standard deviations along with the linear regression and the associated 99% confidence intervals of the linear regression. A "mean" value from a *single trap* is associated with the standard deviation from the upper 99% confidence interval of the regression, thus ensuring that the missing trap values are penalized with a high degree of uncertainty. This method also considers the observed trend of decreasing CV with increasing deposition mass.

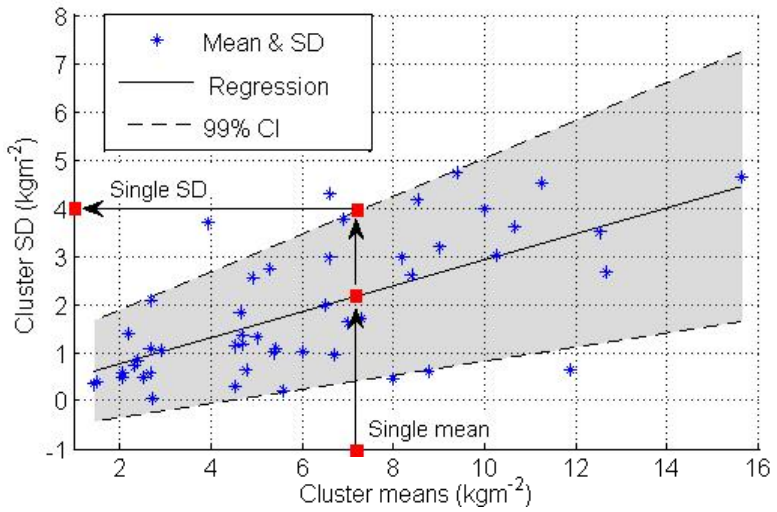

Figure 2.6: Linear regression between SD and mean values derived from the multi-trap clusters.

Step 2: Calculate the dry collection mass
For every trap location a wet collection mass is randomly drawn from the PDFs of step 1. From this wet collection mass the dry collection mass is calculated with randomly selected regression parameters. The normal PDFs of the parameters are derived from the confidence bounds of the parameters. Normality is chosen because the method providing the confidence bounds assumes normality (Student's τ distribution, see explanation of Eq. 2.1.

Step 3: Truncate the dry collection masses from step 2 by the constraint given in Eq. 2.2

Step 4: Construct 95% CI of the empirical PDFs derived from the results of step 3.

b. Nutrient mass

The laboratory results of nutrient analysis are expressed as a proportion of sediment mass (%). This means that the uncertainty of nutrient mass is related to the sediment mass. Moreover, the coefficient of variation of nutrient fraction is comparatively low, as well as the correlation coefficients between sediment mass and nutrient fraction. This implies that the nutrient compounds in the sediments are approximately homogeneously distributed over the study area. Thus the uncertainty of the nutrient fractions can be calculated over a larger spatial unit as for the deposition masses. We chose to derive the overall uncertainty over the whole study area.

Step 5: Derive PDFs of nutrient fractions based on the mean and SD of nutrient fraction calculated over the whole study area. Again we assume normality in the nutrient fraction distribution.

Step 6: Create PDFs of nutrient mass by multiplying randomly selected nutrient fraction from the PDFs in step 5 with the dry collection sediment masses from step 3.

Step 7: Construct the 95% CI for the nutrient masses from the empirical PDFs from step 6.

c. Grain size fraction and pH

In order to account for the observed differences in substrate and pH in the VMD, the uncertainty of grain size distributions and pH is calculated compartment-wise. Variations in pH may well be caused by local redistribution of sediments. The acidic soils, e.g. in the Plain of Reeds, may influence pH, which in turn influences the grain size distribution by flocculation.

Hence, in order to capture the variability of these parameters for an appropriate spatial unit, the uncertainty is evaluated for every monitored compartment. I.e. the statistical moments are calculated from compartment aggregated sample pools. Again we assume normality of the sample distribution over the compartments.

Step 8: Derive PDFs of grain size fractions and pH based on means and SD over compartments

Step 9: Construct the 95% CI from the PDFs results in step 8 for every compartment.

Finally, the results in step 4, 7, 9 are the estimated uncertainty bounds presented as 95% confidence intervals of sediment mass for every sampling location, nutrient masses for the whole study area, and pH and grain size fractions for individual compartments.

Table 2.2: Analysis methods for physical and chemical properties of sediment samples.

Analysis	Methods
Mass	Drying and weighing in the laboratory
D	Robinson pipette method ($sand > 0.063mm > silt > 2\mu m\ clay$)
pH	pH meter: soil : water ratio 1:2.5
TN	Micro Kjeldahl: using $H_2SO_4 - CuSO_4 - Se$, ratio: 100-10-1
TP	Attacked by $H_2SO_4 - HCLO_4$ (1:5) desalinate phosphomolybdate by ascorbic acid, color comparison with Photometer.
TK	Attacked by $HF - HCLO_4$ (10:1) Determine K by Atomic Absorption
TOC	Walkley-Black: oxidation by $H_2SO_4 - K_2Cr_2O_7$, titrated by $FeSO_4$

2.4 Results and discussion

2.4.1 Monitoring results & basic descriptive statistics

A large number of traps was lost or damaged, both due to the exceptionally high flood in this year (MRC [2011b]), and fishing activities in the floodplains. The farmers owning the land where the traps were installed were informed and paid for taking care. However, during the flood season in the VMD the inundated land has legally no owner and everyone can fish everywhere, which partly explains the loss of some traps, as not everybody could have been informed about the monitoring activities. An overall number of 171 traps in 19 compartments could be collected, which is equivalent to 38% of all installed traps.

The number of samples used for the laboratory test is restricted due to a required minimum volume of sediments for nutrient analysis and grain size analysis, integrity of samples after transport from the fields to the laboratory for sediment mass analysis, and available budgets and laboratory capacity. Thus only 161 of 171 traps in 12 compartments could be used to measure the sediment mass. The 161 samples stem from 49 clusters of two or three traps and 26 "*single trap* clusters". In the "*single trap* clusters" the remaining two traps were lost or destroyed by the flood or farmers/fishers. The sample masses were measured after drying at room temperatures in the range of $30 \div 35^oC$ until the masses did not change over several days. This took around 6 weeks. The deposited masses are sample masses subtracted by the trap weight. The trap weights were measured prior to placement on floodplains. The weight of the traps is 180 g $\pm$ 5 g based on weighing of a subset of 10 samples.

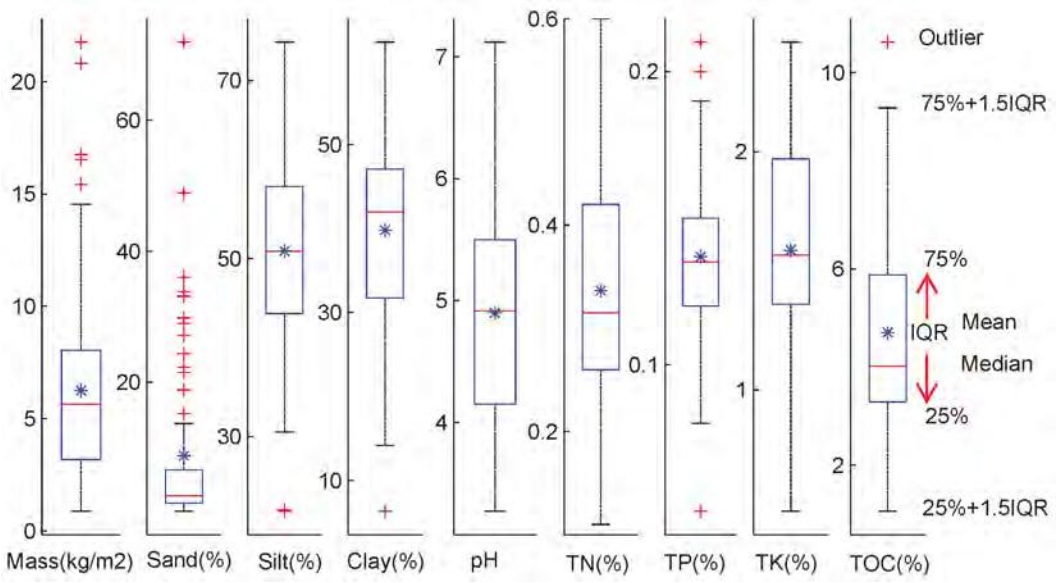

Figure 2.7: Box plots of all data: sediment mass (g), sediment grain size classification of Sand, Silt and Clay (%), potential Hydrogen (pH), Total Nitrogen (TN) (%), Total Phosphorus (TP) (%); Total Potassium (TP) (%) and Total Organic Carbon (TOC) (%).

61 representative samples distributed over 12 compartments were analyzed for the quantification the physical and chemical properties of the floodplains sediments. The physical properties analyzed were the particle size distribution (sand, silt and clay fractions), while the chemical properties were pH, Total Nitrogen fraction (TN), Total Phosphorus fraction (TP), Total Potassium fraction (TK), and Total Organic Carbon fraction (TOC). The nutrient analysis yielded proportional figures to the sediment masses. The analytical methods are listed in Table 2.2.

Fig. 2.7 presents the analysis results and their overall variability for all analyzed samples in box-whisker-plots. Sediment masses show a high variability with minimum and maximum deposition of 1.44 $kg.m^{-2}$ and 21.7 $kg.m^{-2}$ respectively, while the median deposition is 6.0 $kg.m^{-2}$. This high variation is expressed in a high overall coefficient of variation of 0.64. The variability of the nutrient fractions is considerably lower. Minimum and maximum values are always in the same order of magnitude, and the coefficients of variation are 0.36, 0.21, 0.28 and 0.44 for TN, TP, TK and TOC, respectively. This finding supports the hypothesis that the nutrient content of the sediment is relatively uniformly distributed over the delta and that the spatial differences in nutrient input to the floodplains is mainly controlled by the deposition masses, and only to a minor extent by variable nutrient content of the sediments. For pH extreme values up to 3.2 and slightly alkaline samples are observed. The grain size distribution is dominated by the silt and clay fractions with only little and sporadic sand components, as the low percentages and high number of outliers of the sand fraction showed. The coefficients of variation are 0.2, 0.22, 0.17 and 1.53 for silt, clay, pH and sand respectively. This is typical for suspended sediment in the VMD (Wolanski et al. [1996], Thuyen et al. [2000], Hung et al. [2014a]).

Fig. 2.8 shows the variability of every of the 49 sample clusters for deposition mass derived from the sampling repetitions, and for the 12 compartment-wise collected samples for the remaining parameters. The different data aggregation levels, i.e. trap cluster for deposition

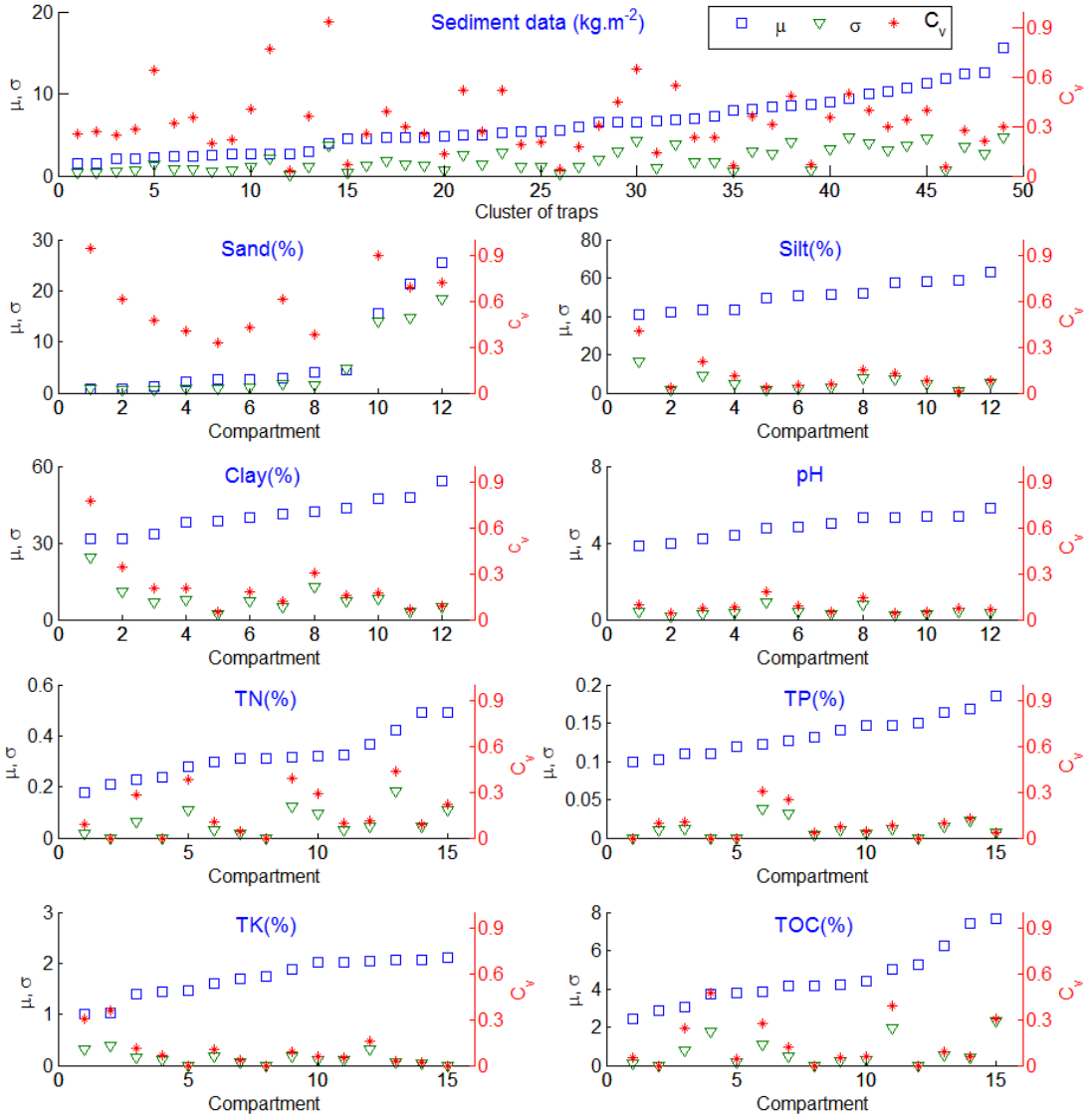

Figure 2.8: The means (μ), standard deviations (σ) and coefficient of variation (CV) of sediment weight on Cluster traps, pH and nutrient data in compartments.

mass and compartments for the remaining parameters, acknowledge the higher variability of the deposition mass and the quantification of the remaining parameters in relative terms, which is to a large extent independent of the actual deposition mass at a single monitoring point. For all parameters mean, standard deviation SD, and coefficient of variation CV are plotted. The clusters, representative compartment samples are sorted according to the mean. The standard deviations are always smaller than the mean resulting in CV's below 1. The deposition mass data shows an interesting trend in declining variability of CV with mean deposition, indicating that the sampling uncertainty is smaller with higher deposition masses. This can be explained by the fact that even little disturbances can have a large effect on deposition in case of only small deposition volumes. For all other parameters besides deposition mass except the sand fraction, the variation within the compartments is comparatively low, as the small CV's indicate (Fig. 2.8). This corroborates the finding that the nutrient content shows only little spatial variation, both within compartments and over the complete sampled domain. These findings imply that (a) the deposition masses contain significant high uncertainties that should be quantified, and (b) the focus of an uncertainty analysis should

be laid on the uncertainty in deposition mass, as this also influences the uncertainty in the estimation of the absolute nutrient deposition.

2.4.2 Uncertainty analysis

In this section the differences in the derived uncertainty estimates from steps 4, 7, and 9 are discussed. Table 2.3 shows a ranking of the parameters by relative uncertainty to the mean based on the the upper bounds of the confidence intervals. The sand fraction has the largest uncertainty bounds with the maximum range from 65% to 203%, while the smallest bounds are found for pH with 36% to both sides. The nutrient mass bounds are significantly wider than the bound of sediment mass, because the uncertainty of the sediment mass is enlarged by the uncertainty of the nutrient fractions. Silt and Clay have quite narrow bounds in terms of their mean, ranging from 39% to 43% and 22% on both sides respectively.

Table 2.3: Uncertainty rank (sorted from low to high mean upper CI) of sediment mass $[kg.m^{-2}.y^{-1}]$*, nutrient mass* $[g.m^{-2}.y^{-1}]$*, grain size (%) and pH. The uncertainty is expressed as 95% CI of PDFs.*

Rank	Component	Mean PDFs		Lower CIs			Upper CIs		
		min	max	min	mean	max	min	mean	max
1	Sand	0.8	25.5	65%	91%	100%	65%	123%	203%
2	TOC	122.4	3109.3	30%	44%	65%	58%	105%	168%
3	TN	8.3	216	27%	42%	64%	49%	98%	155%
4	TK	38	990.1	24%	40%	63%	43%	91%	153%
5	TP	3.1	84.3	21%	38%	62%	40%	85%	139%
6	Sed. mass	2.2	60.6	14%	35%	61%	21%	73%	129%
7	Clay	31.4	54.2	10%	39%	100%	10%	43%	152%
8	Silt	40.7	63.1	2%	22%	80%	2%	22%	80%
9	PH	3.9	5.8	9%	16%	36%	9%	16%	36%

Fig. 2.9 shows the mean and 95% CI of deposited sediment mass before and after the MC analysis, sorted by the measured mean original deposition mass. In overall, the uncertainty bounds are asymmetric due to the constraint from Eq. 2.2. In relative terms the lower bound is always less or at least equal to the upper bound. The single samples show higher uncertainty ranges compared to cluster trap with approximately equal mass. Overall it can be observed that the uncertainty bounds can be considerably large, with a maximum of relative lower bound of 61% and and a relative upper bound of 129%. The minimum relative bounds are 14% (upper) to 21% respectively (lower), cf. Table 2.3. There is a trend towards higher uncertainty with higher sediment mass. This has to be attributed to the wet-dry sampling uncertainty, because this is larger for larger deposition masses (cf. Sect. 2.3.3) and the deposition sampling uncertainty does not show this trend, rather the opposite.. If the deposition sampling uncertainty is low, the overall uncertainty is also well constrained in narrow CI's. The lower CI is closer to the mean and less variable due to the constraint in the wet-dry-sampling correction.

In Fig. 2.10, the uncertainty bounds of deposited nutrients $(g.m^{-2})$ are propagated from sediment weight bounds based on the analyzed nutrient fractions (%). Therefore, the uncertainty bounds show the same characteristics as for the sediment masses (Fig. 2.10). Due

to the additional uncertainty of the nutrient fraction, the relative uncertainty is increased for the nutrient deposition estimates. These features are illustrated in Table 2.3. The upper confidence bounds of nutrient masses are 5÷10% larger compared to sediment for the lower bounds and 10÷20% for the upper bounds.

In contrast to the nutrients, the grain size fractions and pH show different uncertainty characteristics, as they do not depend on the deposition mass (Fig. 2.11). The confidence intervals are small compared to sediment mass and nutrients and essentially symmetric, which is a consequence of the assumption of normal distributed deposition uncertainty. The sand fraction has the highest uncertainty for large sand fraction values, illustrating the sporadic and most likely locally influenced sand content of the suspended sediments in the VMD. The opposite holds true for the clay fraction, where the uncertainty is highest for low clay fractions. This effect has to be attributed to the small particle size and the related sensitivity of the laboratory analysis of the clay fraction, but also to the slow settling of the particles and its susceptibility to only minor hydraulic disturbances and temperature (Hung et al. [2014a]).

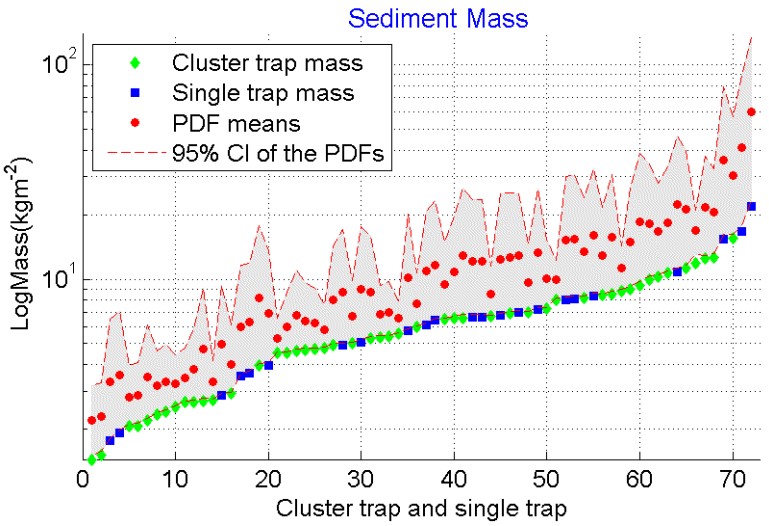

Figure 2.9: Mean (red dots) and confidence intervals (CI, red dash lines) of sediment mass after wet-dry sampling correction and uncertainty analysis, and original trap data. Sediment masses with indication of cluster traps and single trap samples.

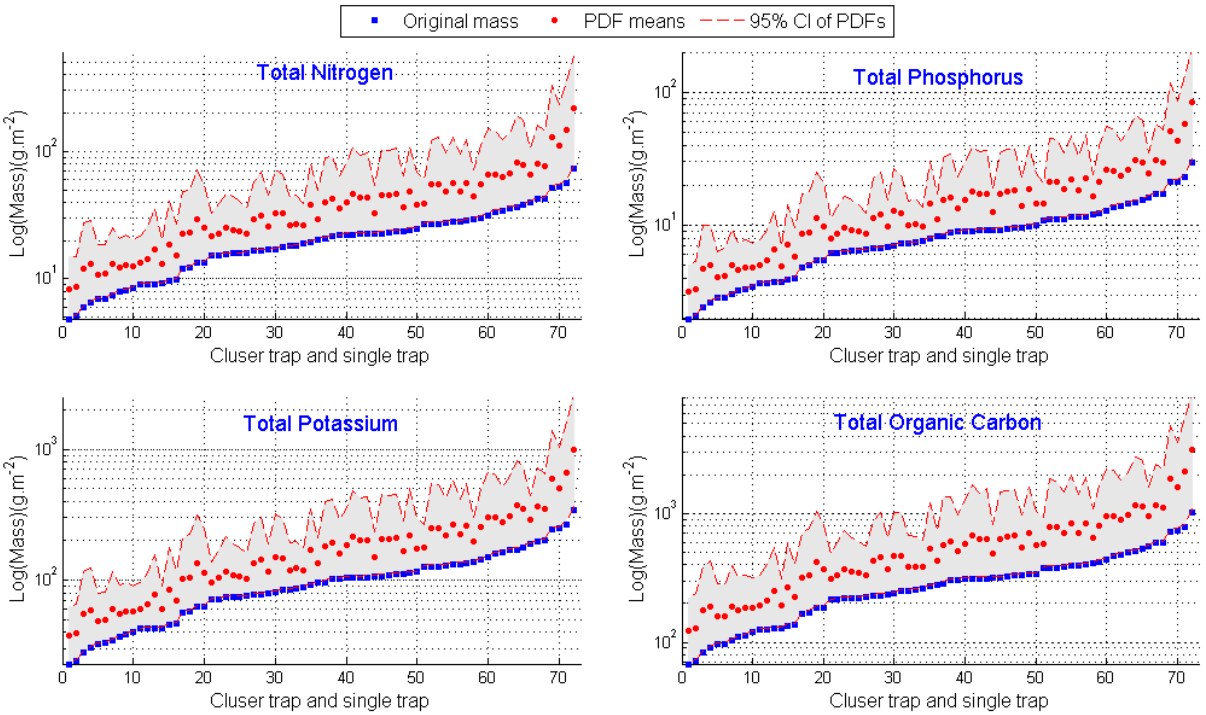

Figure 2.10: Mean (red dots) and confidence intervals (CI, red dash lines) of nutrient masses after wet-dry sampling correction and uncertainty analysis, compared to the original sampled masses.

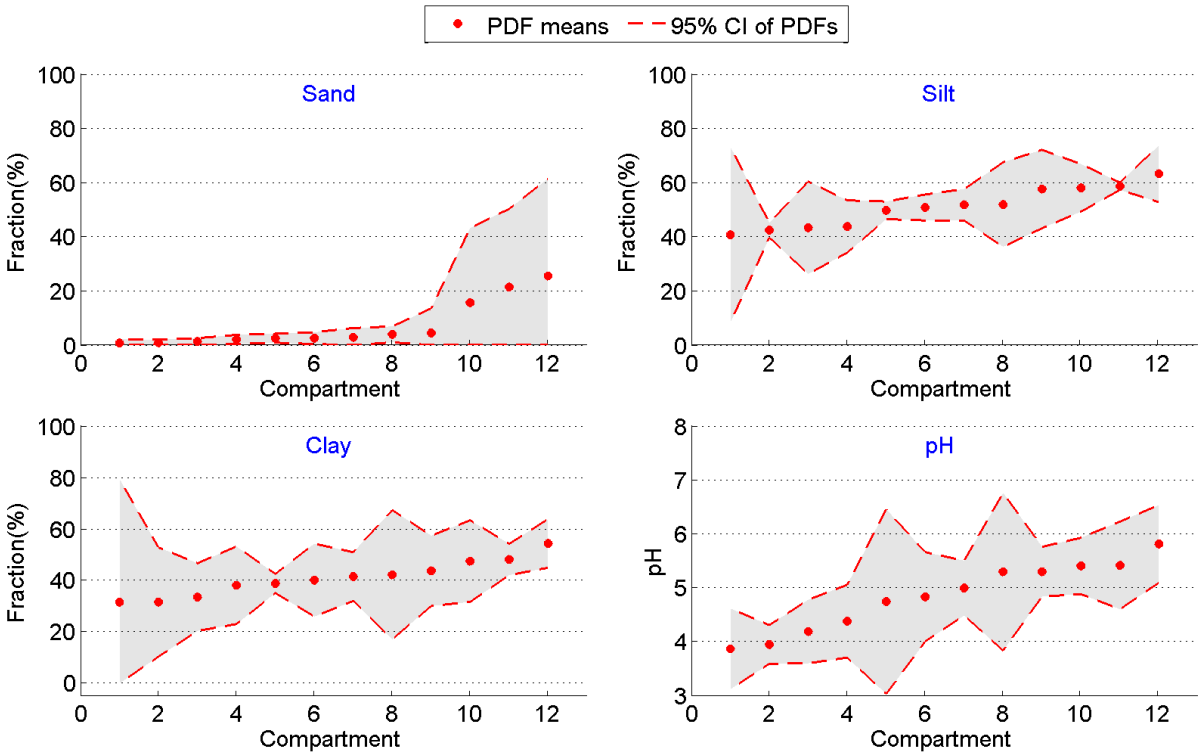

Figure 2.11: Mean (red dots) and confidence intervals (CI, red dash lines) of sand fraction, silt fraction, clay fraction and pH.

2.4.3 Sedimentation and nutrient deposition rates

For an assessment of the deposition rates we use the mean values from the uncertainty analysis. Across all study sites, the sedimentation rates varied from 2.2 $kg.m^{-2}.y^{-1}$ to 60.6 $kg.m^{-2}.y^{-1}$ in the mean, equivalent to 1.8 $mm.y^{-1}$ to 50.5 $mm.y^{-1}$. The mean rate equals 9.5 $mm.y^{-1}$ based on a dry bulk density of 1.2 $ton.m^{-3}$ (Xue, Z., 2010). The nutrient rates are proportional to the sedimentation rates. TOC has the highest rate: the maximum rate is close to 3110 $g.m^{-2}.y^{-1}$ and the mean rate is about 611 $g.m^{-2}.y^{-1}$. The mean rates of TN, TP and TK are 42 $g.m^{-2}.y^{-1}$, 16 $g.m^{-2}.y^{-1}$, and 192 $g.m^{-2}.y^{-1}$ respectively. Table 2.4 provides an overview of the sedimentation rates over all study sites and in low dike and high dike systems. Differentiating the results in low and high dike compartments, it can be shown that the maximum sediment and nutrient deposition in low dike compartments triples the maximum rate in high dike compartments (Table 2.4). Also the minimum values are more extreme in the low dike compartments. However, the average values are 11.6 $kg.m^{-2}.y^{-1}$ and 10.6 $kg.m^{-2}.y^{-1}$ in low and high dike system, respectively. This indicates that on average no significant difference between low and high dike systems could be observed, but the variability in deposition is considerably higher in the low dike compartments ($2.2 \div 60.6$ $kg.m^{-2}.y^{-1}$) compared to the high dikes ($4.7 \div 18.4$ $kg.m^{-2}.y^{-1}$). This is a consequence of the different hydraulic links between the channels and the floodplains of the different dike systems (Hung et al. [2012]). However, in the interpretation of these results the severity of the flood in 2011 has to be taken into account. The high flood peak and long inundation duration likely reduced the differences in floodplain inundation between the two dike systems.

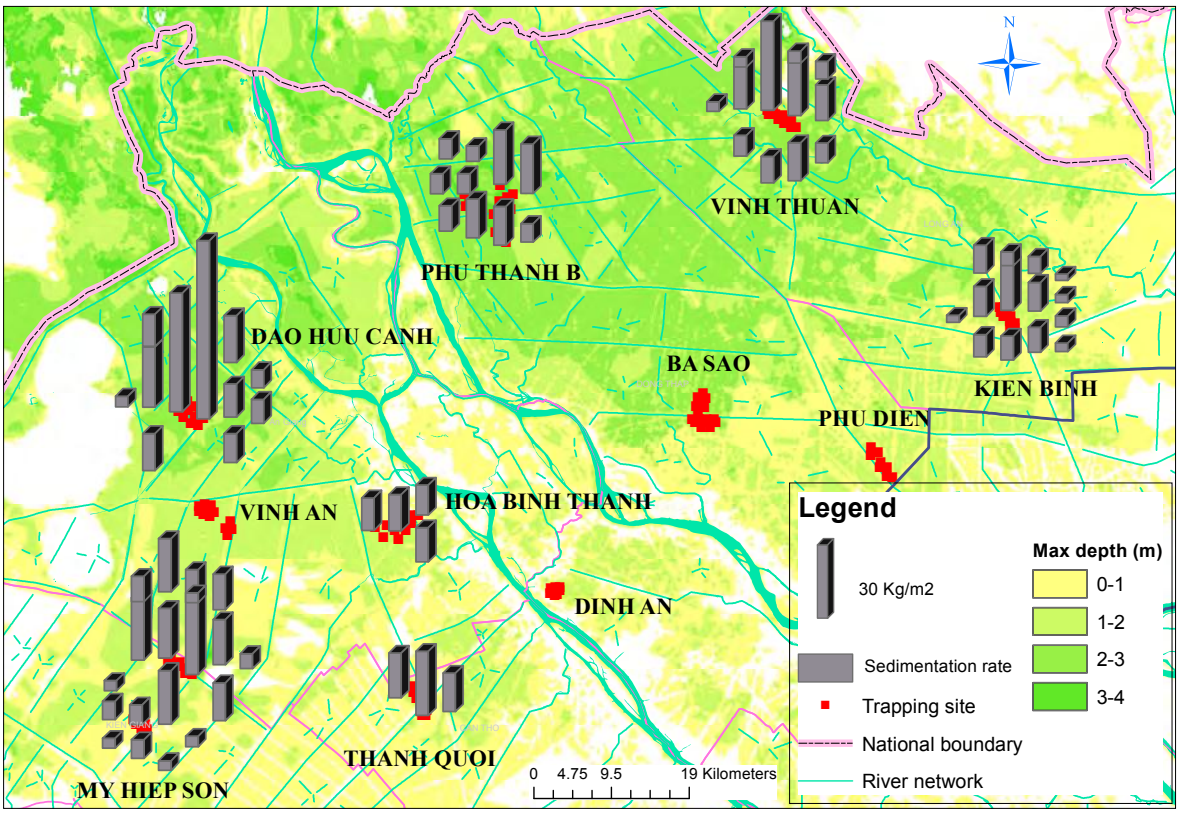

Figure 2.12: Mean sedimentation rate (grey columns) of all monitoring points.

Table 2.4: Mean, minimum and maximum values of sediment and nutrient deposition rates over all study sites, and separated for different spatial units: low dike, high dike, Plain of Reeds, Long Xuyen Quadrangle in flood 2011.

Spatial unit		Sediment ($kg.m^{-2}$)	Sediment ($mm.y^{-1}$)	TN	TP	TK	TOC	Sand	Silt	Clay	pH
					($g.m^{-2}$)				(%)		
	Min	2.2	1.8	8	3	38	122	0.8	40.7	31.4	3.9
Overall	Mean	11.4	9.5	42	16	192	611	7	50.9	40.8	4.8
	Max	60.6	50.5	216	84	990	3109	25.5	63.1	54.2	5.8
Low	Min	2.2	1.8	8	3	38	122	0.8	40.7	31.4	4
dike	Mean	11.6	9.7	43	17	196	623	5.7	50.3	42.3	4.9
	Max	60.6	50.5	216	84	990	3109	21.4	58.5	54.2	5.8
High	Min	4.7	3.9	17	7	78	251	2.6	43.2	31.5	3.9
dike	Mean	10.6	8.9	40	15	180	575	10.8	52.7	36.1	4.7
	Max	18.4	15.3	68	26	309	978	25.5	63.1	43.6	5.4

The differences in grain size distribution between low and high dikes are little, although there is a slight tendency that the low dike compartments exhibit a higher overall variability (Table 2.4). This can be explained by the generally higher flow in the low dike compartments, which are hydraulically fully connected to the channels, whereas the flow in the high dike compartments is controlled and limited by the sluice gate capacities.

The low pH values in Table 2.4 can explained by the acid sulphate soils found in large parts of the VMD floodplains. The total acid soil area is 1.1 10^6 *ha* over total 1.8 10^6 *ha* in floodplain area, i.e. about 60% of the floodplains have acid soils (Soil map – MONRE[1]). Moreover, the extraordinary inundation in 2011 in combination with re-suspension processes might have caused a further reduction in pH in sediment samples.

In order to compare and interpret these figures a comparison with Yangtze River Delta is conducted (Table 2.5). The average suspended sediment concentration (SSC) in the MD and the Yangtze Delta is approximately identical in terms of maximum monthly SSC. The silt and clay grain fractions account for more than 95% with an average of about 40% clay. This is equivalent to published data of the Yangtze Delta (Table 2.5). The similarities between the Mekong and the Yangtze might me partially explained by their shared origin in the Tibetan plateau.

A comparison of floodplain sedimentation in these deltas is difficult as hardly any data are available. However, a comparison with the published sedimentation rate in the Yangtze River Delta shows that the average sedimentation rate in the MD is similar to the result in the Yangtze Delta, but showing a larger variability. This may be interpreted as an impact of the intensive fragmentation of floodplains in the MD, but may as well be an artefact of the data collection and interpretation.

[1]Ministry of Natural Resources and Environment of Vietnam.

Table 2.5: Sediment characteristics of the Mekong and Yangtze at their deltas.

River	Length/Area $km/10^3 km^2$	TDS/TSS $10^6 t.y^{-1}$	Average of max monthly SSC	Grain size *(%)*	Sedimentation $[cm.y^{-1}]$
Mekong	4800/800[(1)]	60/110(150)[(1)]	0.326 $kg.m^{-3}$ Tan Chau station	7% sand, 51% silt 42% clay	$0.18 \div 5.05$
Yangtze	6300/1800[(1)]	180/470[(1)]	0.292 $kg.m^{-3}$ [(2)] Xuliujing station	5% sand 40–45% clay, 40–60% silt [(3)]	1.4-2.5 [(4)]

[(1)] *Milliman, al et. (2011),* [(2)] *Shenliang .C (2003),* [(3)] *Liu J.P. (2006),* [(4)] *Yang S.L. (2003)*

2.4.4 Spatial variability of sedimentation

The spatial distribution of floodplain sedimentation is controlled by the channel and dike systems in the VMD. The channel system is classified as follows: The main channels are “large” channels conveying floods from Tien River and Hau River through the Delta and the associated dikes are typically combined with provincial roads (high dikes). The secondary channels are ”medium” channels branching from the main channels and creating compartments (high dikes or low dikes). Within these large compartments inner ”small” channels exist. These channels are used for agricultural transportation and drainage, and are accompanied by low dikes, if at all.

Normally, a compartment in the Mekong floodplains consists of a secondary ring channel accompanied with high dikes or low dikes, some inner channels with its banks, sluice gates, open culverts, and pumping stations. The flood water from the rivers flows into the channel network and is then redistributed into compartments through hydraulic structures for high dike systems or overflows into compartments in “high stage” in low dike systems (Hung et al. [2012]). The sediment movement into compartment includes advective transport with flow (primary transportation) and an additional but small dispersive component. This means that theoretically the low dike compartments potentially have a higher chance to receive a higher sedimentation than the high dike, as the flow into the compartment is less restricted and the flow velocity is higher on average. However, as this and a previous study (Hung et al. [2012]) indicate, a clear distinction of the floodplain sedimentation between the different dike systems cannot be found. The complex interplay of inundation dynamics, channel and dike systems, and the high number of hydraulic structures creates a differentiated sedimentation pattern without obvious correlations or patterns (Fig. 2.12).

A spatial interpolation of the derived sedimentation data is thus not performed over the whole VMD, but compartment-wise. Inverse Distance Weighting (IDW) interpolation was applied on the mean values. Fig. 2.13 shows exemplarily the Phu Thanh site. Both compartments are located in the center of a main channel ring with a lot of secondary channels and inner channels. The mean sedimentation rate with uncertainty bounds in the high dike O Bao 18 compartment of 14.6 $[9.0 \div 22.5]$ $kg.m^{-2}.y^{-1}$ is significant higher than that in the nearby low dike Phu Hoa compartment 6.3 $[4.9 \div 8.9]$ $kg.m^{-2}.y^{-1}$. Also the spatial variability within the compartment is in this case higher in the high dike compartment than in the low dike compartment. This seems to be contradictory to the postulated higher general variability in low dike compartments, but can be explained by the fact that locally, i.e. in a compartment,

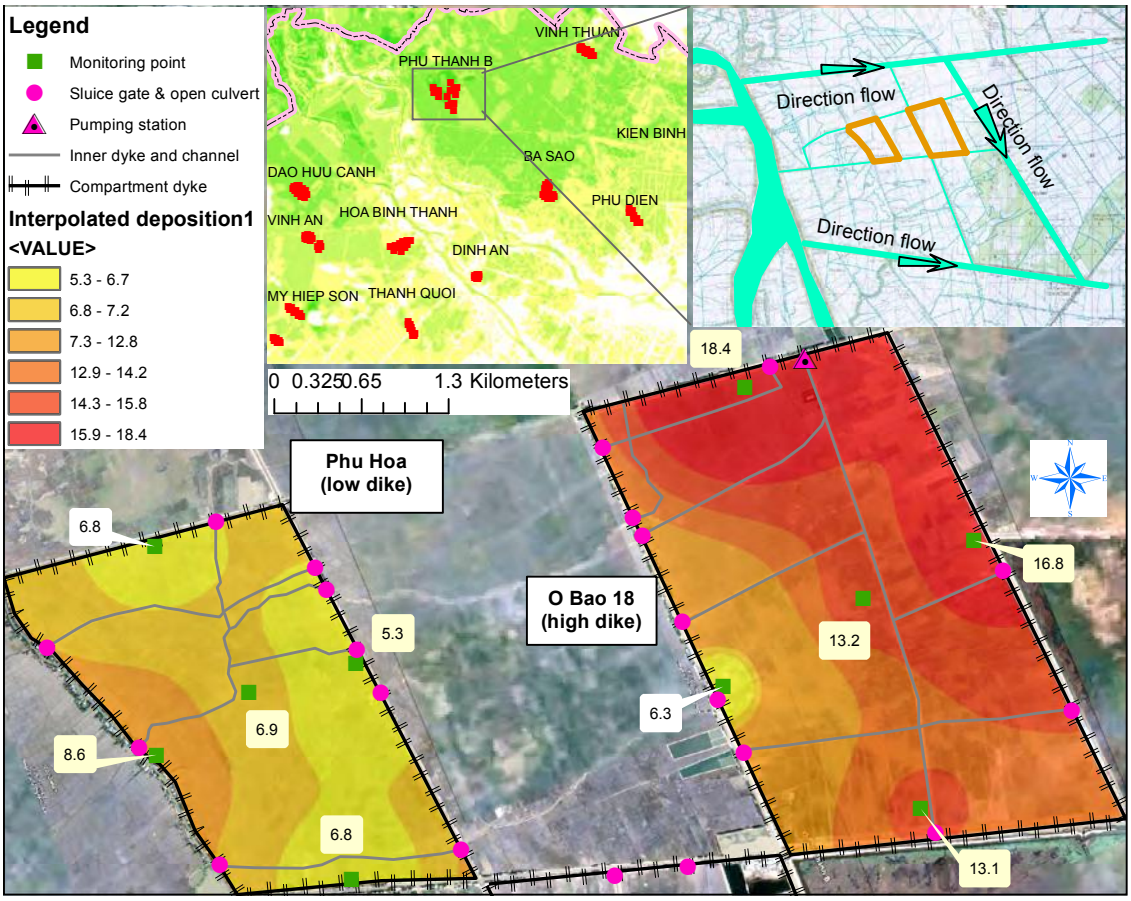

Figure 2.13: Spatial distribution of sedimentation in two nearby compartments in Phu Thanh B sites.

the spatial deposition in high dike compartments is influenced to a large extent by the position and operation of the sluice gates. From these results of these two compartments a slight trend towards lower deposition in the center of the floodplain between the main channels could be postulated, but as data from the surrounding compartments are missing, this cannot be corroborated.

A similar result can be found in the Kien Binh site (Fig. 2.14), where a high dike system in Khu Tram Bom compartment and a low dike in Bay Thuoc compartment were monitored. Both compartments are located next to a main channel, but have different sediment sources (inundation paths) that lead to completely different sedimentation patterns and values. The average sedimentation rate in Khu Tram Bom compartment (high dike) is 8.7 $kg.m^{-2}.y^{-1}$ with an associated uncertainty bound of [6.3 ÷ 12.5] $kg.m^{-2}.y^{-1}$ and much smaller in Bay Thuoc compartment (low dike) 2.6 [2.0 ÷ 3.5] $kg.m^{-2}.y^{-1}$. It can be seen, that higher sedimentation rates are closer to sediment sources, i.e. the sluice gates connecting the floodplain to the main and secondary channels.

Fig. 2.15 shows the interpolated deposition in My Hiep Son compartment. This shows contrary to the previous examples a high variability of sedimentation rates in a low dike compartment. The values of minimum and maximum rates are 3.3 [1.9÷7.5]$kg.m^{-2}.y^{-1}$ and 35.6 [17.1÷56.4] $kg.m^{-2}.y^{-1}$, respectively, compared to 16.1 [9.1÷26.6] $kg.m^{-2}.y^{-1}$, the average rate of this compartment. The CV is with a value of 0.5 in this compartment significantly higher than CVs in high dike compartments. This has very likely to be attributed to the

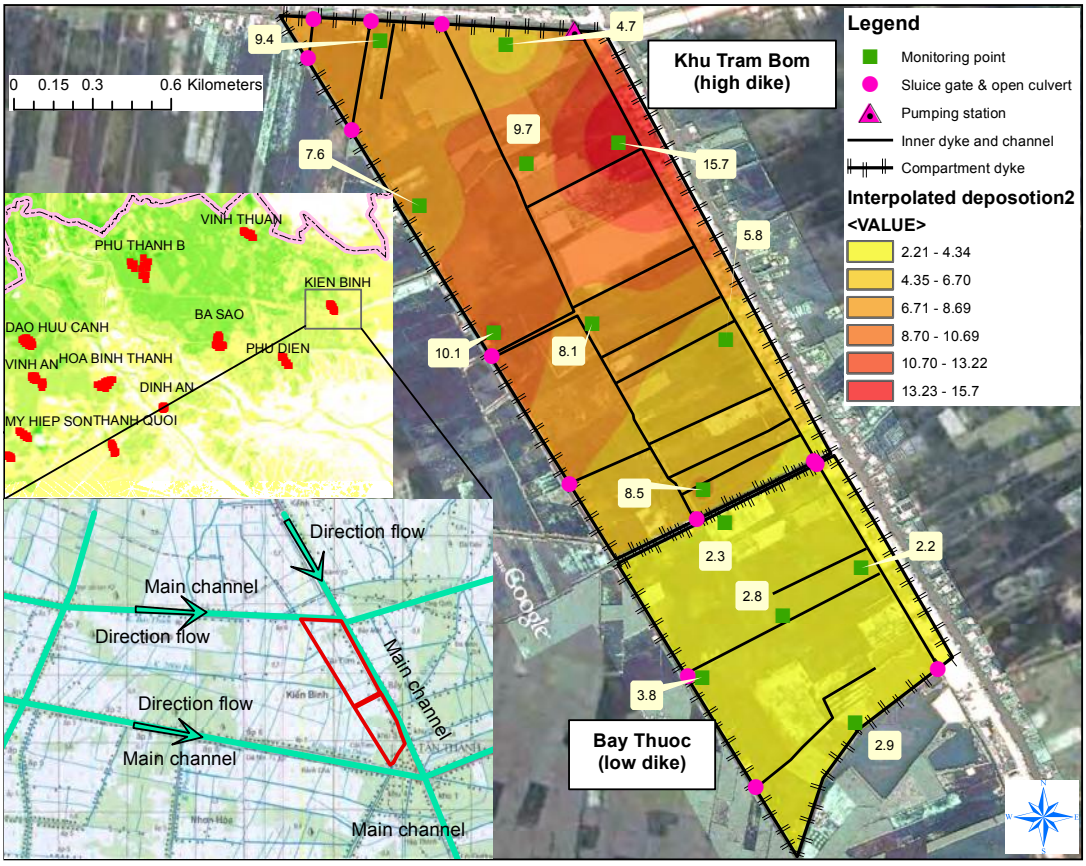

Figure 2.14: Spatial distribution of sedimentation in two adjacent compartments in Kien Binh site – Long An.

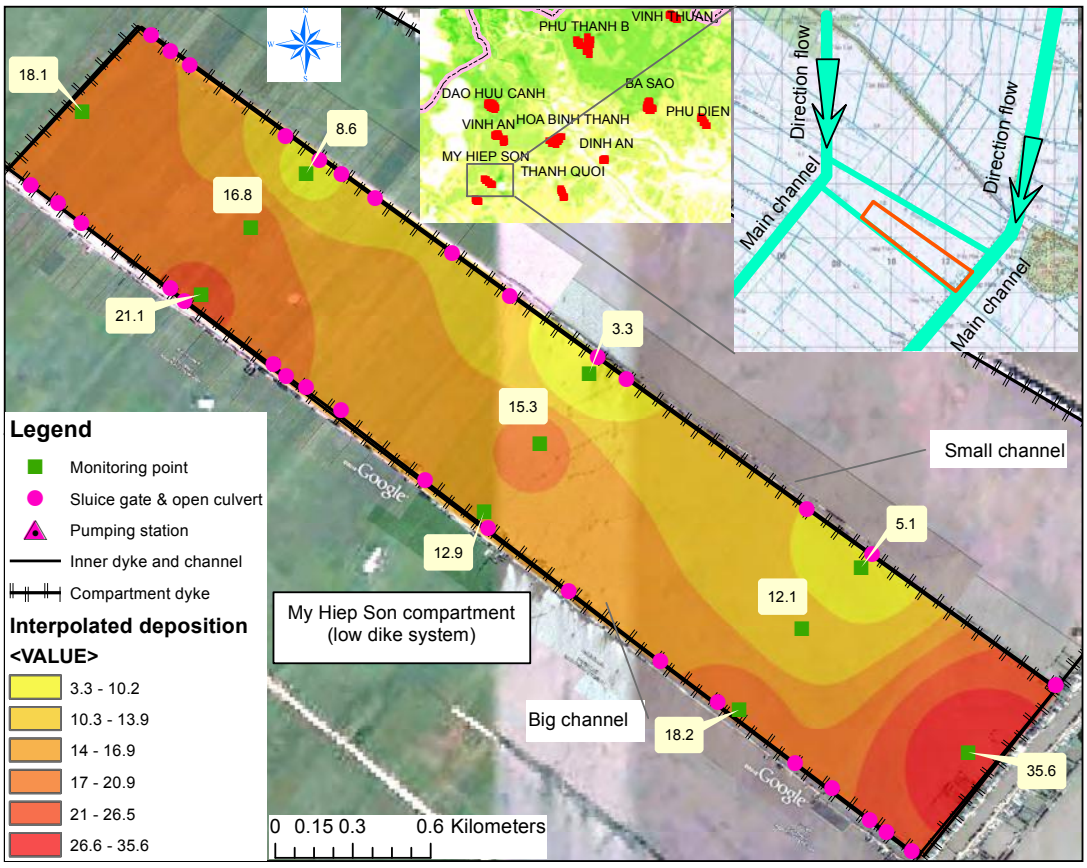

Figure 2.15: The typical pattern of high sedimentation variability in low dike compartments in My Hiep Son-Kien Giang.

Mean sedimentation	Whole VMD	Plain of Reeds	Longxuyen Quadrangle
Overall	11.4	9.1	14
Low dike	11.6	8.2	14
High dike	10.6	10.5	12

Table 2.6: Mean sedimentation values in different spatial units: low dike and high dike, Plain of Reeds/ Long Xuyen Quadrangle and whole VMD.

better hydraulic linkage to a main channel as compared to the previous examples.

Table 2.6 shows the mean values of sedimentation in different larger spatial units, i.e. regions of the VMD. In this analysis, the Long Xuyen Quadrangle receives a higher mean sediment deposition as the Plain of Reeds (cf. Fig. 2.1). However, the deposition within high dike compartments is on the mean comparable between the two regions, but the monitored low dike compartments receive considerably less sediments in the Plain of Reeds, explaining the differences in the overall deposition. Interestingly, if averaged over the whole study regions, the mean deposition in high and low dikes is again comparable. An interesting aspect of this analysis is that over the whole VMD the deposition in low dike compartments shows a higher variability between the compartments, i.e. varies higher between the regions of the VMD compared to the high dike compartments, but within compartments the spatial variability is higher in the high dike compartments. In summary, the results and examples presented above suggest that the fragmentation of the floodplains by the channel and dike systems destroyed the natural consistency and continuity of the floodplains in the Mekong Delta not only hydraulically, but also in terms of floodplain sedimentation.

2.5 Conclusions

This study proposes a procedure to monitor quantity and spatial variability of sediment and associated nutrient deposition in large and complex river floodplains including an uncertainty analysis. The uncertainty estimation consists of the (1) trap installation in clusters to quantify the deposition sampling uncertainty, (2) trap retrieval test to quantify losses by sample collection from inundated floodplains, and (3) a Monte Carlo framework for estimating uncertainty bounds from these uncertainty sources.

This methodology is applied in a large scale study in the Vietnamese Mekong Delta. The mean sediment deposition 11.4 $kg.m^{-2}$ which is equivalent to 9.5 $mm.y^{-1}$. This figure is comparable to published values for the Yangtze Delta, which has the same geographical origin as the Mekong. The related mean deposition of nutrients is 42 $g.m^{-2}$ Total Nitrogen, 16 $g.m^{-2}$ Total Phosphor, 192 $g.m^{-2}$ Total Potassium and 611$g.m^{-2}$ Total Organic Carbon. The sediments are constituted mainly by silt and clay, with little and only sporadic sand proportions. The sediments are generally acidic with an overall mean value of pH = 4.8.

The derived 95% uncertainty bounds of the sediment deposition mass range from -61% to +129% of the mean values for the entire dataset. The nutrient deposition uncertainty is slightly larger, as it directly depends on the sedimentation mass, but the determination of the nutrient content adds another uncertainty source. The uncertainties associated to grains

sizes and pH are considerably smaller, as they are hardly affected by uncertainties in deposition mass. In addition these properties generally do not show a large spatial variation in contrast to the sediment and nutrient deposition. The sand fraction is the only exception in this respect. This finding can be attributed to the fact that the sand fraction in floodplain deposits is generally low and highly influenced by local relocation processes. The sediment source, i.e. the suspended sediment in the Mekong Delta, contains only a very small sand fraction.

The main uncertainty sources are the trap retrieval from still inundated floodplains and likely human interference on the floodplains and floodplain inundation. While the sediment retrieval uncertainties are systematic and quantifiable, the variability caused by human interference and small scale differences in deposition and re-suspension is an uncertainty source that is difficult to attribute to distinct factors. Human interference ranges from direct impact on the sedimentation, by e.g. disturbances, by fishing on the floodplains with nets, to indirect causes by regulating floodplain inundation by sluice gate control and operation of pumps. For the monitoring of floodplain inundation local actions to restrict fishing activities could help, although this is almost impossible to enforce.

Mean sediment deposition values are highly variable, both for the whole set of monitoring points and among the different compartments. The variability among the compartments cannot be attributed to the dike system (low crop protection dikes or high flood protection dikes), as the differences in mean deposition is negligible. However, the mean deposition in low dike compartments showed a higher spatial variability compared to the high dike compartments if analyzed over the whole Vietnamese Mekong Delta, indicating the normalizing influence of the controlled floodplain inundation in the high dike compartments. In contrast to these findings, the spatial variability within individual compartments tends to be higher in high dike compartments, as the sediment source as well as the flow in the compartments are controlled by the location and operation of the sluice gates. Both source and flow can be assumed to be more homogeneous within low dike compartments leading to less spatial variability of in-department deposition. A noticeable influence on floodplain deposition seems to be the distance of the floodplain compartments to the main channels and the location and number of sluice gates. This corresponds to the findings of Hung et al. [2014b] gained in a small test site in the Plain of Reeds of the Mekong Delta.

All findings have to be interpreted in combination with the extraordinary flood in the study year 2011, for which peak flow and duration were the second largest in the observation period of about 80 years. Hence, the observed sedimentation may not be representative for the typical flood situation in the Vietnamese Mekong Delta. We expect that during normal flood years the differences between the low and high dike systems are more pronounced. Therefore, a repetition of the measurement campaign would not only provide additional statistical significance to the presented results, but potentially also lead to a better understanding of the impact of the dike systems on floodplain sedimentation in the Vietnamese Mekong Delta by either corroborating or contrasting the presented results.

Because of the observed low spatial correlation of the floodplain sedimentation over the entire region, an interpolation of the point samples to a large scale floodplain sedimentation map

is not feasible. The derived data are lacking the required autocorrelation and meaningful variograms for geostatistical interpolation. Potentially, a large scale spatial estimation of floodplain deposition could be derived via remote sensing. Optical satellite products can quantify suspended sediment concentrations, from which the deposition could be inferred. The problem with this approach is the high cloud cover during the flood/monsoon period. Therefore, a spatial estimation of floodplain sedimentation has to rely on numerical simulation of the floodplain hydraulics and deposition processes, for which the derived data and uncertainty estimates can provide the essentially required calibration data. Consequently this will be the next step in our analysis of the floodplain sedimentation of the VMD.

In the light of the results and experiences gained in the presented study the following recommendations for floodplain sedimentation monitoring in the Vietnamese Mekong Delta can be derived: The number of monitoring points in the floodplain compartments should be defined according to the floodplain topography, number and location of flood control structures and the presented sedimentation patterns in different floodplains. In rectangular small compartments ($< 100\ ha$) with one sluice gates in each side at least 5 monitoring points in 4 sides and in the center of the compartment should be placed to capture the general sedimentation pattern. In larger compartments ($> 100\ ha$) with several sluice gates in each side the minimal number of monitor points should be proportional to the number of main sluice gates and the compartment area. As the fishing activity on the floodplains proved to be a major threat for the monitoring, negotiations and corporation with not only the land owner but also the local community is essential to protect installed traps.

Chapter 3 Large-scale suspended sediment transport and sediment deposition in the Mekong Delta

Abstract

Sediment dynamics plays a major role in the agricultural and fishery productivity of the Mekong Delta. However, the understanding of sediment dynamics the delta, one of the most complex river deltas in the world, is very limited. This is a consequence of its large extent, the intricate system of rivers, channels and floodplains, and the scarcity of observations. This study quantifies, for the first time, the suspended sediment transport and sediment-nutrient deposition in the whole Mekong Delta. To this end, a quasi-2D hydrodynamic model is combined with a cohesive sediment transport model. The combined model is calibrated using six objective functions to represent the different aspects of the hydraulic and sediment transport components. The model is calibrated for the extreme flood season in 2011 and shows good performance for the two validation years with very different flood characteristics. It is shown how sediment transport and sediment deposition vary is differentiated from Kratie at the entrance of the Delta on its way to the coast. The main factors influencing the spatial sediment dynamics are the setup of river and channel system, channels and dike-rings, the sluice gate operations, the magnitude of the floods, and tidal influences. The superposition of these factors leads to high spatial variability of sediment transport, in particular in the Vietnamese floodplains. Depending on the flood magnitude, annual sediment loads reaching the coast vary from 48% to 60% of the sediment load at Kratie. Deposited sediment varies from 19% to 23% of the annual load at Kratie in Cambodian floodplains, and from 1% to 6% in the compartmented and diked floodplains in Vietnam. Associated annual deposited nutrients (N, P, K), which are associated to the sediment deposition, provide on average more than 50% of typically applied mineral fertilizers typically applied for rice crops in non-flooded ring dike floodplains in Vietnam. Through the quantification of sediment and related nutrient input the presented study provides a quantitative basis for estimating the benefits of annual Mekong floods for agriculture and fishery, and is an important information with regard to the assessment of the impacts of deltaic subsidence and climate change related sea level rise on delta morphology.

3.1 Introduction

The Mekong Delta (MD) is critical to the livelihoods and food security of millions of people in Vietnam and Cambodia. It is known as the "rice bowl" of South East Asia and one of the world's most productive fisheries. This is a consequence of huge floodplains and wetlands, high local flow variability and the high sediment-nutrient load of the Mekong. However, the

Mekong is facing sediment starvation caused by the massive development of hydropower dams (Lu and Siew [2006] , Fu and He [2007], Fu et al. [2007], Kummu and Varis [2007], Kummu et al. [2010], Walling [2008], Gupta et al. [2012], Liu and He [2012], and Liu et al. [2013]). The dams planned or already under construction along the main stem of the Mekong in the middle Mekong basin might alter the sediment regime of the MD dramatically. Kummu et al. [2010] estrimated that hydropower reservoirs could trap 67% of the sediment reaching the Mekong Delta compared to the status quo, in case all the planned dams are built. In a more recent study Kondolf et al. [2014] estimated that in case all planned dams are built 96% of the historical sediment load of the pre-dam period would be trapped. Moreover, the MD is sinking due to human activities (Ericson et al. [2006], Syvitski and Saito [2007], Syvitski et al. [2009], Syvitski and Higgins [2012]). Taking into account the future reduction in sediment load of the Mekong and expected sea level rise, effective subsidence rates of 6 $mm.y^{-1}$ have been estimated (Syvitski et al. [2009]). Understanding and quantifying the sediment and associated nutrient transport and deposition are crucial for the economy of the MD. This knowledge would enable an estimation of the benefits of the annual floods, supplying sediment and nutrients for fisheries and a natural fertilization of the agriculturally used floodplains. It would provide a quantitative base for the ongoing debate on the sustainability of the increasing practice of totally blocking floodplain inundation in the Vietnamese part of the MD in favor of three cropping periods per year. Due to the lack of natural fertilization by floods, this cropping practice requires higher mineral fertilizer application (Ve [2009]). Further, it would allow assessing the contribution of sediment deposition to counteract deltaic subsidence and climate change related sea level rise.

So far, the understanding of sediment and nutrient transport and deposition in the MD is very limited. Regarding larger scale sediment transport and deposition only one study has been published using a combination of 1D, 2D and 3D hydrodynamic models (MRCS/WUP-FIN [2007]. However, the study was limited to the Plain of Reeds (PoR, the north-eastern part of the Vietnamese MD), and considered only the main rivers and channels. It also lacked quantitative measurement data of floodplain deposition for calibrating the model. On the plot scale, a few experimental studies targeting specific aspects exist. These include fine sediment dynamics in the Mekong estuaries (Wolanski et al. [1996]), fine sediment transport and deposition in the Long Xuyen Quadrangle (Thuyen et al. [2000]), sediment deposition and erosion in floodplains (Hung et al. [2014a], Hung et al. [2014b]), and sediment-nutrient deposition in floodplains (Vien et al. [2011], Manh et al. [2013]). None of the published studies provides a quantification of the spatial distribution of sediment transport and deposition for the whole MD, although Manh et al. [2013] sampled the floodplain deposition in 11 different floodplain compartments distributed all over the Northern part of the Vietnamese Mekong Delta. This study provided a first insight into the spatial variability of the floodplain deposition, but a total spatial picture could not be drawn due to the high spatial variability of the deposition and the complex channel network both prohibiting a spatial interpolation of the results.

The heterogeneous and heavily disturbed hydraulic system of the Mekong Delta poses, in combination with the large spatial extent, a particular challenge for the quantification of sediment transport and deposition. The Vietnamese part of the MD (VMD) consists of several thousand floodplain compartments with areas varying from approximately 50 to 500 ha.

While the Cambodian floodplains show a low level of human interference, the VMD floodplains are heavily modified. Typically, a floodplain compartment is enclosed by a ring dike which is surrounded by channels interconnected to a ring. Hydraulic structures (sluice gates, pumps) link the floodplains to the channels. The hydraulic connection between channels and floodplains in the VMD varies depending on dike level, flood magnitude and sluice gate and pump operations (Hung et al. [2012]), causing a very high variability of floodplain sedimentation (Manh et al. [2013]).

Recently, a quasi-2D hydrodynamic model of the whole MD has been developed by Dung et al. [2011a] using DHI Mike 11. This model provides an appropriate compromise between model complexity, spatial coverage and resolution, and computational demand. The model includes a 1D representation of the river and channel network and a quasi-2D representation of the VMD floodplains. The floodplains are represented as orthogonal wide and shallow cross sections separated from the channels by dikes and connected to the channels by control structures such as sluice gates. By this approach the floodplain compartments in the VMD are represented in two dimensions but calculated in 1D. The rather natural floodplains in Cambodia are represented with wide-extended river cross sections in the 1D model.

Given the research gaps identified above and the previous work, this study aims at a spatially distributed model based quantification of the floodplain deposition in the Mekong Delta. In order to quantify the sediment transport and deposition, this study builds on the work of Dung et al. [2011a] and couples the hydraulic model with a cohesive sediment transport model. The combined model is calibrated with daily water levels at 13 stations, daily discharges at 10 stations, inundation extent for several points in time, daily suspended sediment concentrations (SSC) at 2 river stations, SSC at 79 stations for 6 points in time, and annual cumulative sedimentation masses collected at 11 locations in the Vietnamese floodplains. Hence, a very comprehensive data set is used for model calibration encompassing main rivers, channels and floodplains. The model is applied to three flood events covering an extremely low flood (2010), an average flood (2009) and an extremely high flood (2011) (MRC [2011b]).

3.2 Study area

In this study the Mekong delta is defined as the basin area downstream of the gauging station Kratie in Cambodia. This is the first gauging station upstream of Kampong Cham, where bank overtopping initiates the large floodplain inundations on the left bank of the Mekong and the overland flood wave to the Vietnamese part of the delta (Fig. 1). Floods in the Mekong Delta are generated from the tenth-largest river discharge in the world (Gupta [2008]). The Mekong River drains an area of 795,000 km^2 from the eastern watershed of the Tibetan Plateau to the MD. The Mekong River has a length of about 4,909 km and passes through China, Myanmar, Lao PDR, Thailand, Cambodia and Vietnam before reaching the South China Sea. The annual flood pulse in response to the Western North-Pacific monsoon during the months of July to October is the key hydrological characteristic of the Mekong River. The start of flood season in the MD is defined when the mean annual discharge of 13,600 $m^3 s^{-1}$ at Kratie is exceeded (MRC [2007]). The long-term average of annual flood volume is 330 km^3 and with a mean annual flood duration of 137 days starting typically in July (MRC

[2011a]). Reported estimated annual sediment load of the Mekong varies between 50 and 160 *million tons* (Lu et al. [2014]: 50÷ 91 *million tons*; Milliman and Farnsworth [2011]: 110 *million tons*; Walling [2008]: 160 *million tons*). The annual dissolved sediment load was estimated to 60 *million tons* by Milliman and Farnsworth [2011].

In this work the MD is divided into the four subsystems in order to facilitate the discussion of flood hydraulics and sediment transport: (1) Cambodian Mekong Delta, (2) Tonle Sap, (3) Vietnamese Mekong Delta and (4) coastal area (Fig. 3.1, Fig. 3.7 right). In the following, the salient features of each subsystem are described.

The Cambodian Mekong Delta consists of all rivers and floodplains in Cambodia excluding Tonle Sap. This encompasses the Mekong River downstream of Kratie until the Mekong is divided into three branches at the Chatomuk junction near Phnom Penh, the Tonle Sap River diverting water north to the Tonle Sap Lake (TSL) in Cambodia, and two branches transporting water south to the VMD and the sea, namely the Bassac River (Hau River in Vietnam) and the Mekong River (Tien River in Vietnam). These floodplains with a total area of around 11,000 km^2 are in a comparative natural state, i.e. show a low level of human interference in terms of hydraulic structures and channels. During the flood season overbank flow from the Mekong and Bassac Rivers causes large scale inundations in these parts.

The Tonle Sap region includes the Tonle Sap Lake (TSL) and the Tonle Sap River. The flow into the TSL during the rising and high stage of the annual floods is reversed during the falling stage and the following dry season. Hence the TSL acts as a huge buffer retaining flood water and sediment during the flood season and increasing discharge of the Mekong during the dry season. The TSL stores up to 10% of the total wet season flow volume measured at Kratie, and reduces the maximum discharge of Kratie by 16% (MRC [2009]).

The subsystem Vietnamese Mekong Delta VMD starts at the Cambodian-Vietnamese border a few kilometers upstream of gauging stations Tan Chau and Chau Doc and extends to My Thuan and Can Tho at the Tien River and Hau River, respectively, with an area of about 19,500 km^2. The VMD is a highly complex river delta as a result of anthropogenic interference encompassing numerous channels, dikes, sluices gates and pumps. The total length of the channel network is about 91,000 km, resulting in a dike system that is approximately twice as long. 75% of the ≅10 *million* people in the VMD live in rural areas (GSO [2012]), whereas the rural residential areas are preferably distributed along the dike lines. Most of the transportation during the flood season happens on waterways, especially during high flood events. The main channels are directly connected to the Mekong and the Bassac River. Secondary channels distribute water from the main channels to floodplains and smaller channels. The floodplains are thus dissected into numerous, mostly rectangular compartments that are typically enclosed by dike rings of different heights.

The floodplains of the VMD are subdivided into three regions (Fig. 3.1): (1) the Long Xuyen Quadrangle (LXQ), an area of annually inundated floodplains bordering Cambodia and stretching west of the Hau River to the coast, (2) the Plains of Reeds (PoR), an area of annually inundated floodplains also bordering Cambodia but to the East of the Tien River, and (3) the area in between Tien River and Hau River (THA). The inundations in LXQ are mainly caused by the Hau River and to lesser extent by overland flow from the Cambodian

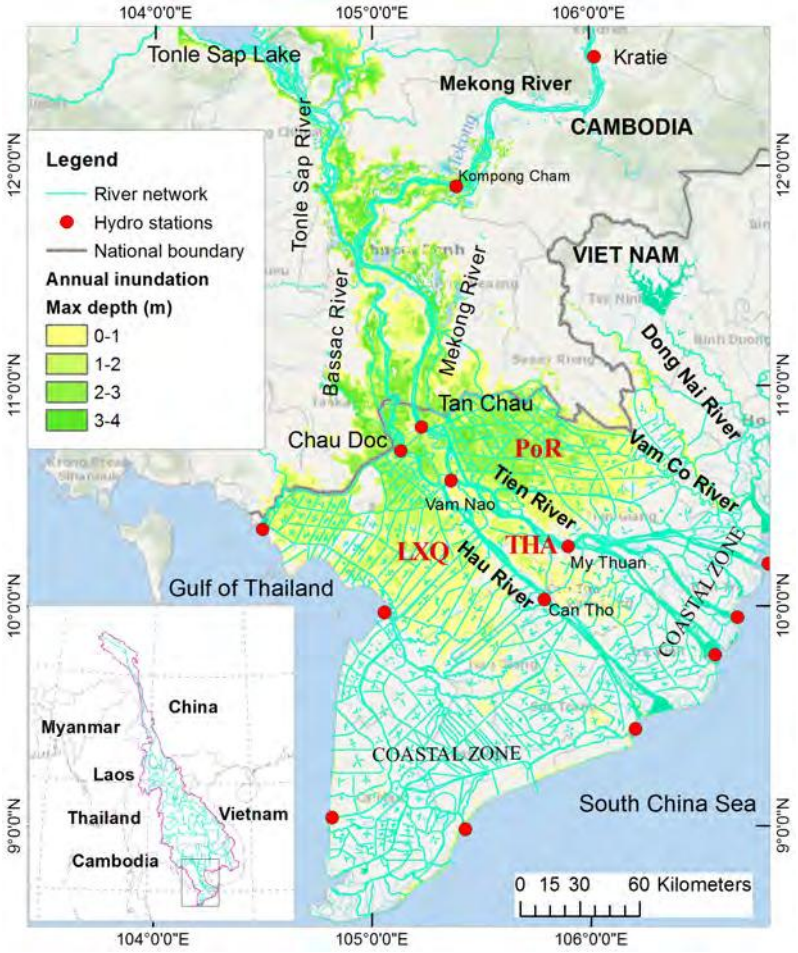

Figure 3.1: The Mekong Delta from Kratie to the coasts, including river networks, main discharge stations and inundated area (average over 10 years).

floodplains. In PoR, floods are caused by the Tien River and by significant overland flow from the Cambodian floodplains providing a second flood pulse, typically with some weeks lag-time to the peak flow of the Hau River.

Almost all floodplains in VMD are compartmented and used for agricultural production. The original floodplains are fragmented by the channel network and enclosed by ring dikes. The compartment areas range from 50 to 500 ha. They are linked to channels through sluice gates. The operation of these gates depends on flood magnitudes, ring dike heights and crop patterns. Ring dike systems are usually classified as low or high dike compartments. In high dike compartments the dike height is designed according to the maximum water level of the record flood in the year 2000. They are equipped with sluice gates and often with additional pumping systems. The flooding of these compartments is usually completely controlled. The total length of the high dike compartments increased rapidly in the past ten years. Remote sensing data show that the triple crop area, an indicator of high dike rings and complete flood control, is concentrated in LXQ and THA (Leinenkugel et al. [2013]). In low dike compartments the flood can be controlled during the rising and falling stages of the flood season only. Overbank flow occurs during high stage of the annual floods. The heights of low dike compartments vary depending on the experience and capacity of famers. The main purpose of these dikes is the support of the farming activities. Dirung the early

stages of the flood the dikes protects the second rice crop from flooding until it is harvested end of July/start of August. When the flood is receding, residual ponding water in these compartments is pumped out at the end of November but leaving enough water for planting the dry season rice crop. In years of extreme or long lasting floods, the water volume may exceed the pumping capacity and the dry season crop is not sown, as e.g. in 2011.

The coastal area subsystem covers the area downstream of My Thuan gauging station in Tien River and downstream of Can Tho station in Hau River to the sea. In this area tidal backwater effects occur throughout the year, and large scale floodplain inundation is rare.

When considering the flood and sediment processes in the MD, the characteristics of these subsystems and of the flood wave entering the MD need to be considered. Hung et al. [2012] divided the flood season into three periods. During the rising and falling stages the hydraulics in the MD are controlled by the river flow entering the Delta at Kratie, tidal backwater effects, and flow diversion from the Mekong into TSL (rising stage) and the reverse flow from TSL to the Mekong (falling stage). The flood stage is considered high when water level in the Mekong are high enough to counterbalance the water level of the TSL and the tidal backwater effects in the Northern part of the VMD (PoR, LXQ, THA) are diminished to a large extent. In addition, the hydraulic regime and sediment dynamics in VMD are strongly influenced by human interferences, and Hung et al. [2012] found a considerable influence of crop schedules and sluice gate operation on floodplain hydraulics.

In summary, the typical flood characteristics in the MD are: (1) buffering of the flood pulse by the Tonle Sap Lake, (2) a secondary flood pulse besides the river pulse caused by large-scale overbank flow over the Cambodian floodplains to the VMD, (3) large-scale, annually inundated areas (>20,000 km^2), (4) extended inundation periods ($3 \div 4$ months), (5) strong human interference in the hydraulic regime and the suspended sediment transport in the VMD.

3.3 Model setup and data

3.3.1 Suspended sediment characteristics in the Mekong Delta

The suspended sediment in the MD is fine-grained. The dispersed grain size was studied by Wolanski et al. [1996], who quantified the grain size by $d_{50} = 2.5 \div 3.9\mu m$ in the freshwater region of the estuary of the Hau River. MRC/DMS [2009] detected a $d_{50} = 3 \div 8\mu m$ in the Tonle Sap River and an even finer distribution in the Tonle Sap Lake. Manh et al. [2013] analyzed sediment deposition at 11 sites over a large area of the VMD and found that the deposited sediment grain size and nutrient content are uniformly distributed over the study sites, with a dispersed grain size distribution of 41% clay (grain size $< 2\mu m$) and 51% silt (grain size $2 \div 63\mu m$). Similarly, Hung et al. [2014b] found a median grain size $d_{50} = 10 \div 15\mu m$ of deposited sediment in over 12 sediment traps on floodplains of the Plain of Reeds, VMD. The reported dispersed grain sizes of $d_{50} = 2.5 \div 15\mu m$ are equivalent to free settling velocities of $W_0 = 1.10^{-5} \div 2.5.10^{-4} ms^{-1}$ using Stoke's law assuming an average measured water temperature $T \approx 30^0 C$, which is a representative mean value for the floodplains of the MD (Hung et al. [2014b]).

However, as the sediment is cohesive (Hung et al. [2014b]), the size of sediment flocs is of higher importance, particularly for the modeling. Wolanski et al. [1996] used image analysis for the measurement of flocs sizes, and observed a floc size of $d_{50} = 40\mu m$ of suspended sediment in the freshwater region of the estuary of the Hau River. Hung et al. [2014b] performed intensive measurements of SSC, sediment deposition, water temperature and water depth on the floodplains in the PoR and derived a floc size of $d_{50} = 35\mu m$ by inverse deposition and erosion modeling. MRC/DMS [2009] measured a floc size of $d_{50} = 29.4\mu m$ in the Tonle Sap River using image analysis. Free settling velocities of the reported floc size range of $d_{50} = 29.4 \div 40\mu m$ are equivalent to $W_0 = 9.10^{-4} \div 1.710^{-3} ms^{-1}$ based on Stoke's law (Hung et al. [2014b]).

Recorded maximum suspended sediment concentrations SSC in the MD are below 500 $mg.l^{-1}$. Given this maximum SSC a hindrance of sediment settling is unlikely, as it is much less than the SSC threshold for hindered sediment settling of $SSC > 10^4 mg.l^{-1}$ (Krone [1962]).

3.3.2 Description of the 1D hydrodynamic and sediment transport model

The Mike11 hydrodynamic model (HD) is based on one-dimensional hydrodynamic equations and solves the vertically integrated equations of conservation of continuity and momentum (the "Saint Venant" equations). The numerical solution is based on an implicit finite difference scheme developed by Abbott and Ionescu [1967].

The sediment model focuses on suspended sediment transport and deposition. The cohesive sediment transport module of Mike11 is based on the mass conservative 1D advection-dispersion (AD) equation:

$$\frac{\delta(A.SSC)}{\delta t} + \frac{\delta(Q.SSC)}{\delta x} - \frac{\delta}{\delta x}\left(AD\frac{\delta C}{\delta x}\right) = -A.K.SSC + C_2.q \tag{3.1}$$

Where SSC is the suspended sediment concentration, D is the dispersion coefficient, A the cross-sectional area, K the linear decay coefficient, C_2 the source/sink concentration, q the lateral inflow, x the space coordinate and t the time coordinate. The main assumptions are: (1) the considered substance is completely mixed over the cross sections implying that a source or sink have mix instantaneously over the cross section; (2) Fick's diffusion law applies, i.e. the dispersive transport is proportional to the concentration gradient.

The falling velocity of sediment flocs mainly depends on sediment concentration:

$$W_s = k.VC^m \; with \; k = \frac{W_0(1 - VC)^\gamma}{VC^m} \tag{3.2}$$

Leading to

$$W_s = W_o(1 - VC)^\gamma \tag{3.3}$$

Where W_s is the settling velocity of flocs $[m.s^{-1}]$, VC the volume concentration of suspended sediment $[m^3.m^{-3}]$, W_0 is the free settling velocity, and m, γ are empirical coefficients.

$W_0[m.s^{-1}]$, is the free settling velocity based on Stoke's law, which is determined by the sediment grain or floc size (d):

$$W_o = \frac{(s-1).g.d^2}{18\vartheta} \tag{3.4}$$

with ϑ = kinematic viscosity coefficient as a function of water temperature (for T = 30^o [C] it equals $\vartheta = 8.310^{-7}[m^2.s^{-1}]$ (Hung et al. [2014a]), s = specific gravity of sediment particles (s = 2.65), and g = acceleration of gravity (g = 9.81 $[m.s^{-2}]$).

The deposition process is described as:

$$\begin{aligned} S_D &= \frac{W_s.SSC}{h^*}(1-\frac{\tau_b}{\tau_{c,b}}) \; for \; \tau_{c,b} > \tau_b = \rho g \frac{V^2}{h^{\frac{1}{3}}(\frac{1}{n})^2} \\ &= 0 \qquad\qquad\qquad for \; \tau_{c,b} \leq \tau_b \end{aligned} \tag{3.5}$$

Where S_D is deposition rate $[kg.m^{-3}.s^{-1}]$ describing the source/sink term in the advection-dispersion equation. W_s is the floc settling velocity $[m.s^{-1}]$, SSC is suspended sediment concentration $[kg.m^{-3}]$, h^* is the average depth through which the particles settle $[m]$, τ_b and $\tau_{c,b}$ are bed shear stress and critical bed shear stress for deposition $[N.m^{-2}]$, ρ is the fluid density $[kg.m^{-3}]$, g the acceleration of gravity $[m.s^{-2}]$, n is the Manning number, h the flow depth $[m]$ and V the flow velocity $[m.s^{-1}]$.

The gradual erosion process is described as

$$\begin{aligned} S_E &= E_o(\frac{\tau_b}{\tau_{c,e}}-1)^{n_1} \; for \; \tau_{c,e} < \tau_b = \rho g \frac{V^2}{h^{\frac{1}{3}}(\frac{1}{n})^2} \\ &= 0 \qquad\qquad\qquad for \; \tau_{c,e} \geq \tau_b \end{aligned} \tag{3.6}$$

where S_E is the rate of erosion, E_o the erosion coefficient, $\tau_{c,e}$ the critical shear stress for erosion and n_1 is the erosion exponent.

The mass in grid point j is given as:

$$M_j = vol_j.SSC_j \tag{3.7}$$

Where M is the mass at given time at given grid point j $[kg]$, SSC is suspended sediment concentration $[kg.m^{-3}]$ and vol is the volume of grid point j.

3.3.3 Hydrodynamic and sediment transport modelling

The quasi-2D hydrodynamic model developed by Dung et al. [2011a] is applied to simulate flood propagation and inundation in the MD from Kratie to the coast including Tonle Sap Lake. Fig. 3.2 shows the river network of the hydrodynamic model of the MD, and the quasi-2D representation of the floodplain compartments is illustrated. A floodplain is enclosed by main and/or secondary channels. The floodplain itself is represented by 'virtual' channels with wide cross sections extracted from the Shuttle Radar Topography Mission (SRTM) DEM. Defining four virtual intersecting channels per compartment permits a quasi-2D simulation of the floodplain. The cross section width of each virtual channel is defined in such a way that the compartment area is preserved. Details can be found in Dung et al. [2011a].

The crest levels of the dikes are modeled as sill levels of sluice gates in each floodplain com-

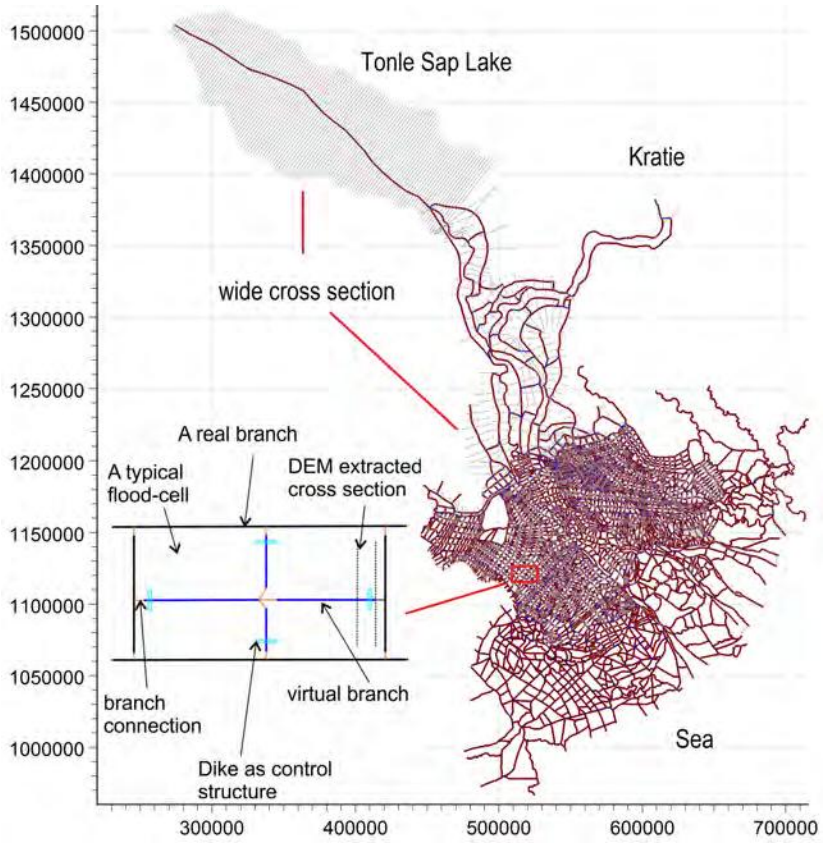

Figure 3.2: Model river network and quasi-2D concept for a typical floodplain compartment in the VMD.

partment in the model. The width of the sluice gates in the model is either the width of sluice gates actually present for high dike compartments, or 50 m for low dikes modeling dike overflow. In the latter case the dike crest levels define the sill levels of the control structures. Data about dikes and control structures were collected by Dung et al. [2011a] from different local and regional authorities.

The calibration of Dung et al. [2011a] revealed systematic errors in the dike crest levels implemented in the model, probably caused by different vertical reference values of the collected dike data. Thus the model dike heights are updated based on an analysis of water masks from satellite images (Kuenzer et al. [2013]) combined with maximum simulated water levels from the hydraulic model (Dung et al. [2011a]). The dike levels of floodplain compartments are corrected by comparing the maximum simulated water levels the with maximum observed flood extents for three flood seasons: the average flood of 2009, the exceptionally low flood of 2010 and the extreme flood 2011.

In the MD only a small number of the sluice gates have real radial or vertical gates, whereas most of the sluice gates are operated by movable high sills using sandbags. The opening time is decided by the land owner depending on the rice crop schedule and the flood magnitude. In the model the operation of real sluice gates is controlled by the water level of the incoming flow and/or a fixed schedule. Data on the operation of these sluice gates was collected from authorities by Dung et al. [2011a]. The remaining artificial sluice gates modeling dike are defined as broad crested weirs,for which available or estimated dike levels were used to define sill levels in the model. Pumping stations are excluded in the model because the pumps are

operated at the end of the flooding period only in order to drain the compartments for the new crop. In this period, water levels and SSC is very low and the effects of pumping can be neglected for the estimation of floodplain deposition.

The model contains 2,340 hydraulic structures consisting of weirs, culverts and sluice gates. This complexity is a challenge for the numerical stability of the cohesive sediment transport model. Hence, the model network of Dung et al. [2011a] is slightly modified to satisfy stability conditions based on the Courant ($Cr = v\frac{\Delta t}{\Delta x} < 2$) and Péclet number ($Pe = v\frac{\Delta x}{D} > 2$). Numerical stability can be achieved by increasing the distance between the computational points Δx to satisfy both Courant and Péclet stability criteria, and by decreasing the time step Δt to satisfy the Courant criterion. Hence, the cross section spacing is increased whereby the important elements influencing the hydraulic conditions (e.g. topography, location of hydraulic structures) are taken into account. A minimum Δx of $700m$ and a time step Δt of the sediment transport model of $3 \div 5$ minutes are chosen. This setup results in model run times of $7 \div 12$ hours for one flood season. This model setup guarantees, numerical stability of the hydrodynamic and sediment transport model and automatic model calibration is thus feasible.

The sediment dynamics in the floodplains can be strongly influenced by local re-suspension due to human activities like net-fishing (Manh et al. [2013]). Thus measured sediment deposition in floodplains includes not only new watershed sediment from upstream but also locally eroded or re-distributed sediment. However, in order to quantify the net delivery of sediments from the watershed to the delta, the disturbances from human activities are ignored in the modeling. This is achieved by setting a very high critical shear stress for erosion in the model ensuring that no erosion occurs in the modeling. This approach is thus not aiming at a closest representation of reality, respectively the measured deposition data, which is almost impossible due to the large interference of human activities on local sedimentation processes. This study rather aims at the quantification of new annual sediment and nutrient input delivered from the Mekong Basin, and its spatial distribution in the Mekong Delta.

3.3.4 Model parameterization

The model parameters to be defined for the HD model are the roughness coefficient (n) and for the AD model the longitudinal dispersion coefficient (D), the free settling velocity (W_0) and the critical shear stress for deposition (τ_d) for the AD model. In order to reduce the degrees of freedom in the parameter estimation, the MD is divided into eleven parameter zones (Table 3.1). Within these zones the calibration parameters are assumed to be constant. This zonation is a refinement of the zones used by (Dung et al. [2011a]), taking into account the different characteristics of main rivers, channels and floodplains in terms of hydrodynamics and sediment transport. In order to reduce the complexity of the calibration even further, not all calibration parameters are calibrated in all eleven zones. Depending on parameter sensitivity and flow characteristics, some parameters are fixed in some zones based on region-specific literature values (Table 3.1).

The Manning roughness coefficient n is calibrated in ten zones. The range of n in the calibration is set to $0.016 \div 0.10$. In the coastal zone, where the flow is governed by ocean tides, n is set to 0.016 (Chow [1959]). The longitudinal dispersion coefficient D controls the dispersive

sediment transport. It represents the effect of the non-uniform flow velocity distribution on suspended sediment concentration. The dispersion coefficient is determined as a function of the mean flow velocity: $D = a|V|^b$ with flow velocity V and coefficients a, b. Model sensitivity runs showed that the suspended sediment moving with the velocity of water (advection) is orders of magnitude higher than the spreading due to non-homogeneous velocity distribution (dispersion). Thus, to reduce to complexity of the calibration, we fix $b = 1$ for the whole MD, i.e. assume a linear dependency of D on V, and calibrate a values for the areas with high variability of flow velocity (channels in the VMD and coastal zone, Table 3.1). The a values in other areas are fixed based on equivalent mean flow velocities and dispersion coefficients of 81 measurements in 30 US rivers (Kashefipour and Falconer [2002]).

Table 3.1: The calibration parameters and the calibration zones: Manning roughness coefficient n, dispersion factor a, critical deposition shear stress $\tau_{c,b}$ $[N.m^{-2}]$ and free settling velocity W_0 $[m.s^{-1}]$. Least Euclidian distance Pareto-optimal parameters (O) and fixed parameters (F).

Zone	n	a	$\tau_{c,b}$	W_0	Description
1	0.032 O	400 F	0.025 F	$1.3.10^{-3}$ F	Mekong River: Kratie to Phnom Penh
2	0.031 O	500 F	0.025 F	$1.3.10^{-3}$ F	Mekong River: Phnom Penh to border
3	0.036 O	50 F	0.025 F	1.10^{-4} O	Cambodian floodplains
4	0.030 O	500 F	0.025 F	$1.3.10^{-3}$ F	Tien River: Border to My Thuan
5	0.026 O	700 F	0.025 F	$1.3.10^{-3}$ F	Tien River: My Thuan to coast
6	0.027 O	500 F	0.025 F	$1.3.10^{-3}$ F	Hau River: Border to Can Tho
7	0.024 O	700 F	0.025 F	$1.3.10^{-3}$ F	Hau River: Can Tho to coast
8	0.034 O	335 O	0.021 O	1.10^{-4} O	VMD channels with Q $> 100\ m^3s^{-1}s$
9	0.025 O				VMD channels with Q $\leq 100\ m^3s^{-1}s$
10	0.018 O	50 F	0.190 O	8.10^{-4} O	VMD floodplains
11	0.016 F	831 O	0.025 F	$1.3.10^{-3}$ F	Coastal zones

The selection of fixed zones for τ_d or W_0 is based on a model sensitivity analysis. 300 Monte Carlo runs were performed with the AD model fixing the dispersion coefficient D and τ_d or W_0 to determine the sensitivity of W_0 and τ_d in each zone. In zones with low sensitivities of the parameters W_0 or τ_d, this parameter was fixed (mainly the large river branches, Table 3.1). In zones with high sensitivities W_0 or τ_d were calibrated (mainly the channels in the VMD and the floodplains, Table 3.1). The fixed value of the free settling velocity (W_0) was calculated using Eq. 3.4 based on measured sediment sizes reported in sect. 3.3.1. For this we used the average floc size determined for floodplains of the Mekong Delta of $d_{50} = 35\mu m$ by Hung et al. [2014b]. For calibrating W_0 we used an extended range of reported dispersed and flocculated grain sizes, $d_{50} = 2.5 \div 80\mu m$, which evaluates to a calibration range of $W0 = 1.10^{-5} \div 7.10^{-3} ms^{-1}$.

Furthermore, Hung et al. [2014b] estimated the deposition shear stress $\tau_d = 0.021 \div 0.029 N.m^{-2}$ for simulating sediment deposition on VMD floodplains. The median value $\tau_d = 0.025 N.m^{-2}$ of that range is used for the fixed τ_d parameters, while an extended range of $\tau_d = 0.01 \div 0.2 N.m^{-2}$ is used for the model calibration. All the fixed and optimized parameter values (result of sect. 3.4) of τ_d and W_0 for the specific zones are listed in Table 3.1.

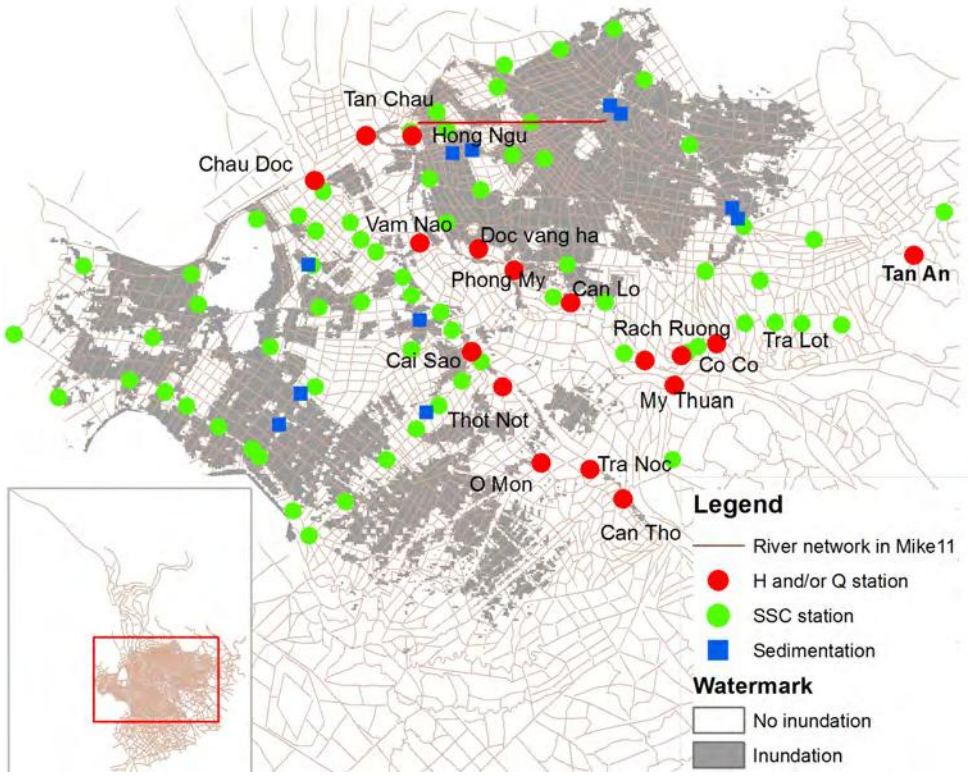

Figure 3.3: Locations of stations used for model calibration .

3.3.5 Measurement data

Measured data used for calibration and validation encompass water level, discharge, inundation extent, *SSC* in main rivers, *SSC* in channels, and floodplain sediment deposition (Fig 3.3. TThe first three variables are used to calibrate the hydrodynamic module, while the latter three variables are used for sediment transport calibration. The flood in 2011 serves as calibration period, because the floodplain deposition data were collected in 2011 only (Manh et al. [2013]).

Daily water level and discharge data were collected for 18 stations. They include 5 stations in the main rivers with both discharge and water level (Tan Chau, Chau Doc, Can Tho, My Thuan, Vam Nao) and additionally 7 water level stations and 5 discharge stations in main channels (Fig. 3.3). For evaluation of the spatial performance of the hydrodynamic model water masks derived from optical MODIS satellite images are used. The simulated inundation extents are calibrated against these inundation maps excluding cloud covered areas. For the calibration of the sediment transport *SSC* data from 79 locations were acquired from the Southern Regional Hydro-Meteorological Center of Vietnam (Fig. 3.3). These measurements were conducted manually every 15 days during the flood period by grab water samples and suspended sediment mass quantification by filtering and drying. The sediment deposition in the compartments of the VMD of the complete flood season 2011 was monitored by Manh et al. [2013], deploying a large number of sediment traps. This study provided mean cumulative sedimentation budgets including uncertainty ranges for 11 compartments distributed over PoR and LXQ.

In addition, Manh et al. [2013] determined the nutrient fractions of the sediment deposited in the sediment traps. Analyzed nutrients are Total Nitrogen (TN), Total Phosphorus (TP),

Total Potassium (TK) and Total Organic Carbon (TOC). The mass fractions of these nutrients varied only slightly in space. Thus the total nutrient content of the sediment can be estimated by an average fraction of 6.7%. This value defines the total deposition of TN, TP, TK, and TOC as fraction of deposited sediment, and is used to estimate the nutrient deposition in the floodplains of the VMD. The deposition of the different nutrients is derived by the following fractions: TN = 4.9 %, TP = 1.9%, TK = 22.5% and TOC = 70.7 % of the total nutrient deposition.

3.3.6 Definition of the sediment model boundary conditions

The simulation of sediment dynamics requires specifying SSC for the upper and lower model boundary at daily resolution. However, daily SSC data are available neither for the upper model boundary nor for the lower boundary. Hence, daily SSC are reconstructed using lower-resolution SSC data.

SSC time series for the lower boundaries at the river mouths were derived from remote sensing data. Water turbidity was derived from multi-sensor optical satellite scenes, and the turbidity was calibrated against in-situ SSC measurements (Heege et al. [2014]). This provided approximately weekly SSC values at the various river mouths. These values are linearly interpolated to daily SSC time series.

For the upper model boundary, daily SSC time series are derived from daily discharge and monthly or sporadic SSC data of the Mekong River at Kratie and neighboring gauging stations. In this analysis, however, one has to consider the reported low quality of the available SSC data (Walling [2005]). Before 2010 only monthly observations of water quality including total suspended solid (TSS) at Kratie are available. TSS was measured taking a single water sample at 0.8 m depth, which is a very rough and possibly strongly biased estimation of the average SSC over the whole river cross section. Recently, the Mekong River Commission (MRC) measured SSC as the average of 5 vertical profiles over the cross section at Kratie. The measurements were taken on 6 dates (every 2 months) in 2010 and on 20 dates from June to December 2011. The reconstruction of daily SSC at Kratie is based on this data set.

Most often, SSC is reconstructed using a sediment rating curve. The 26 measurements at Kratie are significantly correlated to discharge (*significance level* < 0.05) with a *Spearman's rank correlation coefficient* of $\rho = 0.79$. A sediment rating curve is constructed using a second order logarithm power function:

$$SSC_t^{Krat} = 10^{-494.02\ log(Q_t^{Kra})^{-4.52}+2.88} \tag{3.8}$$

In which SSC_t^{Krat} is $SSC[mg.l^{-1}]$ at time t at Kratie, Q_t^{Krat} is discharge $[m^3.s^{-1}]$ at time t at Kratie. The rating curve is shown in Fig. 3.4(A).

Another possibility to reconstruct SSC at Kratie is to correlate SSC at Kratie to SSC measurements at a nearby station with longer daily time series. Considering that the suspended sediment in the MD is very fine (Manh et al. [2013]) and that no significant lateral SSC input downstream of Kratie exists except the flow from TSL, the measured daily SSC at Tan Chau and Chau Doc in Vietnam (see locations in Fig. 3.1) might be used to reconstruct daily SSC

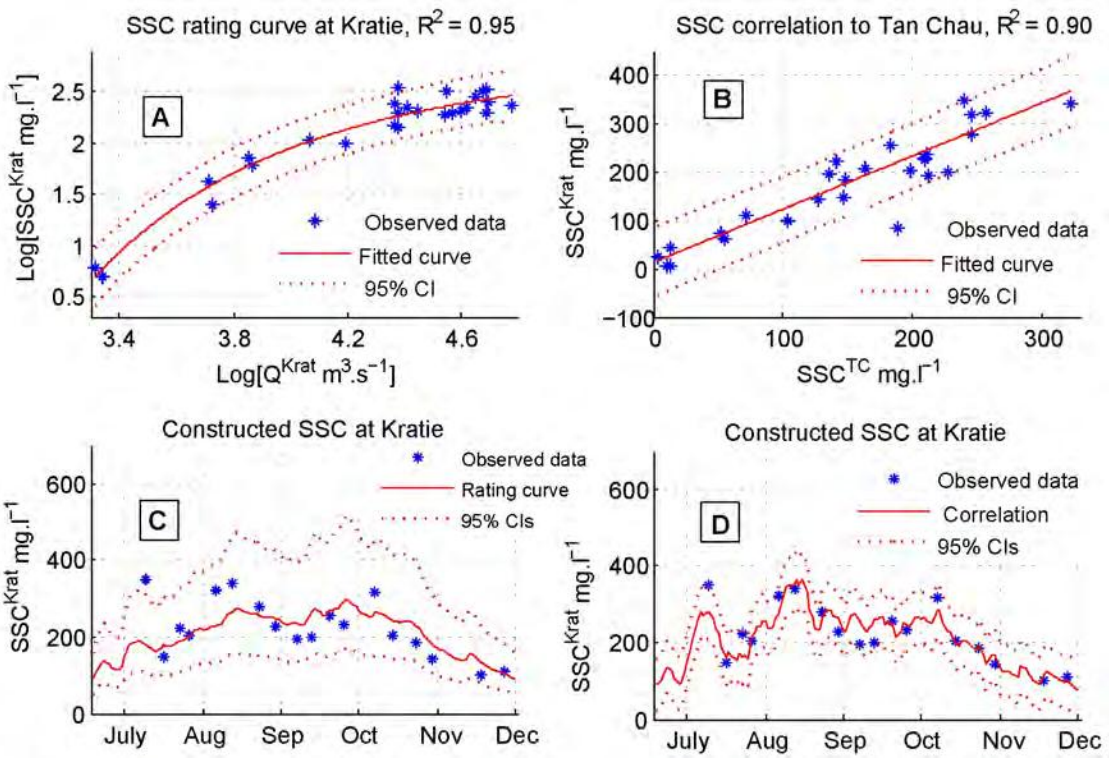

Figure 3.4: (A) Derived SSC for Kratie using sediment rating curve, (B) Derived SSC for Kratie using correlation to SSC at Tan Chau, (C) Comparison of sediment rating curve method with measured data in 2011, (D) Comparison of correlation method with measured data in 2011.

at Kratie. An analysis of the SSC data of Tan Chau and Chau Doc shows that, due to the hydraulic properties of the flow diversion of the Mekong into Mekong, Bassac and Tonle Sap Rivers, the flow into and from TSL influences mainly the SSC in the Bassac River at Chau Doc station (Fig 3.5 C-D). Hence, the daily SSC records of Tan Chau at the Mekong River are used as predictor for SSC in Kratie. The average travel time from Kratie to Tan Chau is $1 \div 2$ days, which is considered as lag in the correlation analysis. We found a close linear correlation ($R = 0.95$) of the measured SSC at Kratie to SCC at Tan Chau with a 1 *day lag*. The linear regression is given as:

$$SSC_t^{Krat} = 1.1\ SSC_{t+1}^{TC} + 12.77 \tag{3.9}$$

In which SSC_t^{Krat} is SSC $[mg.l^{-1}]$ at time t at Kratie, SSC_{t+1}^{TC} is SSC $[mg.l^{-1}]$ at time $t+1$ at Tan Chau. It is noteworthy that the same SSC measurement method is applied at both stations. Fig. 3.4(B) shows the regression of SSC_{t+1}^{TC} vs. SSC_t^{Krat} along with the confidence bounds. The derived SSC time series at Kratie based on these two methods yield very similar total sediment loads (106 *mil.ton* for the rating curve, and 107 *mil.ton* for the linear regression to Tan Chau), however, the SSC time series derived by the rating curve method is rather smooth and does not capture the SSC peaks existing in the measurements of Tan Chau. Hence, the rating curve method seems to suppress some fraction of SSC variability (Fig. 3.4C). Further, the regression based method provides smaller uncertainty bounds (Fig. 3.4D). Based on these two arguments, the regression based method is used to reconstruct daily SSC at the upper model boundary.

Table 3.2: Model performance: calibration, data (locations and number of points), results of calibration (year 2011) and of validation (years 2009 and 2010). The model performances measures are Nash–Sutcliffe efficiency (NSE), Flood Area Index (FAI), Root Mean Square Error (RSME).

Objectives	No. stations /No. data	Calibration (2011)			Validation (2009/2010)		
		NSE	FAI	RMSE	NSE	FAI	RMSE
H (m)	13/daily	0.84	-	-	0.74/nodata	-	-
Q ($m^3.s^{-1}$)	10/ daily	0.63	-	-	0.51/0.74	-	-
Inundation	571/17	-	0.46	-	-	0.39/0.36	-
River $SSC(mg.l^{-1})$	2/daily	0.52	-	-	$0.2^{(1)}$/0.78	-	-
Channel $SSC(mg.l^{-1})$	79/6	-	-	40	-	-	60/nodata
Sedimentation ($kg.m^{-2}y^{-1}$)	11/-	-	-	8.55 $[4.4 - 18.8]^{(2)}$	-	-	5.27/1.28 -

(1) in which NSE = 0.9 at Tan Chau and NSE = -0.56 at Chau Doc
(2) is the RMSE calculated against the mean 95% confidence interval of the measured deposition

3.4 Model calibration and validation

Model calibration and validation cover an extreme event (2011), a normal event (2009) and a low flood event (2010). 2011 was the most severe flood in recent times with a peak discharge in Kratie of 63,103 m^3s^{-1}, which is higher than the historically most damaging flood in 2000. In terms of flood volume, this event is the third largest in the observation period of 88 years (MRC [2011b]). In 2010, the lowest flood volume ever was recorded. The flood peak was 37,103 m^3s^{-1} only, and the flood lasted 6 weeks less than on average (MRC [2011a]). 2009 was an average flood both in terms of peak discharge and volume (MRC [2010b]). The calibration is performed for the extreme flood in 2011, because for this year the most comprehensive data set including floodplain deposition is available. The model is validated against the data of 2009 and 2010. Hence, the model is calibrated for an extreme flood and validated against a normal flood and an extremely low flood, thus providing information about the applicability of the model over the whole possible event magnitude scale.

3.4.1 Model calibration

To reduce the complexity of the calibration and to reduce runtimes, the hydrodynamic (HD) and sediment transport (AD) model components are run and calibrated individually. The HD simulation results are fed as input into the AD model. This separation has the advantage that different computational time steps can be used for the two components, dramatically reducing the required runtime. The automatic multi-objective calibration algorithm developed by Dung et al. [2011a] and based on the NSGA-II algorithm is applied. This enables an objective calibration considering different optimization objectives.

The HD model is calibrated with three objective functions: discharge in rivers and channels, water level in rivers and channels, and inundation extent. The first two objectives are quantified by the mean Nash-Sutcliffe efficiency (NSE) over all considered gauging stations. The spatial inundation performance is quantified by the Flood Area Index (FAI) comparing the simulated extent with the inundation extent derived from MODIS Terra images. Cloud covered areas in the MODIS images are considered as no-data in both observed and simulated

inundation. This multi-objective calibration results in a Pareto optimal set of HD model parameters. From this set we select the set with the least Euclidian distance to the optimal solution for the consequent AD calibration.

The AD model is calibrated with three objectives: SSC in main rivers, SSC in the channels and cumulative sedimentation rates on the floodplains. The Nash-Sutcliffe efficiency is used for the first objective, and the Root Mean Square Error (RSME) is used for the second and third objectives. RSME is selected because the measurements of channel SSC and sedimentation are not continuous in time. RMSE for cumulative sedimentation rate is calculated for the mean and, in addition, for the 95% confidence bounds of the observed deposition derived by Manh et al. [2013]. The AD model calibration results in another Pareto-optimal parameter set, from which the parameter set with the least Euclidian distance to the optimal solution is again selected. The calibration zones and calibrated parameters are given in Table. 3.1.

3.4.2 Model validation

For model validation, the flood seasons 2009 and 2010 are used. Since floodplain sedimentation data from Manh et al. [2013] is available for 2011 only, data from Hung et al. [2014b] are used for validating sediment deposition. Hung et al. [2014b] also used sediment traps to quantify sedimentation in floodplains in 2009 (2 locations) and in 2010 (1 location). This data set is much less comprehensive than the data set of Manh et al. [2013], and is limited to a small study site in the PoR. Further, less data for discharge, water level and SSC is available for 2010 compared to 2011 and 2009. This needs to be considered in the interpretation of the validation results.

The calibration and validation results are summarized in Table 3.2 and Fig. 3.5 (A-E). Overall, the validation shows similar results as the calibration. The validation performs better for discharge and SSC in 2010 which is likely due to much less overland flow, reducing the possible errors stemming from erroneous dike levels and floodplain representation. The agreement between simulation and measurements for SSC at Chau Doc is very low in 2009. This is probably the consequence of the poor quality of measured data at Chau Doc station in 2009 as illustrated in Fig. 3.5 C. Fig. 3.5 (A-D) show that modeled and measured discharge and SSC fit well in 2011 for Chau Doc and in 2009 and 2011 for Tan Chau, implying coherence between SSC and discharge. This coherence is frequently not given in 2009 for Chau Doc indicating data errors.

Overall, the model performance indices (Table 3.2) show a good agreement between simulation and measurements in terms of hydraulics and SSC. However, simulated sediment deposition match less the measured data (Fig. 3.5 E). This is further discussed in section 3.5.2.

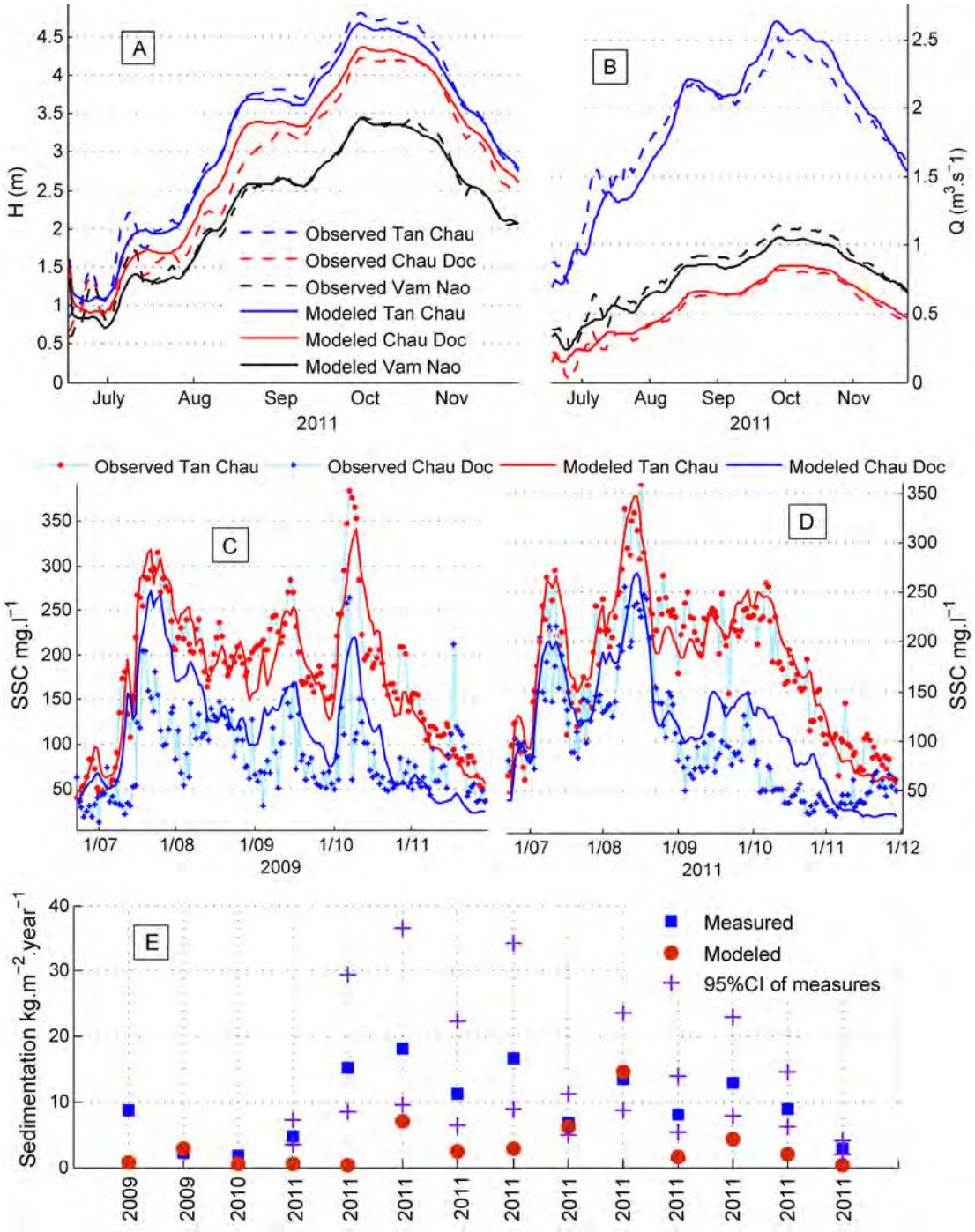

Figure 3.5: Model performance: Top panel: Comparison of measurements and simulation results at stations Tan Chau, Chau Doc and Vam Nao for 2011: [A] daily water levels, [B] daily discharges. Middle panel: Comparison of measurements and simulation results at Tan Chau and Chau Doc: [D] daily SSC for the calibration year 2011, and [C] for the validation year 2009. Bottom panel [E]: Comparison of measured and simulated sedimentation (2 locations in 2009, 1 location in 2010, 11 locations in 2011).

3.5 Results and discussion

Table 3.3 shows the distribution of flood volumes into hydraulic subsystems of the MD. In the extreme event of 2011 12% of the flood volume is distributed to the TSL and Cambodian floodplains, while during normal and low flood events (2009, 2010) this portion amounts to 6-8% only. The flood discharge in Tien River is about three times higher than in Hau river up to the Vam Nao junction connecting Tien and Hau river. After the Vam Nao juncion between discharge of the two main branches of the Mekong is almost equalized (Table 3.3). The hydraulic characteristics of the sub-systems of the MD are illustrated in Fig. 3.6. Tidal influence is found in the entire VMD up to Tan Chau and Chau Doc, while no influence is observable at the Mekong-Bassac diversion around Phnom Penh. The tidal magnitude at Chau Doc (Hau River) is higher than at Tan Chau (Tien River) due to the lower distance to the coast. However, the situation is reversed in the coastal zone, because the semidiurnal tide of the South China Sea mainly influencing the Tien branch is distinctively higher than the amplitude of the diurnal tide in the Gulf of Thailand, which dampens the tidal magnitude at the river mouth of the Hau river compared to the Tien river. The flow velocity in the main river from Kratie to the Vietnamese border is almost always greater than 1 $m.s^{-1}$, while in the VMD channels flow velocities less than 1 $m.s^{-1}$ can occur, particularly during high tide. Very low flow velocities can be observed under the ponding conditions of the TSL and the floodplain compartments in VMD. Typical VMD floodplain flow velocities are in the range of $0 \div 0.05 m.s^{-1}$. The flow velocities on the Cambodian floodplains vary between the river and VMD floodplain velocities, because the flow is less restricted by dikes (Fig. 3.6). Flow velocities in this area are thus governed by the distance to the main river and the topography. These highly differentiated flow patterns determine, in combination with the water depths, the sediment transport and deposition dynamics in the MD.

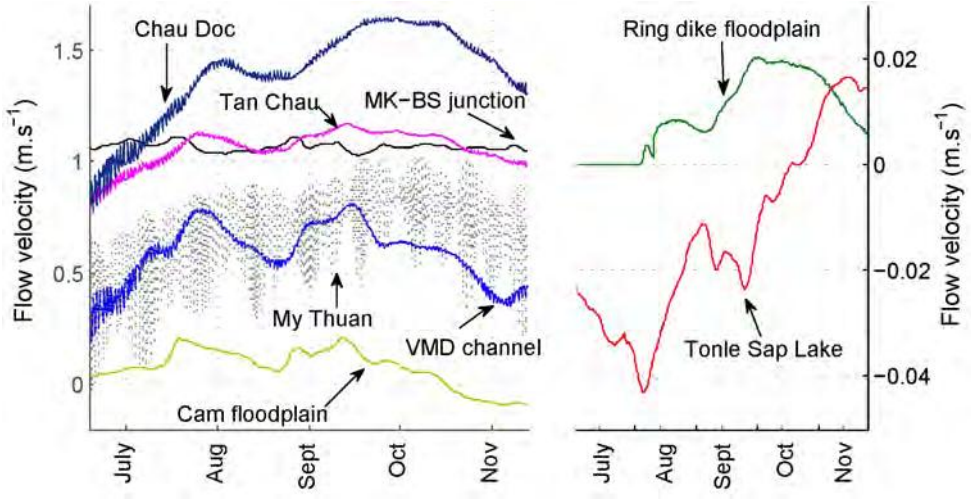

Figure 3.6: Flow velocity time series with 6-hour time steps of all the sub-systems in the MD in 2009. Flow velocities of some key location in the main rivers and in a VMD channel in the PoR (left, MK-BS = Mekong-Bassac), flow velocities in the center of the TSL and a floodplain compartment in the PoR (right).

3.5.1 Sediment transport in the Mekong Delta

In the following, the results regarding SSC transport are given for the subsystems introduced in section 3.2. The sediment fluxes of these subsystems are compared to the values at the upstream boundary Kratie. The results are summarized in Table 3.3, and the variation of the transported sediment from Kratie to the coast is exemplarily shown for 2009 in Fig. 3.7 (right).

Rather significant storage of water and sediment occurs in the subsystem 'Tonle Sap'. The flood volume stored in the TSL ranges from 6% to 12% compared to the flood volume at Kratie for the three simulated flood events. This is equivalent to $14 \div 55\ km^3$. These figures compare well with the average value of $41.8\ km^3$ in the TSL water balance analysis published by Kummu et al. [2014]. The total simulated sediment mass input to the TSL is 2.1 10^6 t in 2010, 5.2 10^6 t in 2009 and 10.6 10^6 t in 2011 (Table 3.3). Since the reverse flow of the TSL to the Bassac River at the end of the flood season has a low SSC, these figures are an estimate of the total sediment loss in the TSL. They compare well with the historical average value of 5.09 10^6 ton estimated by Kummu et al. [2008].

In the subsystem 'Cambodian Mekong Delta', 24÷27% of the suspended sediment load of the Mekong at Kratie is transported into the Cambodian floodplains, and 4-7% is further conveyed by overland flow to PoR and LXQ in the VMD. The remaining proportion is deposited in the Cambodian floodplains or returned to the main rivers.

The total sediment transported to the 'Vietnamese Mekong Delta' varies from 64% for the extreme flood to 71% for the low flood, with a corresponding flood volume of 86% and 93%, respectively. The largest fraction of the sediment is transported through the stations Tan Chau and Chau Doc, ranging from 57% to 68% (corresponding flood volume: 78-89%) for the high and low flood year, respectively. This means the smaller the flood event the higher is the proportion of sediment load passing through Tan Chau and Chau Doc. This has to be attributed to higher sediment trapping in the TSL and the Cambodian floodplains during larger events. Furthermore, it has to be noted that the transport capacity of the Mekong River upstream of the Vam Nao junction is three to four times greater than the capacity of the Bassac River. The differentiation of SSC in the rivers from upstream to downstream is explained by sedimentation in the river bed, dispersion, and the SSC-dilution effect caused by the return flow from TSL. The TSL return flow has much lower SSC than the inflow (i.e. flow from the Mekong) due to the settlement of sediment in the TSL. As the most of TSL return flow enters the Bassac branch, SSC at Chau Doc is significantly smaller than SSC at Tan Chau during the high and falling stage of flood events. During this period SSC at Chau Doc is approximately 50% of SSC at Kratie (Fig. 3.5 C-D).

The transport capacity in Tien River and Hau River is balanced again through the Vam Nao junction. 23÷28% of the overall flood volume and 18÷21% of the sediment load is conveyed from Tien River through Vam Nao channel to Hau River. Downstream of the Vam Nao junction, Tien and Hau River carry approximately the same suspended sediment load. The total suspended sediment transport to the VMD floodplains varies from 13% for the low flood to 17% for the extreme flood. The channels in the VMD floodplains obtain sediment from two sources: the main part stems from the Tien and Hau Rivers and is conveyed through

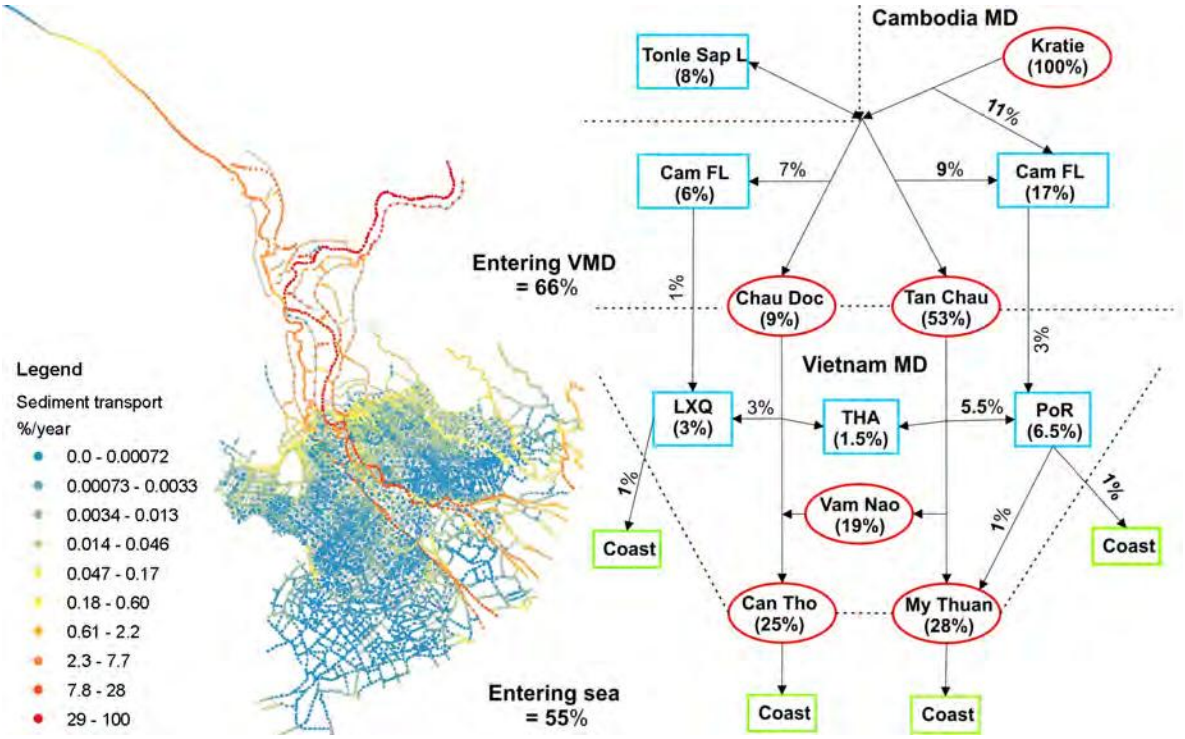

Figure 3.7: Proportion of transported sediment in the whole MD compared to sediment load at Kratie (left), and sediment load transport into subsystems (turquois blocks) and to key stations (red circles), both for the normal flood year 2009.

the channel network to PoR and LXQ. The second part originates from the overland flow from the Cambodian floodplains. SSC of the overland flow is lower compared to SSC in the main rivers as a consequence of the deposition in the Cambodian floodplains. The VMD floodplain compartments trap 1%÷6% of the total sediment load at Kratie. This is equivalent to 9%÷41% of total transported sediment into the VMD floodplains.

The remaining suspended sediment is transported to the subsystem 'coastal area'. In the tidal backwater influenced coastal zone also the fine sediments can be deposited in the river beds (9÷11%). However, the model does not consider salt water intrusion and the effects of density layering on sediment deposition. Thus the simulated river bed deposition in the coastal zone can be taken as a rough indication only. Overall, the total sediment load transported to the coastal area at My Thuan and Can Tho ranges from 48% for the extreme event to 60% for the low flood.

Fig. 3.7 (left) provides an overview of the spatial distribution of sediment transport in the whole MD and Fig. 3.7 (right) shows schematically the variation of the sediment load through the MD. The numbers indicate the fraction of sediment transport compared to the sediment load at Kratie. The largest proportion of sediment is kept in the main rivers and channels. As expected, the sediment loads are not equally distributed in the VMD. Highest SSC value are simulated in and close to the main Mekong branches and along the Cambodian-Vietnamese border (PoR and LXQ), where the channels in the VMD collect the sediment of the overland flow from Cambodia. In the upper VMD the PoR receives higher sediment loads, which are also transported deeper into the floodplain area compared to LXQ. This has three reasons: (1) LXQ is directly influenced by tidal backwater effects from the Gulf of Thailand reducing

Table 3.3: Total sediment load, relative sediment load, flood volume (with reference to Kratie) at key locations in the MD for three flood events.

Subsystem	Flood volume (%)			Sediment load (mil.ton)			Sediment load (%)		
	2009	2010	2011	2009	2010	2011	2009	2010	2011
Kratie	100%	100%	100%	78.4	43.4	104.2	100%	100%	100%
Cam floodplains	11%	9%	16%	21.4	10.3	27.3	27%	24%	26%
Overflow to VMD	6%	4%	9%	3.5	1.5	7	4%	4%	7%
Tonle Sap Lake	8%	6%	12%	5.2	2.1	10.6	7%	5%	10%
Vietnamese MD	92%	93%	86%	51.8	31	66.3	66%	71%	64%
Tan Chau	67%	70%	60%	41	24.7	50.3	53%	57%	48%
Chau Doc	19%	19%	18%	7.3	4.7	9	9%	11%	9%
Vam Nao	26%	28%	23%	14.7	9.3	18.7	19%	21%	18%
VN floodplains	21%	17%	24%	10.9	5.6	17.6	14%	13%	17%
Coast (Sea)	-	-	-	42	25.9	50.5	55%	60%	48%

flow from the Hau River into LXQ, (2) SSC in the Hau River is generally smaller than SSC in the Tien River upstream of the Vam Nao connection, and (3) most of the floodplains with high ring dike systems blocking the inundation of the floodplains are concentrated in LXQ. In THA, the area between Tien and Hau River, almost all floodplains are fully protected by high ring dikes prohibiting floodplain inundation and deposition (if three crops per year are grown, which is the typical pattern). In the coastal areas, flow and thus sediment transport is governed by tidal influences. Most of the channels in this area do not receive significant amounts of sediment from the Tien and Hau Rivers, because the prevailing alternating flow in these channels prevents a constant flow and sediment input from the main rivers into these channels.

3.5.2 Sediment dynamics in the VMD floodplains

In this section the sediment dynamics in the VMD floodplain regions PoR, LXQ and THA are elaborated. These floodplains obtain sediment from two sources: via channels starting from Tien River and Hau River, and via channels collecting overland flow from Cambodia.

During the rising flood stage the bulk of the flow is concentrated in rivers and channels. Overbank flow on Cambodian floodplains does not yet occur, and flow to TSL occurs mostly through the Tonle Sap River. In the VMD, all floodplain sluice gates are still closed to protect the second rice crop of the year, but also the low dikes prevent extensive flooding of the compartments. During this phase water levels rise generally, but in the main rivers and the channel network only. SSC is also rising with the onset of the flood, but SSC decreases with distance from Tien River and Hau River towards the remote parts of PoR and LXQ (see Fig. 3.8 left panel and Fig. 3.9). In both PoR and LXQ, SSC greater than 50 $mg.l^{-1}$ can be found up to a distance of $60 \div 70$ km from Tien River and Hau River, but also the remote parts of the floodplains show noteworthy SSCs in the channels in all simulated flood events (Fig. 3.8 left panel).

During the high flood stage overbank flow occurs on both sides of the Mekong and Bassac Rivers. All sluice gates in low dike compartments and also some of the high dike compartments - depending on the management scheme - are opened after the second rice crop harvest. Later

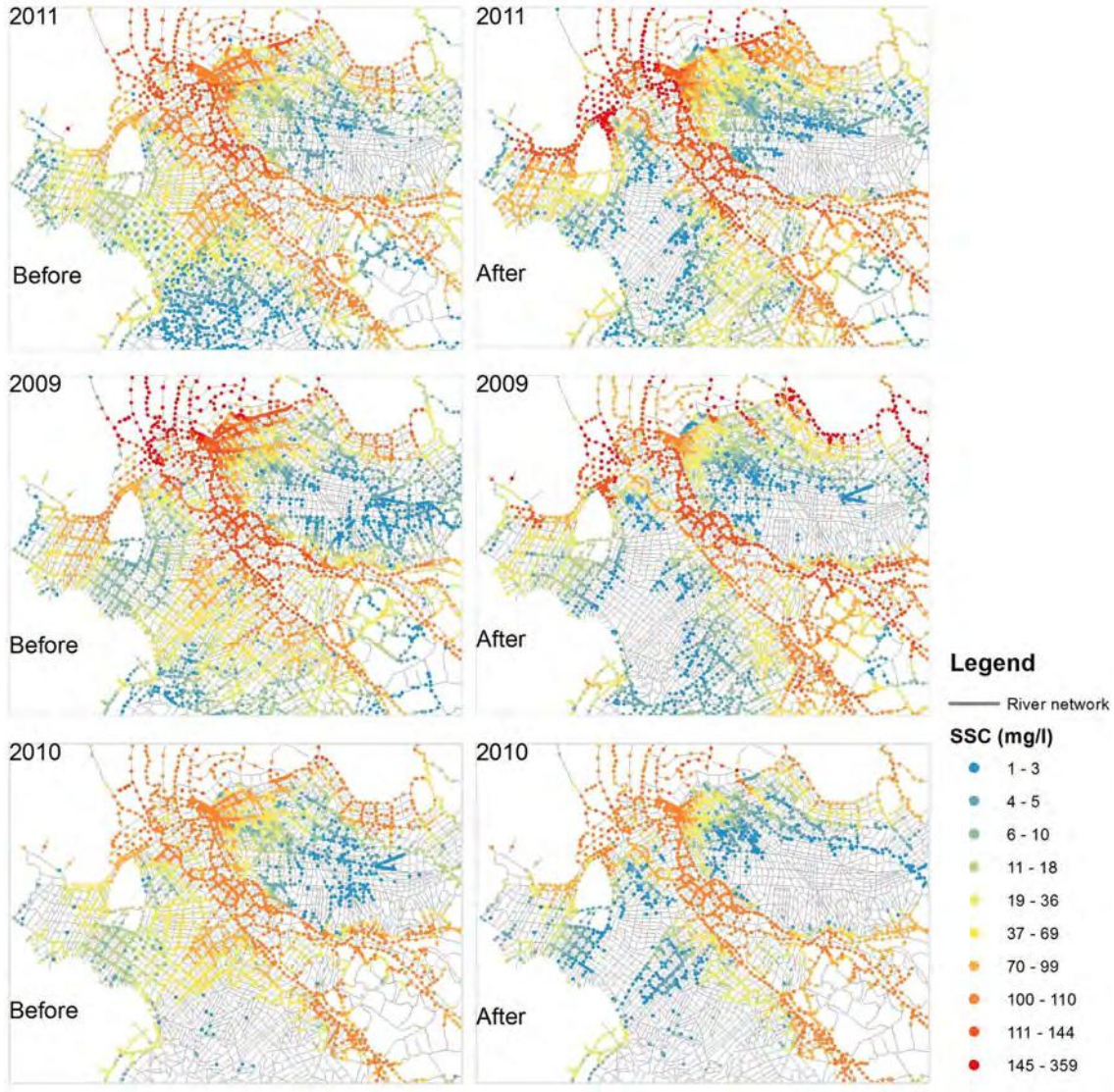

Figure 3.8: SSC distribution in the VMD for three floods: SSC distribution before (left) and after (right) sluice gate opening.

on the low dikes are also overtopped. The VMD floodplains now receive water and sediment from Tien and Hau Rivers and overland flow from the Cambodian floodplains. The SSC patterns depend on the magnitude of the overflow from the Cambodian floodplains, which has significantly smaller SSC compared to Tien and Hau River. In the normal year 2009, floodplain compartments are filled through sluice gates after $2 \div 3$ days. This results in a drastic reduction of SSC in the channels due to sediment deposition in the compartments and in low SSC of the return flow from the compartments to the channels (Fig. 3.8 right panel). Notable SSC are then observed until a distance of 20 km from the main rivers only. SSC in the central and remote parts of the PoR and LXQ is reduced to below 5 $mg.l^{-1}$.

In PoR, $24 \div 37\%$ of the flood volume stems from the Cambodian floodplains. Overland flow from Cambodia enters the border channels, from where it is redistributed to the channels of the PoR and the Vam Co River. Flow from the Tien River also enters PoR through channels which are mainly parallel to the border channels. Due to the hydraulic head imposed by the flood water from the Cambodian floodplains, flow velocities in these channels are

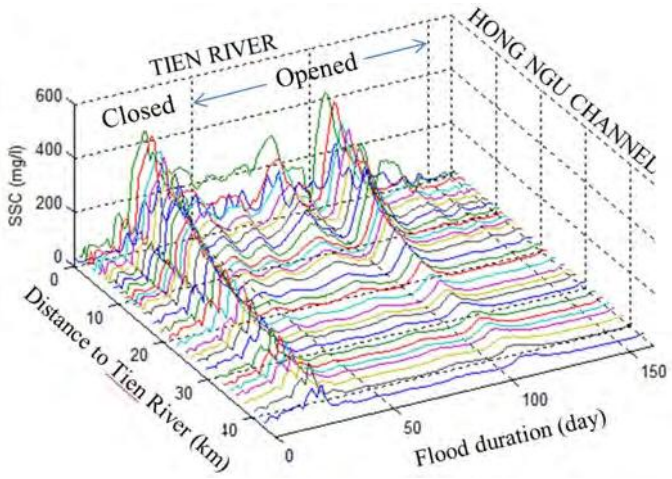

Figure 3.9: Typical SSC reduction in the channels with distance to the main river in the Plain of Reeds, exemplarily shown for the Hong Ngu channel in 2011.

comparatively small. During the later period of the high flood stage the flow into PoR from the Tien River might become stagnant or even reverse during low tide. This is besides the compartment flooding the reason for the low SSC in the southern part of the PoR in October, even close to the Tien River (Fig. 3.8 right panel). In LXQ, floodplains receive 25÷33% of the overland flood volume from the Cambodian floodplains. Like in PoR, the border channel redistributes the water to the channels of LXQ and to the Gulf of Thailand. The difference to PoR is that flood water can flow directly to the sea. The overland flood wave to LXQ is also generally lower than the overland flow to PoR. This results in a lower hydraulic head of the overland flood compared to PoR. Because in LXQ the flow from the Hau River is less dampened by the overland flood wave, higher flows and SSC rates occur in the channels of the southern parts of LXQ compared to PoR, This effect is, however, limited to regions close to the Hau river, because of the direct tidal influence of the Gulf of Thailand at the western part of the LXQ.

In the falling flood stage the flow is reverted from TSL to the Mekong just upstream of the diversion of the Bassac and Mekong branches. The return flow from TSL has low SSC, thus the SSC in the Mekong is reduced by dilution and considerably lower than during the previous flood stages with similar discharges. This SSC reduction particularly affects the Bassac River branch, where the dilution is more substantial due to incomplete transversal mixing between the confluence of the Tonle Sap River to the Mekong and the diversion of Mekong and Bassac. This effect was also highlighted by Kabeya et al. [2008] through stable isotope sampling.

The reduction of SSC with distance to the main rivers and the variation of the reduction during the flood period are illustrated in Fig. 3.9. It shows the simulated SSC of flood 2011 in a typical channel in the VMD, the Hong Ngu channel. It is connected to Tien River and reaches 40 km eastward into PoR. SSC reduction along the Hong Ngu channel differs in the different flood stages. In the rising stage, when the flow from the Tien River into the channel is not impaired by the secondary flood wave from the Cambodian floodplains and when floodplain inundation has not yet occurred in the VMD, SSC is reduced least of all flood stages. SSC in the channel changes considerably after the opening of the sluice gates. Sediment is trapped in the compartments and the return flow dilutes SSC in the channels further. Now SSC is reduced rapidly over the first 10 km distance from the Tien River. At larger distances it remains stable at a very low level of around 20 $mg.l^{-1}$. This corresponds

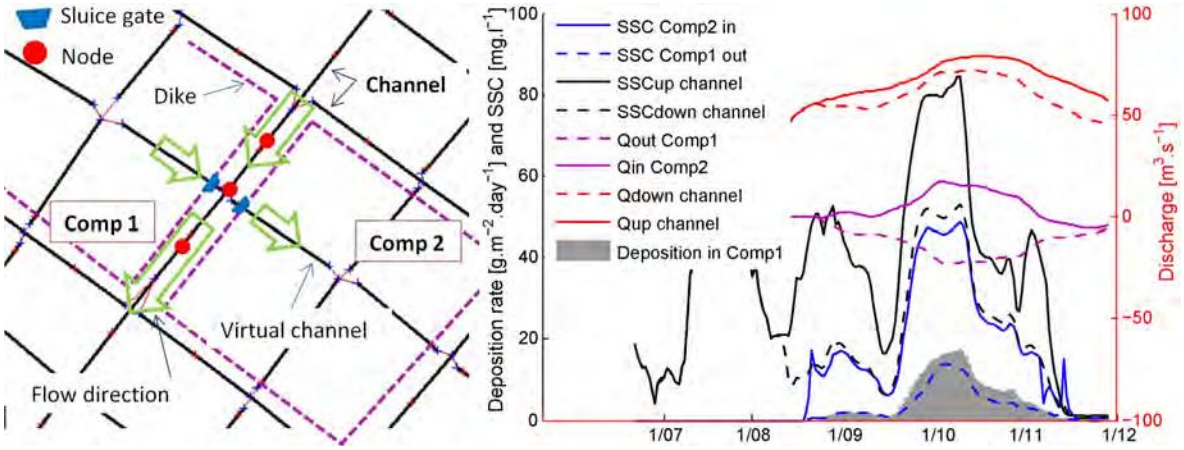

Figure 3.10: Flow direction in channels and two nearby compartments as represented in the hydraulic model (left). Discharge and sediment dynamics between the channel and two nearby compartments and sediment deposition in compartment 1 for 2011 (right).

well to the SSC reduction in the same channel measured in 2008 by Hung et al. [2014a] during this flood stage.

The effect of sluice gate opening on flow dynamics in the channels is exemplarily illustrated for two nearby compartments in Fig. 3.10. It shows discharge and SSC of channels upstream and downstream of two sluice gates, as well as discharge and SSC flowing in and out of the compartments. After the opening of the sluice gates, the compartments are filled within $2 \div 3$ days. After this compartment 1 acts as a wide channel buffering the flow to the channel and to compartment 2. At the same time suspended sediment is entering the compartments and is deposited due to reduced flow velocity. The outflow from compartment 1 with very low SSC dilutes the channel SSC. The diluted flow in the channel partly enters compartment 2, and flows further downstream the channel. This process is the primary reason of SSC reduction in the high and falling flood stages in the VMD.

3.5.3 Sedimentation and nutrient deposition in the VMD floodplains

Floodplain sedimentation is derived from the mass balance in every simulated compartment. The annual sedimentation rate is then calculated from the gross sedimentation per year and the floodplain area. The associated nutrient deposition is estimated from the sediment deposition rate by the average total nutrient proportion of the deposited sediment of 6.7% (Manh et al. [2013]). This proportion quantifies the summed deposition of total nitrogen, total phosphor, total potassium and total organic carbon. Finally, the sediment deposition depth is calculated from the cumulative sedimentation rate and the 1.2 $ton.m^{-3}$ dry bulk density of sediment soil in the MD specified in Xue et al. [2010].

A comparison of simulated sedimentation with measured data in 2011 (Manh et al. [2013]) and in 2009 and 2010 (Hung et al. [2014b]) is shown in Fig. 3.5 E. A general tendency of the model to underestimate the monitored deposition can be observed. The underestimation is particularly pronounced for the high flood 2011. Here in 9 of 11 locations the simulated deposition is below the lower 95% confidence bound associated to the measurement data (Manh et al. [2013]). This underestimation is likely a consequence of different reasons:

1. In the floodplains the sediment grain size is very fine and small disturbances can already

cause erosion and re-suspension. Hung et al. [2014b] showed that erosion can occur locally and over limited time periods in the floodplains. Also, the typical net-fishing activities on the floodplains very likely cause a considerable amount of re-suspension. Furthermore, the settling velocity depends on water temperature. (Hung et al. [2014b]) showed by measurements that bottom layer SSC and thus sediment settling velocity on floodplain fluctuates diurnally due to temperature changes. These effects are not described in the presented large-scale model.

2. The study focuses on the sediment delivered to the MD from the Mekong watershed. Erosion and re-suspension are suppressed by the model setup using a very high critical erosion shear stress for the whole model domain. Hence erosion from bed layers and banks of channels is not simulated, and sediment input to the floodplain compartments might thus be smaller in simulation than in reality. This local erosion might be one reason for the significantly smaller simulated sedimentation rates. However, as the SSC values in the channels are well simulated, the impact of this possible error source on the results might also be low.

3. Most of the sluice gates are operated by land owners using sandbags. The uncertainty and variability inherent in the dike levels and sluice gate operation which is almost impossible to cover completely in the modeling might impact the simulation of floodplain deposition. Based on field experiences and the work of Dung et al. [2011a] this factor is likely to have the highest impact on the simulation results.
   But despite this underestimation, the simulations are valuable, because they quantify the deposition of the newly arriving sediment to the VMD, excluding the local re-suspension and erosion. In addition, the model enables an analysis of the spatial distribution and variability of sediment deposition over the whole MD.

Table 3.4: Cumulative sediment and nutrient deposition mass in different spatial units in VMD floodplains (absolute mass and relative to Kratie), and spatial variability of sedimentation rate, deposition depths and nutrient deposition rates in the VMD.

Zone	Item	Unit	2009	2010	2011
VMD	Sedimentation	10^6 ton	2.27	0.43	6.56
		% of Kratie	3%	1%	6%
	Nutrients	10^3 ton	152.5	28.8	439.9
PoR	Sedimentation & Nutrients	PoR/VMD	58%	68%	66%
LXQ		LXQ/VMD	28%	23%	23%
THA		THA/VMD	14%	8%	10%
VMD	Sedimentation ($kg.m^{-2}$)	Min	0.05	0.01	0.1
		Mean	1.02	0.36	2.1
		Max	27.2	6.85	58.44
	Depth (Mean)	(mm)	0.9	0.3	1.8
	Nutrients (Mean)	($g.m^{-2}$)	68.5	24.4	141

Table 3.4 lists the cumulative sediment and nutrient deposition for the regions PoR, LXQ and THA) and over the whole Vietnamese floodplains. The total sediment deposition in VMD

varies from 0.43 *mil.ton* in the low flood year 2010 to 6.56 *mil.ton* in the extreme flood 2011. This is equivalent 1%÷6% of the total sediment load of the respective years at Kratie within the three flood events. The majority of the sediment is deposited in PoR (58÷68%), while THA receives only 8÷14%. The deposition in LXQ varies less and amounts to 23÷28%. This distribution is explained by the comparatively small floodplain area and the high number of high dike compartments in THA and LXQ.

Since the nutrient deposition is directly linked to sedimentation, the pattern of nutrient deposition is identical to the sedimentation pattern. For the extreme flood 2011, 292.10^3 ton, 102.10^3 ton and 45.10^3 ton of nutrients are deposited in PoR, LXQ and THA, respectively.

Table 3.4 also gives the spatial variability of sedimentation rates, nutrient rates and sediment depths for the three floods. This result basically depicts the effect of higher deposition in large flood events due to higher SSC, larger inundation extent and longer duration of compartment inundation. The range of sedimentation rates over the whole VMD in 2011 is 0.1÷58 $kg.m^{-2}y^{-1}$, while it is just 0.01÷6.8 $kg.m^{-2}y^{-1}$ in 2010. This large range of deposition for a given flood season illustrates very high spatial variability, and can be explained by very different distances to the main sediment sources and the heterogeneous operation schedules of sluice gates. The mean deposition in THA is considerably higher than in the other regions, because the distances to main rivers and channels never exceed 10 km (Fig. 3.1). In summary, the delta-wide average sedimentation rates are 0.36 $kg.m^{-2}y^{-1}$, 1.02 $kg.m^{-2}y^{-1}$, and 2.1 $kg.m^{-2}y^{-1}$ in the low, normal and extreme flood, respectively, with annual mean sedimentation depths of 0.3 mm, 0.9 mm and 1.8 mm, and average nutrient deposition of 24 $g.m^{-2}y^{-1}$, 68 $g.m^{-2}y^{-1}$, and 141 $g.m^{-2}y^{-1}$. These average figures compare well to the estimated recent annual aggradation rate of 0.5 $mm.y^{-1}$ given for the whole Mekong Delta by Syvitski et al. [2009].

In order to quantify the benefit of nutrient deposition in inundated compartments, we compare the cumulative nutrient deposition rate with the average total amount of N, P, K fertilizers that is applied to rice crops in the wet season (Khuong et al. [2007]. The cost of fertilizers and pesticides amount to approximately 40% and 15% of the total costs per rice crop season Thong et al. [2011], Phuong and Xe [2011]). Table 3.5 shows the average N, P, K deposition in floodplains and the N, P, K requirements for a rice crop. Depending on the event, the floods supply 13÷75% N, 10÷58% P, and 145÷835% K to the floodplains. Under normal flood conditions as in 2009 flooding can provide more than 50% of the typically applied rice crop fertilizers. This is a significant reduction of the costs for mineral fertilizers used in high dike compartments blocking the inundation.

Event	$N(kg.ha^{-1})$		$P(kg.ha^{-1})$		$K(kg.ha^{-1})$	
2009	33.6	36%	13	28%	154.2	406%
2010	12	13%	4.6	10%	55	145%
2011	69.1	75%	26.8	58%	317.2	835%
required	92.1		46		38	

Table 3.5: Mean nutrients supply from flood events to floodplains nutrient requirements for a rice crop in the wet season, and the percentage of nutrients supplied by flood sediments.

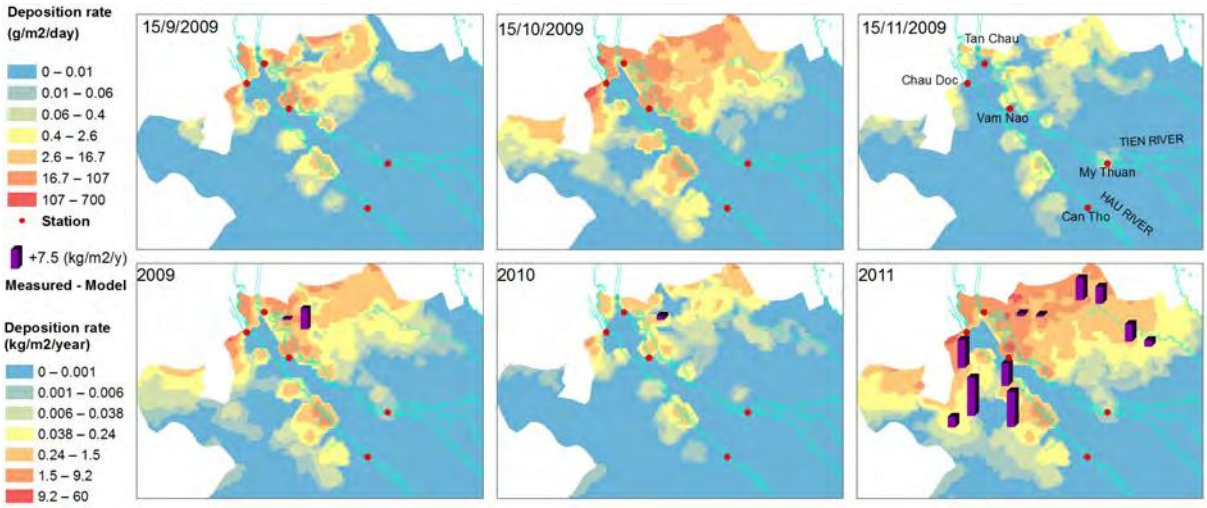

Figure 3.11: Map of sedimentation in the VMD floodplains. Top: Sediment deposition rate ($g.m^{-2}.day^{-1}$) during the period of compartment opening (left), during flood peak discharge (center) and during the period of compartment closing (right) in the normal flood of 2009. Bottom: Cumulative sediment deposition ($kg.m^{-2}.day^{-1}$) in 2009, 2010 and 2011. The bars indicate the differences between measured and simulated cumulative sediment deposition.

Fig. 3.11 (top row)) shows the spatial variability of sedimentation rate in the VMD floodplains over the flood season 2009. These maps are interpolated using Kriging based on the deposition rates of the 1D representation of the floodplains in the hydrodynamic model. In middle September a number of sluice gates are opened or overtopped. These are mostly located along the border of Vietnam to Cambodia, where the water levels rise first. During this period the daily sedimentation rates are quite high because of high SSC of channel water flowing into the floodplain compartments. In middle October all the low dike compartments and some high dike compartments are overtopped or opened, i.e. a large proportion of the floodplains is inundated. The daily sedimentation rates during this peak discharge period are very high, especially in the vicinity of the Tien and Hau Rivers and the border channels. In PoR almost all compartments are inundated and trap sediment, but the sedimentation rates reduce with distance from the Tien River and the border channel. Thus the deposition rate becomes quite low in the southern part of PoR. In THA most of the compartments are closed and the high dikes prevent inundation during the peak discharge. Sedimentation occurs only in some compartments along the border and close to the rivers. In these compartments the deposition rate is very high. Similarly, sediment deposition cannot occur in the central part of LXQ, where a large number of high dike compartments exist and the sluice gates remain closed during the high flood period. Like in THA, sedimentation in LXQ is mainly concentrated along the border and in close proximity of the Hau River. At the end of November the flood is receding in the upper part of the VMD and many compartments are closed to start a new crop season. Patterns of sedimentation rates are similar to those in September, but with much lower rates.

The bottom row of Fig. 3.11 shows maps of the annual deposition for the simulated flood events. In the extreme flood 2011, the inundated area is not much larger than during the normal flood 2009, but sedimentation rates differ strongly. Total sedimentation in 2011 is more than three times the deposition in 2009 (cf. also Table 3.4). This is the result of the

higher flood magnitude and longer flood duration. The opposite holds true for the extremely low flood 2010: low water levels and short inundation duration allow only very low sediment deposition. The total sedimentation rate is just 19% and 6% of the total rate in the normal and extreme year, respectively. The sedimentation in the low flood year is mostly concentrated in the compartments close to the border channels and main rivers. Sediment is not depositedin central LXQ and very little sediment is trapped in central PoR. Fig. 3.11 (bottom row) also shows the differences between measured and modeled sedimentation (vertical bars). The smallest differences are observed in upper PoR, where the sampling locations are closer to the sediment sources, i.e. Tien River and overland flow from Cambodia. In the remote areas in PoR and LXQ the simulated SSC is very small as Fig. 3.8 and Fig. 3.9 illustrate. The main sediment source seems to be local erosion in channel beds, river banks and floodplains, which is likely to be the major source for the differences between measured and simulated sedimentation.

3.6 Conclusions

This study presents a comprehensive approach to quantify suspended sediment and sediment-related nutrient transport and deposition in the whole Mekong Delta. The heterogeneous system is described by a quasi-2D model linking a hydrodynamic and a cohesive sediment transport model. A two-stage model calibration approach using six objective functions was applied. By this approach different types of observed point and spatial data are taken into account with the aim to obtain the best possible model representation of the large-scale water and sediment transport. It can be concluded that, for the first time, a large-scale quantification of sediment and sediment-related nutrient transport and deposition for the whole Mekong Delta has been achieved.

The model considers only sediment originating from the Mekong basin and entering the Mekong Delta at Kratie. Re-suspension and erosion in channels and floodplains are explicitly excluded through appropriate model parameterization. As a consequence, the simulations tend to underestimate sedimentation in the floodplains. This effect is particularly pronounced in the remote areas of the Vietnamese Mekong Delta at large distance from the main rivers (parts of the Plain of Reeds PoR and Long Xuyen Quadrangle LXQ). In these regions very low suspended sediment concentrations prevail, and hence erosion and re-mobilization is more important for floodplain sedimentation compared to regions closer to the main rivers and channels. Particularly sediment re-mobilization is highly influenced by human activities, particularly net fishing in channels and floodplains, but also channel bank erosion caused by ship and boat traffic is also a potential local sediment source. However, the understanding and quantification of these processes require further field investigations and a more complex model setup including local erosion.

The model quantifies spatial and temporal variations of the suspended sediment transport and sediment-nutrient deposition from Kratie at the entrance of the Mekong Delta to the coast. A very high variability of floodplain sedimentation was observed in the VMD. Generally, higher rates occur in closer distances to sediment sources. During the rising flood stage no sedimentation in floodplains occurs due to closed sluice gates. The channel network is effective

in transporting and distributing sediment, also deeply into remote floodplain areas. During flood peak stage flood water can enter floodplain compartments and sediment deposition is initiated. The outflow from compartments dilutes SSC in the channels, which causes in turn a high heterogeneity of SSC in the dense channel network of the VMD. Furthermore, SSC becomes very small with larger distances from the sediment sources which contributes to the very high variability of floodplain sedimentation.

Based on these findings, the following recommendations can be deduced in order to achieve higher sediment deposition and a lower spatial variability across the VMD: (1) The overflow of the border channels with low SSC currently entering the VMD floodplains should be re-directed. This could be achieved by increasing the capacity of the border channels and directing the water to Vam Co River in PoR, or to the Gulf of Thailand in LXQ. This should cause higher SSC stemming from Tien and Hau river in remote areas of the floodplains. (2) The channels starting from Tien River and Hau River should be enlarged to be able to convey higher sediment mass towards the floodplains. (3) From a management point of view, crop schedules in PoR and LXQ should be adapted to keep sluice gates open for longer periods, and compartments/sluice gates in larger distance to sediment sources should be opened earlier than the nearer compartments. Optimizing the operation of sluice gates on a larger scale is the best solution to transport and trap sediment in the floodplain compartments of PoR and LXQ in the VMD with no additional investments in infrastructure . The presented work does thus support a similar recommendation given by Hung et al. [2014a].

The presented quantification of the nutrient input by sediments presents an opportunity to assess the nutrient deficit to be expected in the high dike compartments in the VMD. It would allow a data based cost-benefit analysis of natural inundation versus dike construction and implementation of three crop per year cropping pattern.

The study also shows, as expected, that the Mekong River basin is a net contributor of sediment to the Mekong Delta. The annual spatial average floodplain deposition of $0.3 \div 1.8$ mm, which can be much higher locally, is an important, in fact the only counterbalance to land subsidence, as well as to some extend sea level rise in the MD (Syvitski et al. [2009]). As particularly the actual and expected sea level rise exceeds the floodplain deposition, any changes leading to reduced deposition poses a serious threat to the Mekong Delta. This includes local changes in the delta like complete blocking of floodplain inundation for an increased agricultural production, but also sediment starvation of the Mekong river caused by increased damming in the Mekong Basin (Kondolf et al. [2014]; Kummu et al. [2010]). The most dramatic effects would be increased flood hazard and erosion, particularly of main river beds and shore lines.

The model results might also be helpful for detailed studies of this latter point by providing sediment loads entering the sea. This information can be used as boundary conditions for studies on sediment transport and erosion along the coast and the subaqueous delta. This is currently also a hot topic, as the coastline of the Mekong Delta is subject to considerable erosion (Tamura et al. [2010], Anthony et al. [2013]).

Finally, the model can be used to quantify impacts of planned and ongoing dam construction in the Mekong Basin in terms of floodplain deposition and sediment distribution in the

Mekong Delta. In a similar manner the impact of the current and expected sea level rise on the sediment transport in the MD can be estimated. These points will be covered in a follow-up study.

Chapter 4 Future sediment dynamics in the Mekong Delta: impacts of hydropower development, climate change and sea level rise

Abstract

The Mekong Delta is under threat due to human activities that are endangering livelihood of millions of people. Hydropower development, climate change and the combined effects of sea level rise and deltaic subsidence are the main drivers impacting future flow regimes and sedimentation patterns in the Mekong Delta. We develop a sensitivity-based approach to assess the response of the floodplain hydrology and sediment dynamics in the Delta to these drivers. A quasi-2D hydrodynamic model including suspended sediment dynamics is used to simulate the sediment transport and sediment deposition in the whole delta including Tonle Sap Lake for a baseline (2000-2010) and a future (2050-2060) period. For each driver we derive a plausible range of future states and discretize it into different levels, resulting in 216 combinations. Our results thus cover all plausible future pathways of sediment dynamics in the delta based on current knowledge. Our results indicate that hydropower development dominates the changes in sediment dynamics of the Mekong Delta, while sea level rise has the smallest effect. The floodplains of the Vietnamese Mekong Delta are much more sensitive to the changes compared to the other subsystems of the delta. The median changes of the three drivers combined indicate that the inundation extent would increase slightly, but the overall floodplain sedimentation would reduce by approximately 40%, and the sediment load to the South China Sea would diminish to half of the current rates. The maximum changes in all drivers would mean a nearly 90% reduction of delta sedimentation, and a 95% reduction of the sediment reaching the sea. Our findings provide new and valuable information on the possible future development of floodplain hydraulics and sedimentation in the Mekong Delta, and identify the areas that are most vulnerable to these changes.

4.1 Introduction

The Mekong Delta (MD) sustains the livelihood and food security of millions of people in Vietnam and Cambodia. It is known as "rice bowl" of South East Asia and has one of the world's most productive fisheries (Ziv et al. [2012]). This high productivity is a consequence of the annual flood pulse and large amount of suspended sediments transported by the Mekong River to its extensive floodplains (Arias et al. [2014], Lamberts and Koponen [2008]). The sediment load transported by the flood pulse to the floodplains provides nutrients for agriculture and plays a major role for the high biodiversity in the whole delta system. However, recent assessments classify the MD among the most vulnerable regions in the world due to climate change related sea level rise (Watson et al. [2013]) and other human activities

linked to the economic development of the six countries in the Mekong River Basin (MRB) (Syvitski and Saito [2007], Syvitski et al. [2009]). The ongoing hydropower development in the MRB impacts the flow regime (Lauri et al. [2012], Piman et al. [2013]) and changes the sediment load entering the MD (Kummu et al. [2010]; Kondolf et al. [2014]). Economic development within the delta induces land subsidence, which in turn enhances the effect of climate change related sea level rise (Ericson et al. [2006], Syvitski [2008], Syvitski et al. [2009], Doyle et al. [2010]).

In total, 136 hydropower plants are being built or planned throughout the MRB. According to the current plans, 31 dams are under construction, 82 dams will be completed within 20 years and nearly all of the 136 dams will be built within the coming 40 years (MRC [2011c]). These dams will trap considerable amounts of sediments, which in turn is very likely to strongly reduce the sediment input to the delta (Kummu et al. [2010]; Kondolf et al. [2014]). There is a particularly strong hydropower development in the Chinese part of the MRB known as the Langcang cascade (Fig. 4.1), which comprises approximately only 23% of the total basin area and provides 15% of the total annual flow volume, but is responsible for 65% of the total suspended sediment load (Kummu et al. [2010]). A number of studies have estimated the consequences of hydropower development in the Lancang on sediment load (Lu and Siew [2006], Fu and He [2007], Fu et al. [2007], Kummu and Varis [2007], Walling [2008], Liu and He [2012], Liu et al. [2013], Kameyama et al. [2013]). The sediment load reduction of reservoirs is commonly quantified by sediment trapping efficiency (TE). These studies find TE values of the Lancang cascade being within the range of 80-90% just downstream of the cascade and of approximately 50% at the Mekong Delta. An implementation of all 136 dams across the whole Mekong Basin is likely to result in massive reduction of sediment load in the Mekong Delta. Estimated TE varies from 78-81% by Kummu et al. [2010], to 85-90% by ICEM [2010], and 96% by Kondolf et al. [2014]. Hydropower development will also alter the flow regime in the lower MRB and will increase the flows in the dry season and decrease those in the wet season (Keskinen et al. [2012], Räsänen et al. [2012], Lauri et al. [2012], Piman et al. [2013]).

Climate change is expected to act as another main driver changing the hydrology in the MRB (Eastham et al. [2008], Hoanh [2010], Västilä et al. [2010], Kingston et al. [2011], Lauri et al. [2012]), however its impact on the flow regime of the Mekong River is highly uncertain (Lauri et al. [2012], Kingston et al. [2011]). Hoanh [2010] and Västilä et al. [2010] use only one Global Circulation Model (GCM) and thus their findings are not reflecting GCM uncertainty as shown in Kingston et al. [2011] and Lauri et al. [2012]. Eastham et al. [2008] examine eleven GCMs but they do not, however, downscale the GCM output to the MRB and their results are thus associated with very large uncertainty. Impact studies which have used a GCM ensemble approach along with downscaling have obtained a large range in future Mekong streamflow (Kingston et al. [2011], Lauri et al. [2012]), mainly as consequence of different GCMs. Kingston et al. [2011] study the uncertainty resulting from different GCMs and different global warming assumptions on the flow at the Mekong River gauge Pakse having a more reliable historical discharge record compared to the next downstream station Kratie, which indicates the upper boundary of the MD. Lauri et al. [2012] used two emission scenarios and five GCMs to illustrate effects and uncertainties of climate change

projections, and compared this to the expected changes caused by hydropower development. For the period 2032-2042, they find that hydropower development is very likely to have a much larger impact on the flow regime, particularly for the lower Mekong basin, compared to projected climate change impacts.

Another important driver of changes in the hydrology and sediment dynamics of the MD is sea level rise (SLR). The flow regime, and with that the sediment dynamics of the delta, are sensitive to changes in sea level (Manh et al. [2014]). Higher sea levels would cause higher backwater effects, which in turn alter the water levels and flow velocities in the river system and the floodplain inundation. As a consequence also the sediment dynamics, i.e. the erosion and sedimentation, is expected to change, with distinct spatial differences. Also the flood hazard in the delta is likely to change with higher sea levels. For deltaic regions often effective sea level rise values are defined. Effective sea level rise is a combination of sea level rise caused by climate change and deltaic subsidence. Available studies (Ericson et al. [2006], Syvitski et al. [2009], Doyle et al. [2010], MONRE [2012], Syvitski and Higgins [2012]) indicate that, with economic development and population growth, deltaic subsidence is increasing and playing an important role in effective sea level rise. The main anthropogenic causes for deltaic subsidence are subsurface resource exploitation (oil, gas, groundwater) and accelerated ground compaction by urban growth (Syvitski et al. [2009]).

It can be summarized that climate change and hydropower development along the Mekong River and its tributaries are expected to alter the hydrological regime and the sediment load at the upper boundary of the MD, while climate change related sea level rise and deltaic subsidence influence the lower boundary. Hence, the hydrology and sediment dynamics of the MD are subject to a superposition of these drivers of change. Moreover, the delta consists of an intricate system of rivers, channels and floodplains. A large degree of human interventions in the floodplains contribute to a highly variable hydrological system (Hung et al. [2012], Hung et al. [2014a], Hung et al. [2014b]) and to very heterogeneous patterns of sediment transport and deposition (Manh et al. [2013], Manh et al. [2014]). To date, there is no study available which quantifies the cumulative effects of these drivers on future hydraulics and sediment dynamics in the Mekong Delta in a spatially explicit manner. The purpose of this paper is to close this gap.

To this end, we assess the response of floodplain hydraulics and sediment dynamics of the MD to a plausible range of changes in the upper and lower boundary of the delta. We achieve our aim by using a sensitivity-based approach for all three above identified drivers. The plausible future pathways are used to drive a quasi-2D hydrodynamic model (Manh et al. [2014]), including suspended sediment transport module, for the whole MD. The model enables us to quantify the floodplain hydrology and sediment transport providing the spatial distribution of sediment deposition within the delta.

4.2 The Mekong Delta

The Mekong River is one of the major rivers of the world. It drains a total land area of 795,000 km^2, from the eastern watershed of the Tibetan Plateau to the South China Sea. The mean annual flood volume of the Mekong is approximately 475 km^3 (MRC [2009]). The

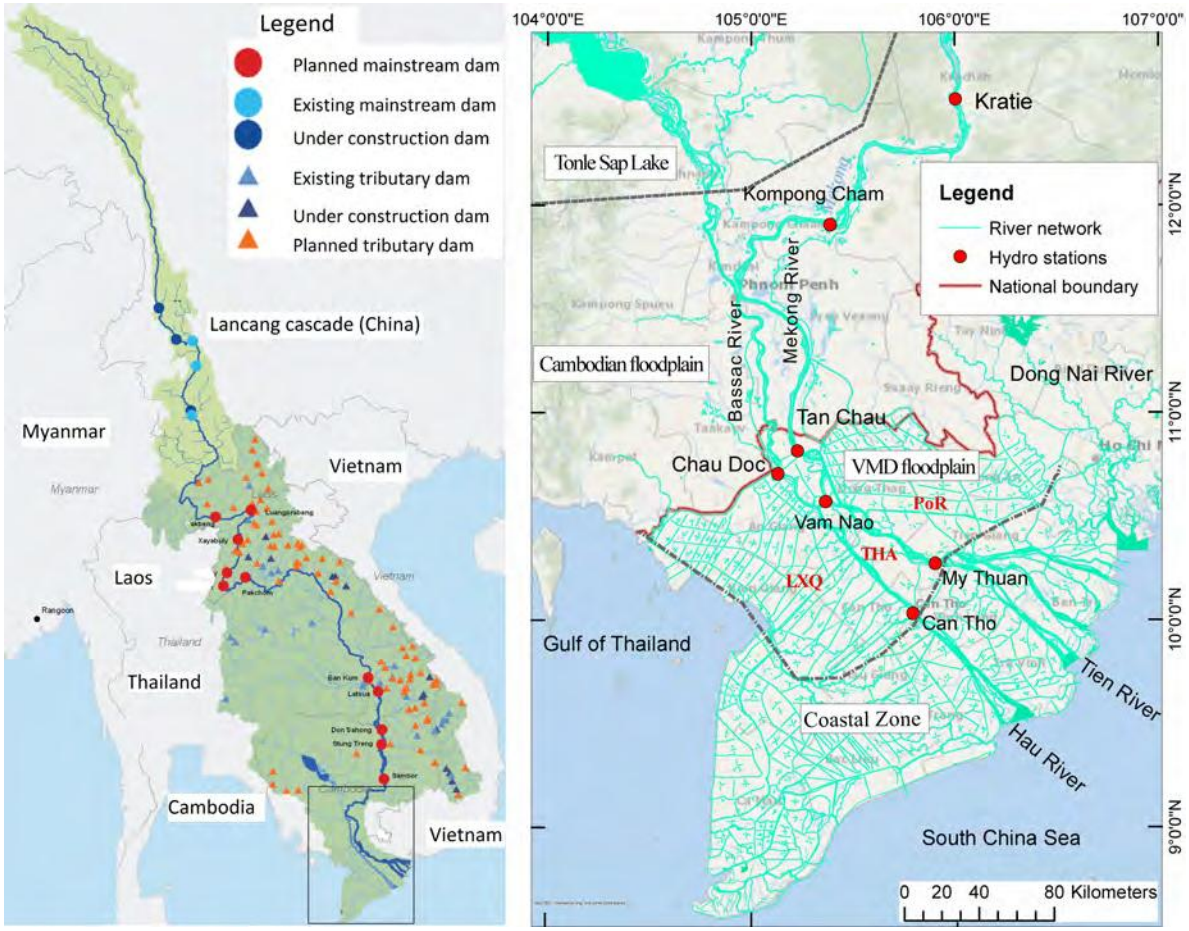

Figure 4.1: Left panel: The Mekong River Basin including the hydropower dam locations (MRC [2011c]). Right panel: The Mekong Delta (MD) from Kratie to the seas including the main hydrological stations, the subsystems of the MD and the floodplain areas in the VMD.

annual flood pulse in response to the Western North - Pacific monsoon and partially to the Indian monsoon during July to October is the key hydrological characteristic of the Mekong River. Estimates of the mean annual suspended sediment load of the Mekong at Kratie, just above the MD (see Figure 4.1), vary from 50 to 160 mil.ton (Walling [2008]; Milliman and Farnsworth [2011]; Lu et al. [2014]), and about 50-65% of this load is contributed by the upper part of the basin in China (Roberts [2001], Walling [2008], Wang et al. [2011]).

The MD is a large-scale and complex river, channel, and floodplain system with highly variable hydrodynamic characteristics (Hung et al. [2012]). The sediment load transported to the MD has a very fine grain size (Hung et al. [2014a]) and contains high nutrient fractions (Manh et al. [2013]). Sediment-related nutrient deposition in the floodplains is a significant source of natural fertilizers for the rice crops in the delta (Manh et al. [2014]).The sedimentation rates in the floodplains show a high variability in space, caused by the interplay of the complex river and channel network, two tidal systems and human regulation of floodplain inundation (Manh et al. [2013], Manh et al. [2014]).

In this paper we divide the MD into four subsystems (Fig. 4.1): Tonle Sap, Cambodian Mekong Delta, Vietnamese Mekong Delta and coastal zones. The subsystem Tonle Sap consists of the Tonle Sap Lake (TSL) and the Tonle Sap River. During the rising stage of the

flood season the Tonle Sap River diverts water with high suspended sediment concentration (SSC) in northern direction to the Tonle Sap Lake (Kummu et al. [2008]). During the falling stage water from the TSL flows back to the Mekong River and further downstream to the Vietnamese part of the delta. This return flow has very low SSC, and Manh et al. [2014] estimate that 5% to 10% of the total sediment load entering the MD at station Kratie has been trapped in the TSL during the low flood in 2010 and the high flood in 2011, respectively. This is supported by the findings of Kummu et al. [2008] for the period of 1997-2003.

The subsystem Cambodian Mekong Delta (CMD) comprises the entire MD in Cambodia excluding the Tonle Sap subsystem. During the flood season, overbank flow from the Mekong and Bassac Rivers inundates the Cambodian floodplains. These floodplains are mostly in a morphological natural state. Approximately 19%-23% of the total sediment load at Kratie is deposited in these floodplains (Manh et al. [2014]).

The Vietnamese Mekong Delta (VMD) stretches from the national border just north of the cities Tan Chau and Chau Doc to the stations My Thuan and Can Tho at the Mekong River (Tien River in Vietnamese) and Bassac River (Hau River in Vietnamese), respectively (Fig. 4.1). The VMD consists of three regions: Long Xuyen Quadrangle (LXQ) west of the Hau River, Plains of Reeds (PoR) east of the Tien River, and the region between the Tien and Hau Rivers (THA). The VMD floodplains receive flood water from the Tien and Hau Rivers with high SSC, and from the overland flow originating from the Cambodian floodplains with lower SSC. The VMD is characterized by very strong human interference. Channels, with a total length of 91,000 km and dikes on both sides, form thousands of floodplain compartments. These compartments are linked to the channels by sluice gates, which are operated according to the rice crop water demand. Hence, sediment transport and deposition are highly variable in the VMD, depending on the setup of channels and compartments, on the flood magnitude, on the operation of sluice gates, and on the height of the dikes. Further, the tidal regime influences the hydrodynamic situation and the sediment transport. The sediment deposited in the VMD floodplains ranges from 1% in a low flood year to 6% in a high flood year relative to the total sediment load at Kratie (Manh et al. [2014]).

The subsystem coastal zone is strongly affected by the semi-diurnal tide from the South China Sea (East Sea in Vietnam) and the diurnal tide from the Gulf of Thailand (West Sea in Vietnam). The tidal magnitude in the Gulf of Thailand is smaller compared to the magnitude in the South China Sea, thus the tidal effects differ in their magnitudes in different parts of the coastal zone. The coastal zone receives approximately 48-60% of the sediment entering the MD at Kratie (Manh et al. [2014]).

4.3 Methodology and data

Given the unpredictability of actual future hydropower development in the MRB and the large uncertainties in climate change impacts, we apply a sensitivity-based impact approach instead of a scenario-based approach. As argued by Prudhomme et al. [2010], this scenario-neutral approach allows rapid appraisal of impacts for different sets of boundary conditions, for example, when new climate change or hydropower development projections are available, without the need to undertake a new impact analysis.

4.3.1 Sensitivity-based, scenario-neutral approach

The sensitivity-based, scenario-neutral approach proposed by Prudhomme et al. [2010] is applied to quantify possible future sediment dynamics in the MD. In our assessment we consider the complete spectrum of changes that can be differentiated into three drivers: (1) hydropower development in the MRB influencing the streamflow and sediment load at station Kratie, the upper boundary of the MD, (2) climate change impact in the MRB and associated influence on streamflow and sediment load at Kratie, (3) effective sea level rise and its impact on floodplain hydraulics and sediment dynamics at the lower boundary of the MD. For each of these drivers of change, the plausible range is derived and discretized into five levels (details are given in Sections 4.3.2, 4.3.3, 4.3.4, Table 4.1 summarizes the selected ranges). When each level of each driver is combined, considering also the baseline (no change relative to the present state), altogether 216 (6 x 6 x 6) possible combinations of upper (Kratie) and lower (sea) boundary conditions are obtained. The division into five levels is a trade-off between computational demand and the high degree of variability in suspended sediment transport in the MD (Manh et al. [2013], Manh et al. [2014]). Hereinafter, the following notations are used: 'D' for the impacts of dams, 'C' for climate change impacts in the MRB, and 'S' for effective sea level rise; '0' for baseline, '1' to '5' for the five levels from the lower bound to the upper bound of the plausible ranges.

We apply the approach proposed by Prudhomme et al. [2010] mainly because of the large uncertainty associated with future hydropower development and climate change impacts in the MRB. For example, today it is unclear whether all the dams will actually been built, and what their characteristics and date of implementation will be. Using a conventional scenario approach would require to select a number of plausible scenarios and propagate them through the MD model. New projections, new knowledge or new political boundary conditions could require undertaking the impact analysis again. In contrast, the scenario-neutral approach allows rapid appraisal of new information, as long as the drivers and their combinations are contained within the defined scenario space. Another advantage is that this approach can be based on diverse studies. All input that is needed is the plausible range for the future impact of the different drivers. This information can be taken from available studies. Hence, different assumptions and inconsistencies between studies do not play a major role, as would it be the case for the conventional scenario approach.

We select the period 2000-2010 as baseline. The MD has undergone massive changes during the last decades, such as the recent implementation of floodplain compartments in the VMD, with large consequences on the spatial distribution of inundation extent, height and duration and associated sediment transport, thus we do not consider pre-2000 states. We use the MD sediment model set up by Manh et al. [2014] which represents the state of the delta during this time period. Also, this period encompasses a wide spectrum of floods, from the very low flood season of 2010 to the extreme flood of 2000. The year 2000, with peak discharge of 57,000 $m^3 s^{-1}$, was taken as design flood for flood defences in the following years (Hung et al. [2014a]). In contrast 2010, the flood peak reached only 37,000 $m^3 s^{-1}$, being the lowest flood volume in the 86-year observation period, and the flood was also six weeks shorter than on average (MRC [2011a]). Thus our reference period includes a wide range of events depicting the increased variability of flood discharges in the last decades, as reported by Delgado et al.

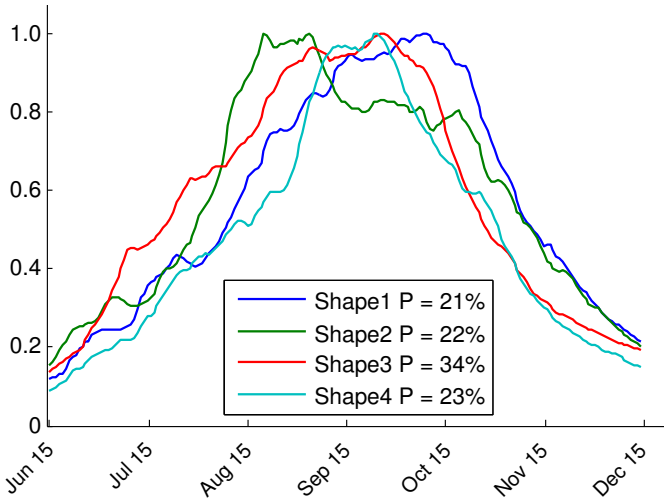

Figure 4.2: Four typical flood season hydrographs at Kratie gauge station resulting from a cluster analysis. The percentages show the empirical probabilities associated to the shapes for the 86-year observation period (adapted from Dung [2011b]).

[2010] For the future time horizon we select the period 2050-2060, when all the 136 dams are expected to be in operation according to the current plans (MRC [2011c]), and when projected climate change related sea level rise will significantly impact the hydraulic regime in the MD (IPCC [2014]).

The duration and volume of the seasonal flood hydrograph play important roles in the spatial distribution of sediment transport and deposition in the MD (Manh et al. [2014]). Thus the baseline discharge time series is generated from the average peak discharges over the baseline period 2000-2010 and typical hydrograph shapes over the entire time horizon (1924-2010) of discharge measurements at Kratie. The hydrographs contain typically one or two peaks while the timing of the peak varies from August to September. Dung [2011b] identified four typical hydrographs by means of a cluster analysis, pooling the 86 annual hydrographs observed at Kratie into four classes (Fig. 4.2). In order to take this variability into account, each of our 216 combinations is run with four typical hydrograph shapes. The resulting sediment transport patterns in the MD are averaged across the four cases using the past frequency of the four cases as weight in the averaging.

4.3.2 Impact of hydropower development on the upper boundary

The impact of hydropower development on the streamflow and sediment load at Kratie, the upper boundary of the MD, is described by the sediment trapping efficiency (TE) of the reservoirs and the change in the peak (ΔQ_D) of the flood season. The plausible range for TE is assumed to be 30-96%. The upper bound is taken from Kondolf et al. [2014], who estimated a basin wide trapping efficiency of 96% in case all 136 dams were built. The lower bound has been estimated by Kummu et al. [2010] and includes the dams already built and those currently under construction. However, both cited studies take the 1970s as baseline, i.e. when no dams existed. These values are rescaled to the baseline period 2000-2010 for which Kummu et al. [2010] estimate TE = 20%. Thus, $TE = \frac{(30\%-20\%)}{(100\%-20\%)} = 12\%$ and $TE = \frac{(96\%-20\%)}{(100\%-20\%)} = 95\%$ are the lower and upper values of the plausible TE range relative to the baseline 2000-2010, respectively.

The upper bound of the plausible range for streamflow changes as a consequence of hydropower development is taken from Lauri et al. [2012]. They simulate the MRB hydrology

assuming all 136 dams were built. The difference in the daily streamflow at Kratie between this situation and the baseline is considered as the impact of the hydropower development on streamflow. A similar simulation for the dam operation impact on streamflow assuming that only the dams built and those already under construction are realized does, however, not exist. Hence, the lower bound of the range of streamflow change had to be estimated in a different way. We use the cumulative active storage of the reservoirs in the MRB as a proxy. This storage capacity for the lower bound (only the dams built and under construction) is 55% in relation to the storage capacity of the upper bound (all 136 dams) (Kummu et al. [2010]). This value is then rescaled to the baseline in Kummu et al. [2010], for which a storage value of 25% was estimated. Thus, storage for the lower bound is $\frac{(55\%-25\%)}{(100\%-25\%)} = 40\%$ of the upper bound storage. We further assume that the streamflow change is proportional to the change in active storage, and thus we multiply the result for the upper bound derived from Lauri et al. [2012] by 0.4 to obtain the streamflow change for the lower bound. Fig. 4.3 shows the upper and lower bounds of the change in streamflow for the flood season as a consequence of hydropower development. For each day of the flood season, the streamflow is averaged over the eleven years of the baseline and future periods, respectively. We assume that the five levels of TE and streamflow change apply jointly, i.e. a certain case for hydropower development is associated with the same level for TE and streamflow change.

In addition, an attempt was made to include the discussed conversion of the planned eight Mekong main stem dams in the Lower Mekong Basin (LMB) from reservoirs to run-of-river hydroplants. In this case the planned active storage would be reduced to almost zero, resulting in TE = 0 when using Brun's method. Thus, in terms of trapping efficiency, a case assuming all main stem dams are realized as run-of-river plants is equal to a case of no main stem dams being built. This is equivalent to TE = 50-68% (Kummu et al. [2010], Kondolf et al. [2014]) in the presented sensitivity analysis above.

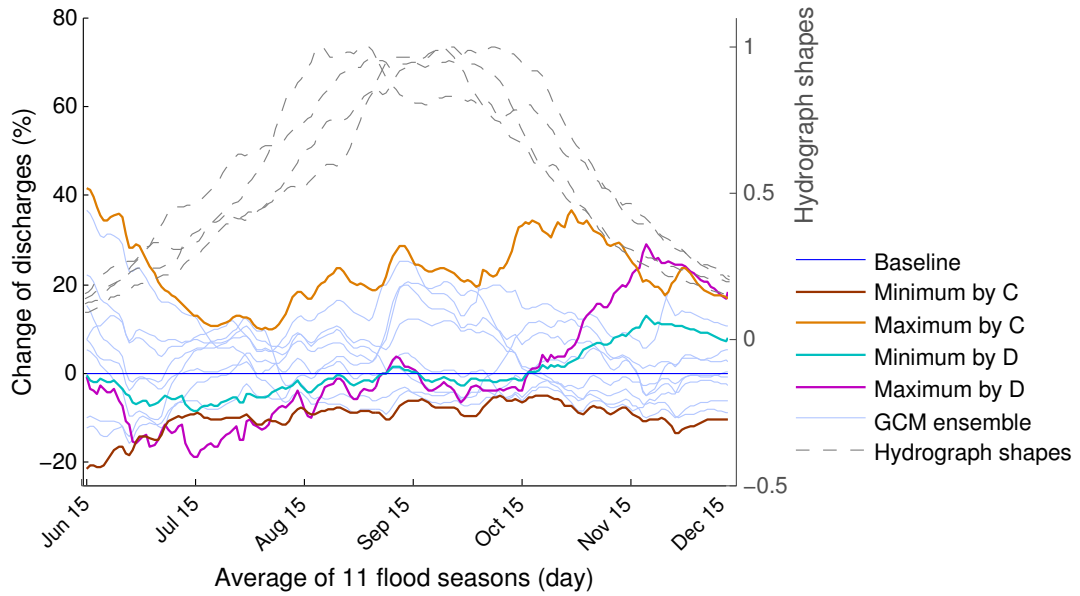

Figure 4.3: Change in daily streamflow during the flood season for the period 2050-2060 in relation to the baseline period 2000-2010 as consequence of climate change and hydropower development, respectively (based on Lauri et al. [2012]).

4.3.3 Climate change impact on the upper boundary

To estimate the plausible range of discharge change in Kratie under climate change (ΔQ_C), the results from Lauri et al. [2012] are used, because this is the most comprehensive study available for the MRB to date. It considers two emission scenarios (IPCC SRES B1 and A1b) and five GCMs, and includes a downscaling procedure. Fig. 4.3 shows the change in daily streamflow at Kratie for the ten climate change scenarios for 2050-2060 in relation to the baseline period 2000-2010. For each day of the flood season the streamflow is averaged over the eleven years of the baseline and future periods, respectively. The upper and lower bounds of the plausible range of the climate change impact are derived by selecting the upper and lower values of the ten scenarios for each day of the flood season (Fig. 4.3).

4.3.4 Impact of sea level rise on the lower boundary

The effective SLR (ΔH_S) is a combination of deltaic subsidence (ΔH_{sub})and climate change related SLR (ΔH_{slr}). The ΔH_{slr} is taken from IPCC [2014] which estimates the global mean sea level rise in the range of 17÷38 *cm* for the period 2046÷2065 compared to the baseline 1986÷2005. This range encloses the results of MONRE [2012], in which climate change related SLR based on IPCC [2007] is downscaled to the South China Sea and the Gulf of Thailand, surrounding the MD.

Deltaic subsidence in the MD is given by Syvitski et al. [2009] as:

$$\Delta H_{sub} = -S + C_N + C_A + M \tag{4.1}$$

S: Annual sedimentation rate in the delta, $S = 1[mm.y^{-1}]$ in a normal flood year (Manh et al. [2014]).
C_N: Natural compaction of the soil layers in the delta, $C_N = 3[mm.y^{-1}]$ (Syvitski [2008], Syvitski et al. [2009]).
C_A: Accelerated compaction due to human activities such as gas exploration, groundwater exploration, $C_A = 2[mm.y^{-1}]$ for the MD (Ericson et al. [2006]).
M: Crustal vertical movement the Earth's mass, $M = 1[mm.y^{-1}]$ for the MD (Syvitski et al. [2009]).

The range of deltaic subsidence for the considered future period varies from 5 *cm* in case only M (1 $[mm.y^{-1}]$) is active to 25 *cm* in case all factors apply ($-S+C_N+C_A+M = 5[mm.y^{-1}]$ for 50 years). Thus the plausible range of future effective SLR, i.e. the combined effect of climate change related SLR and deltaic subsidence, $\Delta H_S = \Delta H_{sub} + \Delta H_{slr} = 22 \div 63$ [cm].

Table 4.1: Plausible ranges of the three drivers of changing boundary conditions. Percentages indicate changes relative to the baseline period 2000-2010..

Drivers	Variable (unit)	Plausible range			No. of runs
		Lower bound	Upper bound	No. of intervals	
Hydropower development (D)	TE (%)	12	95	5	216 runs
	ΔQ_D (%)	-19	34		x 4 typical
Climate change (C)	ΔQ_C (%)	-21	42	5	hydrographs
Effective sea level rise (S)	ΔH_S (cm)	22	63	5	at Kratie

4.3.5 Sediment transport model for the Mekong Delta

The quasi-2D cohesive sediment transport model developed by Manh et al. [2014] is used to simulate sediment transport and deposition in the MD. It is an extension of the hydrodynamic model developed and applied for the MD by Dung et al. [2011a]. It simulates flood propagation, inundation and associated suspended sediment transport and floodplain sediment deposition in the MD from Kratie to the coast including Tonle Sap Lake (Fig. 4.1). The model describes river and channel network in 1D. Floodplain compartments in the VMD are represented in a quasi-2D way. The model contains 2340 floodplain compartments enclosed by dike rings and the associated hydraulic structures consisting of weirs, culverts and sluice gates. In order to quantify sediment deposition originating from the MRB only, re-suspension within the MD floodplains is suppressed in the simulation. The model was calibrated and validated using a comprehensive dataset including water and sediment observations in rivers, channels and floodplains. It showed good agreement with measurements (Manh et al. [2014]). Details about model structure and setup, calibration, validation and general model performance can be found for the hydrodynamic module in Dung et al. [2011a] and for the sediment dynamics in Manh et al. [2014], respectively.

The model is driven by streamflow and SSC time series at Kratie (see Fig. 4.1). The sediment load at Kratie is thus a very important variable for the simulation of sediment deposition in the MD. For the future conditions representing the impact of climate change and hydropower development, times series of streamflow are derived from existing models, but the impact on sediment load is either not simulated (for climate change projections) or given in an aggregated form (TE values for hydropower development projections). A catchment model simulating the sediment dynamics in the MRB does not exist to date. In order to obtain daily SSC values at Kratie we assume that the close relationship between SSC and streamflow (Manh et al. [2014]) holds also for the future period. The derived sediment rating curve of Manh et al. [2014] is rescaled by TE to accommodate the reduction in sediment load. Hence, daily SSC at Kratie is derived for given streamflow and TE by:

$$SSC_t^{Krat} = [1 - \frac{TE}{100}]\ 10^{-494.02\ log(Q_t^{Kra})^{-4.52}+2.88} \tag{4.2}$$

In which SSC_t^{Krat} is $SSC[mg.l^{-1}]$ at time t at Kratie, Q_t^{Krat} is discharge $[m^3.s^{-1}]$ at time t at Kratie. TE is the basin wide sediment trapping efficiency (%).

4.4 Results

Future sediment transport and deposition in the MD is analyzed based on the plausible ranges of drivers shown in Table 4.1 and their discretization into five levels for each driver. For each case of the 216 combinations, the spatial distribution of streamflow, suspended sediment concentration and sediment deposition in the MD is simulated throughout a complete flood season. To be able to present these results in a condensed way, the changes (relative to the baseline period) in the following variables are given and discussed: (1) annual sediment load to the four subsystems of the MD, (2) annual sediment deposition in the Vietnamese floodplains (spatial distribution and deposition aggregated over all compartments), and (3)

peak water level of flood season at station Tan Chau at the upper border of the VMD (Fig. 4.1). To understand the impacts of the different drivers, the sensitivity runs representing changes caused by a single driver only are presented first, followed by the cumulative impact.

4.4.1 Impacts of hydropower development

Hydropower development will reduce streamflow during the rising and high stage of the flood season, as well as sediment load to the MD. Table 4.2 shows the decline in annual sediment load for the different subsystems and in annual sedimentation for the VMD. For a given hydropower development level, the reduction in both variables is similar throughout the MD. However, the compartments of the VMD are proportionally most strongly affected for low to medium dam development. This is caused by the combined effect of reduced sediment input into VMD floodplains, which is already lowest among all subsystems in the baseline period, and the reduced flood peak water levels causing a reduction in the inundation extent. Fig. 4.4 (A-B) shows how this reduction varies with TE. Depending on the level of hydropower development, the flood peak is reduced by 30÷68 *cm* at Kratie and 15÷35 *cm* at Tan Chau, respectively. Sediment load at Kratie changes to -12÷-95% and sedimentation in the VMD floodplains is reduced by 21÷96%. Sediment load reduction to the sea varies from -14÷-95%.

Fig. 4.5 (D-panel) shows the change in spatial distribution of annual sedimentation in the VMD for three hydropower development levels (minimum D, medium D, maximum D), excluding the effects of climate change and sea level rise. Sedimentation is significantly reduced at all three levels. In general, the sedimentation rates but also the sedimentation area are reduced with increasing TE. Already under the medium D level the floodplain sedimentation is largely reduced compared to the baseline. Maximum sedimentation is reduced to just 14 $kg.m^{-2}.y^{-1}$ (cf 40 $kg.m^{-2}.y^{-1}$ in baseline), occurring in close vicinity of the main rivers only. In the maximum D level, these rates are reduced even further to 1.3 $kg.m^{-2}.y^{-1}$, which is equivalent to an almost complete loss of floodplain sedimentation for most parts of the VMD floodplains.

4.4.2 Impacts of climate change

Climate change impacts in the MRB affect the flood magnitude and volume, and associated sediment transport during the flood season. The plausible range of climate change may decrease or increase flooding and associated sediment transport. However, the majority of climate change scenarios used points to an increase with higher average flood discharge, prolonged inundation duration and larger inundation areas. These changes in hydraulic characteristics are associated with higher sediment concentration, sedimentation rates and larger sedimentation extent, as illustrated in the difference maps of Fig. 4.5 (C-panel).

Table 4.2 illustrates that, similar to the hydropower development levels, the floodplains in the VMD show the highest sensitivity to changing boundary conditions. The change in annual sediment load varies from -12% to +36% at Kratie and from -12% to +40% in the VMD floodplains, leading to changes in annual sedimentation in the VMD floodplains from -30% to +137%. The range of the future change in flood peak at station Tan Chau extends from -30 *cm* to +80 *cm* and from -60 *cm* to +150 *cm* at Kratie relative to the baseline level (Fig. 4.4 C-D). Sediment load to the sea varies from -10 ÷ +30%.

Table 4.2: Change in sediment load (SL) in different subsystems of the Mekong Delta and sediment deposition in the Vietnam Mekong Delta (VMD) relative to the baseline for single impacts and selected cases of cumulative impacts. (Notation: S = effective sea level rise, D = dam development, C = climate change; 0-5 denote the levels, 0: baseline, 1: lower bound of plausible range, 5: upper bound; CMD stands for Cambodian Mekong Delta; TSL for Tonle Sap Lake; VMD for Vietnamese Mekong Delta).

	Simulation	SL at Kratie	SL to CMD	SL to TSL	SL to VMD	SL to VMD floodplains	Sedimentation in VMD floodplains	SL to the seas
	S0D0C0 [mil tons]	83.8	23.9	-7.5	52.5	12.4	4.1	40.1
D impacts	S0D1C0	-12%	-12%	-15%	-14%	-17%	-21%	-14%
	S0D2C0	-33%	-35%	-38%	-37%	-41%	-46%	-36%
	S0D3C0	-53%	-55%	-57%	-57%	-60%	-64%	-56%
	S0D4C0	-74%	-76%	-77%	-77%	-79%	-81%	-76%
	S0D5C0	-95%	-96%	-94%	-95%	-96%	-96%	-95%
C impacts	S0D0C1	-12%	-11%	-13%	-12%	-19%	-30%	-10%
	S0D0C2	0%	0%	0%	-1%	-1%	0%	-1%
	S0D0C3	12%	10%	13%	12%	21%	37%	9%
	S0D0C4	24%	17%	27%	26%	46%	84%	20%
	S0D0C5	36%	28%	40%	40%	70%	137%	30%
S impacts	S1D0C0	0%	0%	0%	0%	2%	7%	-1%
	S2D0C0	0%	1%	0%	0%	3%	11%	-2%
	S3D0C0	0%	1%	0%	0%	4%	14%	-2%
	S4D0C0	0%	1%	0%	-1%	5%	18%	-2%
	S5D0C0	0%	2%	0%	-1%	6%	23%	-3%
Cumulative impacts	S1D1C1	-25%	-24%	-26%	-25%	-31%	-40%	-23%
	S2D2C2	-37%	-35%	-38%	-38%	-39%	-39%	-37%
	S3D3C3	-51%	-50%	-50%	-51%	-48%	-41%	-52%
	S4D4C4	-71%	-71%	-69%	-71%	-67%	-58%	-72%
	S5D5C5	-94%	-94%	-92%	-94%	-92%	-89%	-94%
	S1D3C1	-62%	-62%	-63%	-62%	-66%	-73%	-60%
	S2D3C2	-56%	-55%	-57%	-57%	-58%	-59%	-57%
	S4D3C4	-45%	-45%	-44%	-45%	-36%	-19%	-48%
	S5D3C5	-39%	-41%	-37%	-39%	-24%	8%	-43%

The change in spatial sedimentation patterns in the VMD floodplains varies considerably depending on the level of climate change (Fig. 4.5 C-panel). The annual sedimentation changes from 4.1 *million tons* for the baseline period to 2.9, 5.6 or 9.7 *million tons* for the minimum, medium or maximum climate change level, respectively. The median climate change level predicts an increase in sedimentation rates and areas with a net gain in sedimentation. The latter point is most prominent in the remote parts of the VMD, i.e. eastern parts of the PoR. But also the remaining parts of the PoR receive larger amounts of sediment. This increase is much less visible in the LXQ, which is a direct consequence of the already present high number of high dike compartments and the current management scheme, as well as the significant backwater effects from the tide in the Gulf of Thailand, which limits flow and thus sediment transport into the LXQ. For the maximum climate change level a similar pattern can be observed, only with higher sedimentation rates and an even further extent of the sedimentation into the remote parts of the PoR. In the minimum level with decreasing flow and sediment load, the sedimentation pattern is similar to the baseline with moderately reduced sedimentation rates.

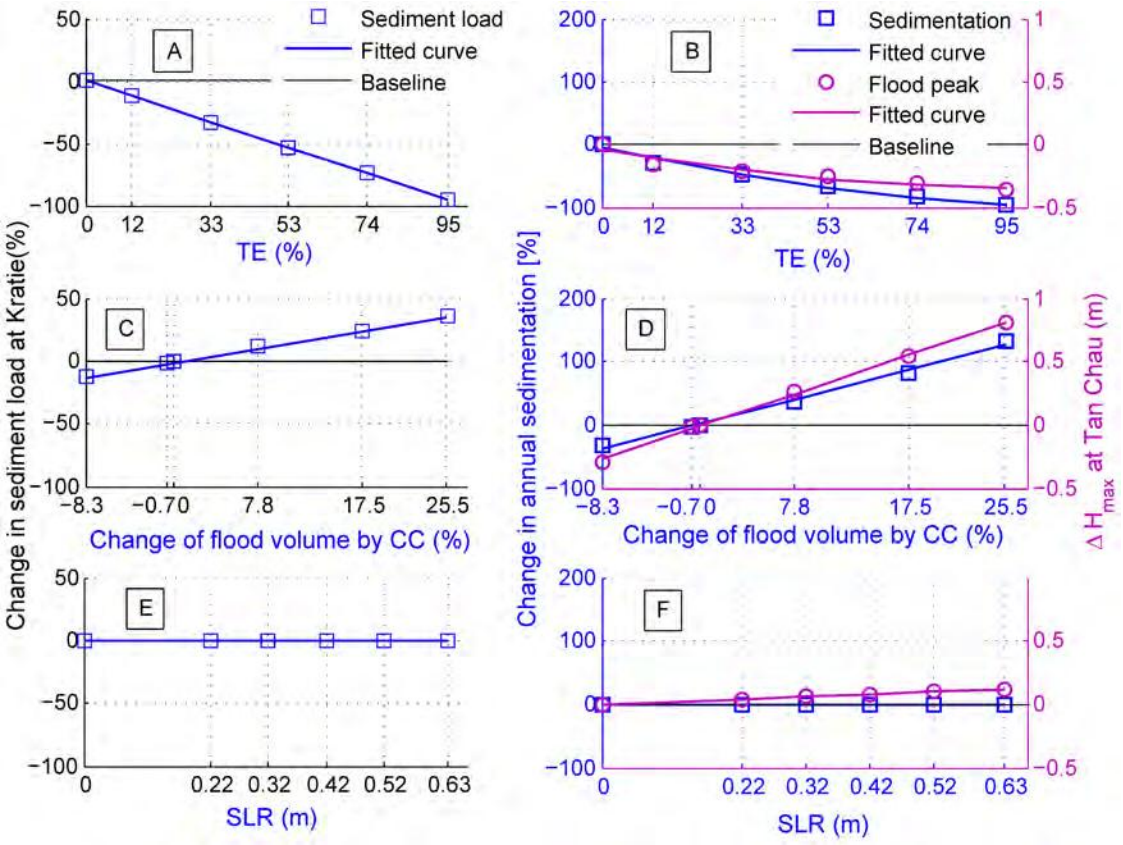

Figure 4.4: Single impacts of drivers. Changes in sediment load at Kratie (left column), and changes in annual sedimentation in the VMD and annual flood peak at station Tan Chau (right column) caused by A-B: hydropower development (TE), C-D: climate change (CC) impact in the MRB, and E-F: sea level rise (SLR).

4.4.3 Impacts of effective sea level rise

Sea level rise mainly impacts the sediment transport into the VMD floodplains and the sedimentation in the dike compartments of the VMD. A higher sea level results in higher water levels of Tien River and Hau River which increase the sediment load into the VMD floodplains by 2-6% and sedimentation in the dike compartments by 7-23% (Table 4.2; Fig. 4.4 E-F; Fig. 4.5 S-panel). The higher sedimentation in the VMD floodplains without increase of sediment supply from upstream reduces the sediment transport into the coastal area by 1÷ 3% (Table 4.2). and sediment load to the sea changes by -1% to -3%.

Sea level rise leads to additional dike compartments being flooded and thus expands the sedimentation area compared to the baseline level (Fig. 4.5 S-panel). Most of these additional sedimentation areas show very low sedimentation and are located in the remote parts of PoR where the tidal influence is limited by the larger distance to the coast. LXQ is much closer to the coast than PoR and thus directy influenced by the tide from Gulf of Thailand restricting the flow of SSC into the area. Thus hardly any changes in sedimentation can be observed in this area. The areas of higher future sedimentation are mostly located close to the main channel at the border of Cambodia and Vietnam.

4.4.4 Cumulative impacts on sediment transport and deposition

An overview of the possible future changes in sediment dynamics due to the combination of the three drivers is presented in Fig. 4.6, where annual sediment load to the different subsys-

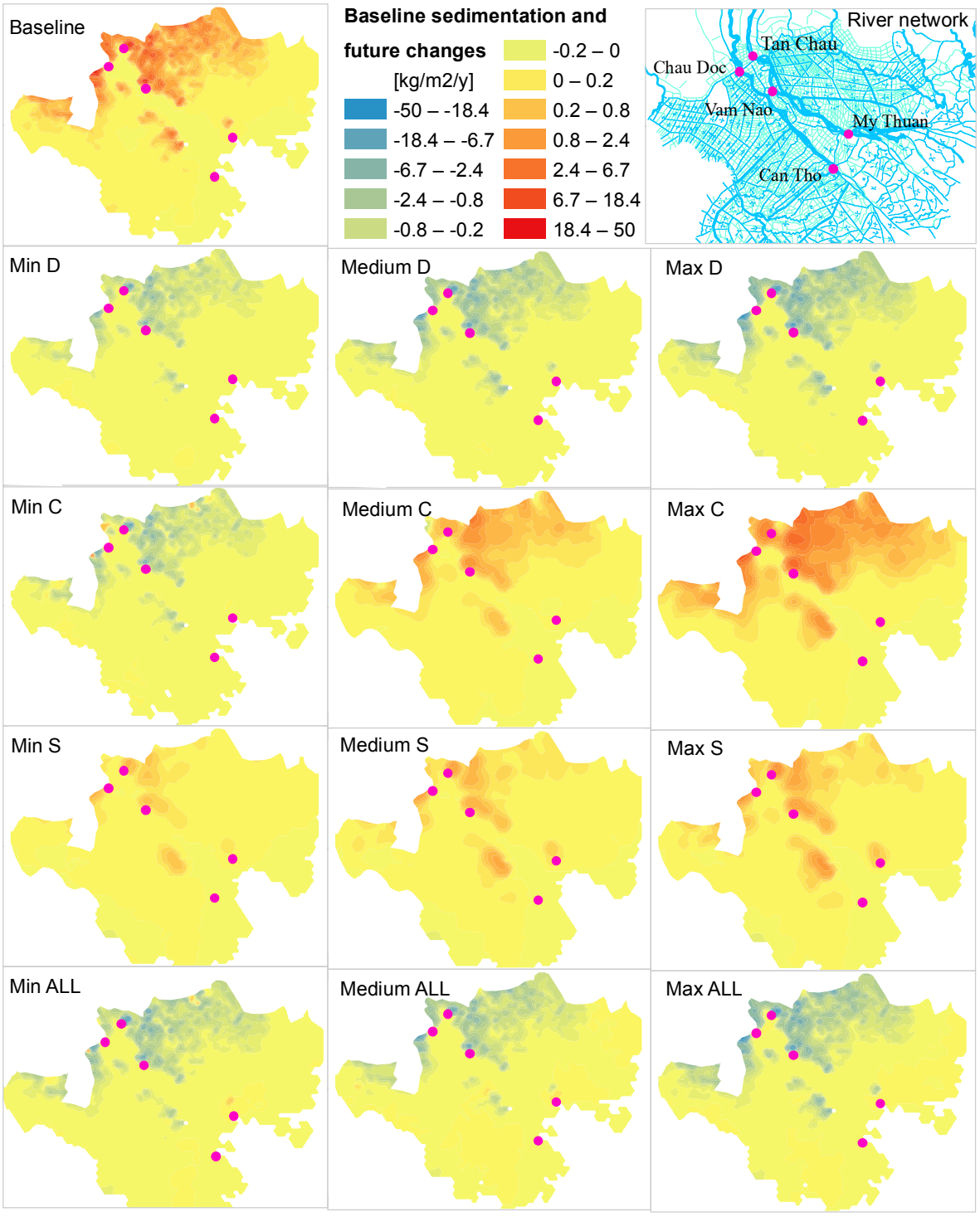

Figure 4.5: Spatial distribution of annual sediment deposition in the floodplain compartments of the Vietnam Mekong Delta (VMD) for the baseline condition, and the minimum, medium and maximum conditions of single drivers (hydropower development: D, climate change: C, sea level rise: S) and of combined drivers (ALL). The baseline map shows the simulated annual deposition, while all other maps show the differences in deposition to the baseline. The dots indicate the main gauging stations in the VMD for spatial reference.

tems of the MD and annual sedimentation in the Vietnamese floodplains are plotted for all 216 combinations. These results are grouped according to TE, representing different levels of hydropower development. It can be observed that the reduction of sediment load by sediment trapping of reservoirs drives the change in sediment dynamics in all subsystems, from Kratie through the entire delta down to the sea. Climate change has a second-order effect. It has, however, a large effect on the sedimentation in the Vietnamese floodplains. For most of the levels, climate change increases the sediment load and deposition, thus partly compensating the sediment trapping by reservoirs. Sea level rise has the smallest effect. It has impact only on the lower areas and, in addition, induces changes that are smaller than those by climate change. The results further reveal that the VMD floodplains are most sensitive to changes caused by the considered drivers.

Medium level of hydropower development (TE = 53%) is equivalent to the case of all planned dams being built without the implementation of the mainstream dams along the Lower Mekong River or with the mainstream dams realized as run-of-river hydropower plants (Kummu et al. [2010]). For this level of hydropower development, the annual sediment transport to the MD is reduced by 39-61% (Table 4.2). This reduction in sediment load propagates downstream and leads to similar reductions in the other subsystems. However, due to the large sensitivity of the Vietnamese floodplains to climate change and sea level rise, the sediment deposition in VMD varies from -73% to +8% (Fig. 4.6, Table 4.2).

Table 4.3: Annual floodplain sedimentation S [million tons] in diked compartments of the VMD as function of annual flood peak H [m] at gauge Tan Chau for given values of hydropower trapping efficiency TE [%].

Group	Fitted equation	Goodness of fit
TE=0	$S = 1.99H^2 - 12.61H + 20.44$	$R^2 = 0.998$
TE=0.12	$S = 1.86H^2 - 12.12H + 20.54$	$R^2 = 0.997$
TE=0.33	$S = 1.43H^2 - 9.41H + 16.12$	$R^2 = 0.997$
TE=0.53	$S = 1.06H^2 - 7.13H + 12.53$	$R^2 = 0.998$
TE=0.74	$S = 0.61H^2 - 4.18H + 7.47$	$R^2 = 0.998$
TE=0.95	$S = 0.12H^2 - 0.84H + 1.51$	$R^2 = 0.997$

For the condition of all dams built with the current design, the sediment load to the MD is dramatically reduced (TE = 95%), and sedimentation in the MD is very low due to the low suspended sediment concentration in the main rivers. Even the combined effect of the highest levels of climate change and sea level rise does not strongly change this result: the reduction in sedimentation in the VMD is 96% for the case where only maximum hydropower development is considered (S0D5C0), while it is 89% for the case where all three drivers have their strongest impact (S5D5C5) (Table 4.2).

If only those dams will be implemented which are under construction as of today, the case TE = 12% applies. In this condition the impacts on the sediment dynamics are small for the subsystems with low sensitivity to climate change and sea level rise. However, climate change and sea level rise may have a large impact on the sedimentation in the VMD. Depending on the levels, sedimentation may vary between -52% and +105% (Fig. 4.6). In case of TE = 0%, i.e. no further hydropower development, climate change and sea level rise have a mild impact

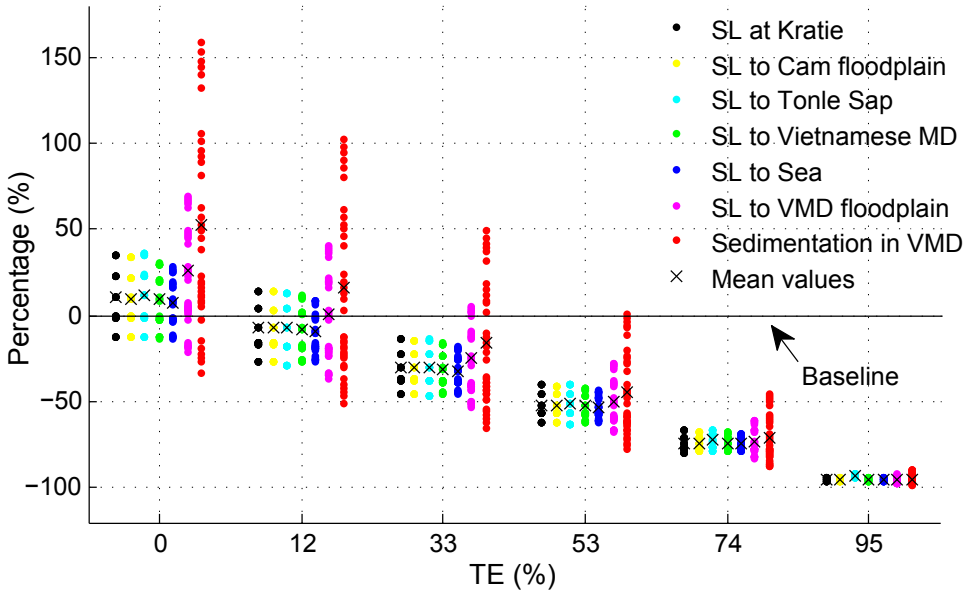

Figure 4.6: Change in sediment load (SL) and deposition relative to the baseline period in key areas of the Mekong Delta (MD). The 216 combinations are classified according to the six levels of trapping efficiency (TE) values. For each TE class 36 combinations (6 climate change levels x 6 sea level rise levels) are plotted. Frequently, groups of six levels can be distinguished for a given subsystem. These groups represent the different levels of climate change. The six levels within each group are the variability due to sea level rise. Note that sea level rise does not affect the upper areas of the MD, hence some of the cases lead to identical results for the upper areas. For the lower areas the 36 combinations form six clusters. These clusters are the effect of climate change, whereas the spread within each cluster shows the sea level rise effect.

on the sediment transport to the upper subsystems (e.g. from -12% to +35% at Kratie). However, a stronger impact is found on sedimentation in the VMD floodplains, ranging from -30% to + 137% in case of C only (Table 4.2, Fig. 4.4) and from -33% to +158% in case of C and S together (Fig. 4.6).

To have a more detailed view on the impacts of the three drivers on the VMD floodplains, Fig. 4.7 shows the peak flood [m] at Tan Chau, the upper border of the VMD, and the annual sedimentation in the floodplain compartments for the complete scenario space. The plausible ranges of the three drivers lead to a large range of sediment deposition and flood peak levels. Annual sedimentation varies from 0.1 *million tons* to 11.2 *million tons* while maximum water level varies from 3.9 m to 5.5 m. Again, the dominant role of hydropower development on sedimentation is visible, leading to strongly decreasing sediment deposition with increasing TE. Climate change and sea level rise have a very small effect on sedimentation in case of total hydropower development. This is different for smaller TE values (0%, 12%, 33%). For example, for TE = 33%, annual sedimentation varies from 1.5 *million tons* to 6.5 *million tons* depending on the level of climate change and sea level rise. The effect on flood peak shows, however, a different behavior, as climate change is the dominant control on flood peak. Hydropower development or sea level rise reduces or increases, respectively, the maximum water level in the flood season but to a much smaller extent than climate change. The aggregated results of the 216 levels can be described by curves fitted to the data of different TE values. The respective equations (compiled in Table 4.3)can be used to

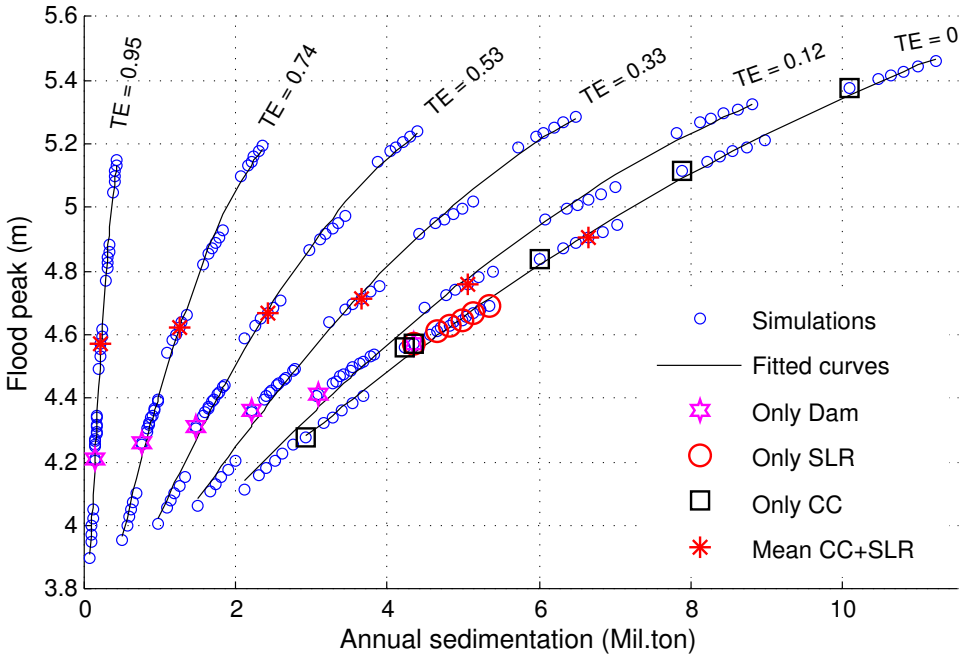

Figure 4.7: Annual sedimentation in the floodplain compartments of the Vietnam Mekong Delta (VMD) and annual flood peak at station Tan Chau (see location in Fig. 1) for all 216 combinations (blue circles) classified by trapping efficiency (TE) levels. Single effects and the mean value of the combined effect of climate change and sea level rise are marked. (Notation: S = effective sea level rise, D = dam development, C = climate change).

predict annual sedimentation in the compartments of the VMD for given TE and flood peak at station Tan Chau.

Fig. 4.5(ALL-panel) shows the combined spatially explicit impacts of the three drivers on sedimentation in the VMD. As discussed above, sediment trapping by dam construction is the dominant driver for floodplain sedimentation resulting in an overall sedimentation decrease across the VMD. However, the most significant changes are expected for the PoR, depicted by the high differences in sedimentation to the baseline. The effects are much less visible in the LXQ, which is mostly caused by the lower sedimentation in general in this area due to lower SSC reaching the area compared to PoR, the tidal impacts of the Gulf of Thailand, and the high number of high dike compartments blocking floodplain inundation (assuming that the current management practices do not change in future). The latter factor is the main reason for the negligible changes compared to the baseline in large parts of the LXQ (Fig. 4.5 ALL-panel).

4.5 Discussion and conclusions

In this study we quantified the impacts of climate change and hydropower development in the Mekong River Basin (MRB) and effective sea level rise on the sediment dynamics in the entire Mekong Delta (MD) for the future time period 2050-2060. A particular focus was a spatially differentiated quantification of the impacts of these drivers on floodplain sedimentation in the Vietnamese Mekong Delta (VMD). Currently, the uncertainties about the future evolution of these three drivers and consequently their impacts on the hydrology and sediment transport over the MRB are very high. Hence, we adopted a sensitivity-based approach and

investigated the impacts on the MD for plausible ranges of drivers. The combination of six different levels of development, including the present state as baseline, for each driver lead to 216 driver combinations, which are assumed to cover the entire range of possible future pathways, given the current knowledge.

This study is the first to assess the response of floodplain hydraulics and sediment dynamics in the entire Mekong Delta to a plausible range of change drivers for the upper and lower boundary of the delta. Existing studies assess the impact of the drivers on streamflow and/or sediment load reduction in the MRB only, i.e. excluding the MD. Thus possible changes in sediment dynamics and hydraulics in the rivers and particularly the floodplains of the MD are still largely unknown. The findings presented in this study thus extent the current knowledge in many aspects.

We found that hydropower development dominates the changes in the sediment dynamics of the MD in case of medium to high hydropower development. Under these circumstances sediment trapping by the reservoirs reduces dramatically the provision of sediment to the MD, with climate change acting as a second-order effect. Even the highest level of climate change, which increases the flood peak and the sediment input to the MD, does not significantly counteract the hydropower sediment reduction effect. Overall, sea level rise has the smallest effect on sediment dynamics. If median changes of all factors are assumed as the most likely pathway for sediment dynamics in the MD for the period 2050-2060, our findings indicate that the inundation extent would slightly increase in the VMD, particularly in the PoR, but the overall floodplain sedimentation is likely to be reduced significantly.

We further found that the floodplains in the VMD respond much more sensitive to changes in the drivers compared to the other subsystems of the MD. The observed changes include changes in sediment deposition, but also the spatial extent of floodplain sedimentation. Within the VMD floodplains, the Plain of Reeds (PoR) sees the largest changes, while changes in the Long Xuyen Quadrangle (LXQ) are much less mainly due to the current practice of blocking floodplain inundation by numerous high dike floodplain compartments.

4.5.1 Possible environmental consequences of high hydropower development

The presented results put the existing studies on basin wide sediment trapping by hydropower dams (Kummu et al. [2010], Kondolf et al. [2014]) into the context of impacts on the MD. In case all 136 planned dams will be built, drastic reductions of sediment input to the MD and floodplain sedimentation are expected. This is very likely to have dramatic consequences for ecology, agriculture and fishery in the MD. For example, Manh et al. [2014] showed that floodplain sedimentation can provide on average 50% of the nutrient requirements for rice crops, which is one of the reasons for the high agricultural productivity. This would be reduced to negligible amounts already with a basin wide sediment trapping efficiency of 53%. The important fishery sector is likely to suffer from sediment starvation because fish productivity is adapted to the nutrient and turbid conditions (Kummu and Varis [2007]; Valbo-Jørgensen et al. [2009]),and dams would block essential fish migration routes (Ziv et al. [2012]). The high impact of sediment and flood pulse could be mitigated, to some extent, by designing hydropower plants as run-of-river type plants. Another important aspect with

possibly severe environmental consequences is the increased erosion of the MD when sediment loads are decreasing. This is already observable (Tamura et al. [2010], Anthony et al. [2013]), but will be most likely aggravated by extended dam construction.

4.5.2 Uncertainties and future research directions

When using our results, one has to consider that the likely increased erosion within the riverbeds after damming is not considered explicitly. Particularly for the case of all 136 dams being built (TE = 95%), reduction in sediment load to the MD subsystems and in floodplain sedimentation could be smaller in the first years after dam closure due to 'cannibalism' of the river on its bed (Kondolf et al. [2014]). However, after stabilization of the riverbeds to a new equilibrium, sediment loads will be inevitably reduced in the long run. A dedicated morphological study of the Mekong River would be useful to reduce the uncertainty of this driver in our assessment. The presented combination set provides, however, estimates also for smaller sediment trapping rates, which can be used in case it becomes clear that bank erosion compensates sediment trapping significantly.

Another uncertainty source in this study is the link of SSC to discharge at Kratie derived through a sediment rating curve and the assumed linear reduction of SSC with future increased sediment trapping. However, we expect that the sediment dynamics of the whole Mekong system are described realistically, although the absolute values contain an, from our point of view, acceptable amount of uncertainty (as always when sediment rating curves are used). A watershed model for the MRB, which would include all major processes, such as sediment trapping of reservoirs and riverbed deposition/erosion, would reduce this uncertainty. But given the low quantity and quality of SSC measurements in the Mekong Basin (Walling [2008]), uncertainties would definitively remain due to insufficient model calibration.

We used the climate change impacts on hydrology of Lauri et al. [2012],which showed high uncertainty in the projection of the future flow regime. However, GCMs are developing fast and using the most recent runs of the GCMs might reduce this uncertainty. Therefore, the climate change impacts on the Mekong hydrology should be regularly updated to reflect the most up-to-date projections.

These future research directions could provide more information on the drivers, and thus the span of the plausible ranges could be reduced. This would lead to a smaller scenario space of sediment dynamics in the MD. However, as long as the ranges of the drivers defined here are not exceeded, appropriate future pathways are already at hand by the presented approach.

4.5.3 Concluding remarks

Given the high pace of dam development in the basin and projected climate change impacts on hydrology and sea level, the Mekong Delta is most likely facing significant changes in the foreseeable future. These changes might have severe impacts on the nature of the delta and on the livelihoods of millions of people. Our results call for urgent reconsideration of the future pathways in the Mekong River Basin. If the development continues with the current pace, our findings deliver valuable information on how and where the impacts on sediment dynamics are largest and they might be used as a starting point for mitigation measures.

Chapter 5 Main results and conclusions

The findings of this study contribute to the understanding of present status and future prospects of sediment transport and sediment deposition in the MD, especially in the ring dike floodplains in Vietnam. The study combine experimental work and numerical simulation to quantify and to project sediment transport and sedimentation in the delta.

The findings of the measurement campaign indicate that the deposited sediment is in cohesive grain size, and that the grain size and fractions of sediment-associated nutrients are homogenously distributed in the entire MD. Very high variability of sedimentation rate over the MD is found due to the fragmentation by the channel and ring-dike systems. The human interference in the floodplains strongly impacts the sedimentation rate. These findings provided data for the setup and calibration of a sediment transport model.

The model calibration procedure considers multiple objectives aiming at optimized spatial and temporal performance. By this procedure, a cohesive sediment transport model was developed and calibrated for the whole MD for the first time. The modelling quantified the distributions of sediment loads, suspended sediment concentrations and sediment deposition for the subsystems of the delta. Depending on the flood magnitude, annual sediment loads reaching the coast vary from 48% to 60% of the annual sediment load at the upper boundary (Kratie). Deposited sediment varies from 19% to 23% of the annual load at Kratie in Cambodian floodplains, and from 1% to 6% in the compartmented and diked floodplains in Vietnam. The result also provided tempo-spatial distributions of sedimentation rates and nutrient deposition rates in ring dike floodplains. Annual deposited nutrients (N, P, K), which are associated to the sediment deposition, provide on average more than 50% of mineral fertilizers typically applied for rice crops in non-flooded ring dike floodplains in Vietnam. Through the quantification of sediment and related nutrient input, the presented study provides a quantitative basis for estimating the benefits of annual Mekong floods for agriculture and fishery, and is an important information with regard to the assessment of the impacts of deltaic subsidence and climate change related sea level rise on delta morphology.

A sensitivity-based approach was applied to assess the response of the floodplain hydrology and sediment dynamics in the Delta to changing boundary conditions for the period 2050-2060. The drivers of change include hydropower development, climate change and the combined effects of sea level rise and deltaic subsidence. For each driver we derive a plausible range of future states and discretize it into different levels, resulting in 216 combinations. The results thus cover all plausible future pathways of sediment dynamics in the delta based on current knowledge. The results indicate that hydropower development dominates the changes in sediment dynamics of the Mekong Delta, while sea level rise has the smallest effect. The floodplains of the Vietnamese Mekong Delta are much more sensitive to the changes compared to the other subsystems of the delta. The median changes of the three drivers combined indicate that the inundation extent would increase slightly, but the overall

floodplain sedimentation would reduce by approximately 40%, and the sediment load to the Sea would diminish to half of the current rates. The maximum change in all drivers would mean a nearly 90% reduction of delta sedimentation, and a 95% reduction of the sediment reaching the sea. These findings provide new and valuable information on the possible future development of floodplain hydraulics and sedimentation in the Mekong Delta, and identify the areas that are most vulnerable to these changes.

5.1 Experimental measurement of floodplain sedimentation

5.1.1 Sedimentation monitoring on floodplains

The experimental approach proposes a procedure to monitor quantity and spatial variability of sediment and associated nutrient deposition in large and complex river floodplains including an uncertainty analysis. For the particular situation in the MD sediment mat traps were developed with a specific design suitable for trap retrieval from still inundated floodplains. Laboratory experiments were conducted to correct the sediment mass from traps retrieved from inundated floodplains. The parameter uncertainty associated to the correction function was determined and considered in the final uncertainty assessment of the deposition data. Furthermore, the cluster installation of three traps at each monitoring point allows a quantification, for the first time, of the sampling uncertainty of sediment deposition in floodplains. This design is particularly useful for the MD floodplain conditions and massive amount of traps. For smaller scale or other systems, sediment traps with the proposed design can be used as well, however the size and number of the traps at each location and in each floodplain should be re-scaled to the problem at hand.

The mat traps collect the cumulative deposition including new sediment from the upstream basin and locally re-suspended sediment. This needs to be considered when interpreting the results. The amount of locally re-suspended sediment is still an open question and its determination should be targeted by further studies.

5.1.2 High uncertainty in floodplain sedimentation

A Monte Carlo based uncertainty estimation is attached to the monitoring scheme. It consists of the (1) trap installation in clusters to quantify the deposition sampling uncertainty (aleatory uncertainty), (2) lab experiments of trap retrieval to quantify losses by sample collection from inundated floodplains (epistemic uncertainty). In order to reduce uncertainties, the trap size and the number of traps in the clusters should be increased. Larger traps could reduce both aleatory and epistemic uncertainties, while larger trap clusters could reduce aleatory uncertainty. The size and number of the traps is eventually a trade-off between measurement scale, resources and required data resolution.

The measured sediment deposition masses in floodplains are quite uncertain. The main uncertainty sources are the trap retrieval from inundated floodplains and human interference on the floodplains and floodplain inundation. The sediment retrieval uncertainties are systematic and quantifiable, while the variability caused by human interference and small-scale differences in deposition and re-suspension is an uncertainty source that is difficult to attribute to distinct factors. Human interference ranges from direct impact on the sedimentation, e.g. by

disturbances caused by fishing on the floodplains with nets, to indirect causes by regulating floodplain inundation by sluice gate control and operation of pumps. These uncertainties cause many difficulties in sedimentation modeling, because a detailed consideration of the disturbing factors is impossible to achieve in large-scale modeling studies.

5.1.3 Large-scale sediment properties

The measured data set of the large-scale floodplains provided new findings and reconfirmation of previous findings at smaller scales. The new findings include large-scale spatial variabilities of grain sizes and nutrient fractions, sedimentation rates for different floodplain types and regions, and the variability within dike-ring floodplains. The sedimentation rates are highly variable, both for the whole set of monitoring points and among the different compartments. The sediment properties, based on laboratory analysis, are generally cohesive, with grain sizes mostly in the clay-silt fraction. The high variability caused by human activities is an important property of sedimentation in the MD floodplains. The derived data provides crucial information for selecting and setting up of a large-scale sediment transport model described in chapter 3.

5.2 Present situation of sediment dynamics in the Mekong Delta

5.2.1 Large-scale sediment transport model of the MD

A large-scale cohesive sediment transport model was developed based on the quasi-2D hydrodynamic model of Dung et al. [2011a] and the experimental data. Through this model a large-scale quantification of sediment and sediment-related nutrient transport and deposition for the whole Mekong Delta has been achieved for the first time. The quasi-2D representation of floodplain compartments was implemented in the VMD only, because floodplain compartments can be found in the VND only. The low level of fragmentation of the CMD floodplains allows a simpler floodplain representation. Thus, the CMD floodplains are implemented in 1D by using wide cross-sections orthogonal to the main rivers. Hence, the model cannot quantify the spatial distribution of sedimentation in the CMD floodplains in detail, as the sedimentation is given for the cross section as a whole.

It is also noteworthy that the model excludes local erosion caused by human interferences on floodplains. The advantage of this approach is to provide a distinct quantification of the new annual sediment imported to the delta, thus allowing to quantify the annual flood benefit in terms of nutrient deposition. However, the model cannot simulate the possible remobilization of new sediment, but this effect is assumed to be rather small compared to the possible mobilization of old sediment occurring during the initial floodplain inundation. This approach is thus not aiming at the closest representation of reality, which is almost impossible due to the large human interference on local sedimentation processes. It is rather aiming at a quantification of the new annual sediment and nutrient input and spatial distribution in the Mekong Delta.

The hydraulic structures in the model include dikes, sluice gates and gate operations. These data stem from different sources which might cause inconsistencies and model errors. To

minimize these errors, the data was revised by an analysis of water masks from satellite images combined with maximum simulated water levels from the hydraulic model. However, some uncertainty remains, and higher resolution data of hydraulic structures are needed for further refinement of the model.

5.2.2 Calibration strategy for large-scale multi-objective domains

The calibration strategy of the large-scale sediment transport model consists of a zonation of the model domain, a sensitivity analysis of parameters and a two-stage calibration. The zonation and sensitivity analysis determined the minimum number of calibration parameters, while two-stage calibration is applied to reduce the degrees of freedom in the optimization problem. The hydrodynamic module with three objective functions and sediment transport module with three other objective functions were calibrated individually. This approach significantly reduces the complexity of multi-objective optimization and the runtime of calibration. Given appropriate data, this approach could be applied in any other hydrological system if the computation power resource is limited and the model results in first stage are independence from the model results in the second stage. However, this procedure is not applicable where flux density is highly variable and the interaction of hydrodynamic and sediment transport is significant.

5.2.3 Sediment transport and sediment deposition

The sediment dynamics in the whole MD are quantified for the first time. The results are an important step forward in understanding the suspended sediment transport and deposition in the Mekong delta including sediment load and sediment deposition in the subsystems of the delta. For the Tonle Sap Lake the result are in line with other sediment studies, but for other subsystems the results are the first to be published. Comparing the results between VMD and CMD, the sediment load and sediment deposition in CMD is much higher than in VMD. It means that the dike-ring systems in VMD floodplains are strongly influencing the sediment transport and deposition. It also means that if the channels and dike systems are redesigned, the floodplains could get higher sediment load and consequently sedimentation. Suggestions for the redesign derived from the model results are given in chapter 3.

The dike levels and sluice gates play a key role in controlling sediment deposition in ring-dike compartments causing different patterns of sedimentation during different flood stages. A general recommendation derived from the model results is that the sluice gates should be controllable throughout the flood season, and a cost-benefit analysis should be performed to determine the optimal dike levels and sluice gate operations over the VMD.

By ignoring the re-suspension process, the model results enable a quantification of the nutrient deposition rate stemming from the Mekong Basin. The deposited nutrient rates (N,P,K) in low dike systems are equivalent to more than 50% of mineral fertilizers annually applied to a rice crop in Vietnam. This quantification can be used to assess the nutrient deficit caused by fully flood controlled dike systems in the VMD. It does also allow a cost-benefit analysis of natural inundation versus dike construction and implementation of three crops per year.

5.2.4 Contributions of the understanding of sediment-related aspects

The study shows that the Mekong River Basin is a significant sediment contributor to the Mekong Delta. The annual spatial average floodplain deposition of 0.3-1.8 *mm* is a unique and important source that counterbalances land subsidence, as well as to some extent sea level rise in the MD. In order to increase or at least keep that source the sediment trapping of the dams in the Mekong basin has to be minimized and the complete blocking of floodplain inundation for an increased agricultural production should be revised.

The model results quantify sediment load and sediment concentration for the subsystems of the MD. This information can be used as boundary conditions for detailed studies on sediment transport and erosion along the rivers, the coast and the subaqueous delta. This is currently also a hot topic, as the coastline of the Mekong Delta is subject to considerable erosion (Tamura et al. [2010], Anthony et al. [2013]).

As the model ignored erosion and re-suspension processes, it can be used to quantify impacts of the changes in upstream and downstream boundary conditions to the sediment dynamics in the MD directly. The changes include hydropower development, climate change, sea level rise and land subsidence very important but unsolved issues in the discussion about the future of the MD.

5.3 Future sediment dynamics in the Mekong Delta

5.3.1 Sensitivity-based approach

As the large-scale study domain is affected by several change drivers, using a conventional scenario approach for projecting future sediment dynamics may have a very limited meaning. Hence, a sensitivity- based approach was chosen, by which all possible future pathways of sediment dynamics in the MD are illustrated. The approach can cover the uncertainties inherent in the estimation of future hydropower development, climate change and sea level rise and their combinations. By setting appropriate wide ranges of changes, the combinations can cover new projections, new knowledge or new political boundary conditions in years to come. The approach also allows rapid appraisal of new information, as long as the drivers and their combinations are contained within the defined scenario space. Another advantage is that this approach can utilize the results of diverse studies. All input needed is the plausible range for the future impact of the different drivers. This information can be extracted from available studies. Hence, different assumptions and inconsistencies between used studies do not play a major role, as would be the case for a conventional scenario approach.

5.3.2 The most influencing change driver and the most affected area

The results show all possible combinations of upstream and downstream change driver on the future sediment dynamics. Thus, it allows ranking the most influential driver for each subsystem and the areas most responsive to the changes. This ranking is contributing to the understanding of the overall future evolution of sediment dynamics in the MD, and the evolution under each single driver. The identification of the dominant impact of hydropower development is an important result potentially contributing to a comprehensive environmental impact assessment of hydropower development in the MRB to downstream areas. It extends

the knowledge on hydropower and climate change impacts in the Mekong River Basin, which normally ends at the upstream boundary of the MD (Kratie). The identification of the most sensitive area - the VMD floodplains - is crucially important, as a first step, for targeting mitigation measures and future development plans in the MD.

5.3.3 Future pathways of sediment dynamics

Although the impact analysis result in a wide range of possible futures, the median results of future characteristics are defined by higher flood magnitude and lower sediment load into all the subsystems. The sedimentation in VMD floodplains is characterized by expanded spatial distribution with significant lower sedimentation rates. The affected area is mainly in PoR rather than in LXQ. The other subsystems are uniformly responding to changes of the upstream boundary, and the Tonle Sap and Cambodian subsystem are not affected by the changes at the downstream boundary. Overall, the medium future sediment dynamics of the MD show a loss of 51-53% suspended sediment in the channel network, and a 44% reduction of sedimentation in floodplains.

Given the high pace of dam development in the basin and predicted climate change impacts on hydrology and sea level, the Mekong Delta is most likely facing significant changes in the foreseeable future. These changes might have severe impacts on the nature of the delta and consequently livelihoods of millions of people. Our results thus reinforce the previous findings of the possible drastic impacts of the ongoing development and call for urgent reconsideration of the future pathways in the Mekong. Would the development continue with the current pace, our findings deliver valuable information on how and where the impacts on sediment dynamics are largest. This information might be used as a starting point for mitigation measures.

5.4 Outlook

This thesis provided a wealth of data and model results and, for the first time, a quantification of the spatio-temporal variation of sediment dynamics in the MD for the present and future states. To further improve this knowledge and to design specific mitigation measures, the following activities are proposed:

Monitoring sediment:

To improve the sedimentation monitoring in the MD, the number of monitoring points in the floodplain compartments should be defined according to the floodplain topography, number and location of flood control structures and the presented sedimentation patterns in different floodplains. Fishing activities are the most disturbing factors for the sediment traps, thus support from landowners and local communities is essential to protect installed traps and improve measurement data.

For an improved understanding and simulation of the sediment transport in channels and floodplains in VMD intensive field campaigns need to be performed in order to quantify the human interference in the deposition/erosion process during the flood season.

A higher resolution of SSC measurements in the MRB, especially daily measurements of

SSC in mainstream stations in Cambodia are needed for more reliable sediment boundary condition. In addition, measurements of SSC in main channels in daily or neap-spring tides resolution are also needed in the VMD to improve model performance in the intricate floodplain-channel system of the VMD.

Refinement and update of MD model: Topological data of rivers, channels, floodplains and hydraulic structures should by updated and implemented in the MD model regularly to catch ongoing floodplain modificartions. A finer resolution, especially for the floodplains in Cambodia, is also advisable. The dike and sluice gate data including operations in the VMD should be upgraded for better describing the floodplain dynamics and the human dimension in the model.

Development of a catchment sediment model: A conceptual watershed model including dam operation, dam sediment trapping and riverbed deposition/erosion would be very helpful for a better prediction of the sediment delivery from the MRB to the MD and the impact of the change drivers.

Bibliography

M. Abbott and F. Ionescu. On the numerical computation of nearly-horizontal flows. *J. Hydraul. Eng.*, 5:97–117, 1967.

E. J. Anthony, M. Goichot, G. Brunier, P. Dussouillez, M. Provansal, and F. Dolique. Widespread erosion of the Mekong River Delta: from construction to destruction phase? *Mekong Environ. Symp. 2013*, HCM city -, 2013.

H. Apel, A. H. Thieken, B. Merz, and G. Bl. Flood risk assessment and associated uncertainty. *Nat. Hazards Earth Syst. Sci.*, 4:295–308, 2004.

H. Apel, A. H. Thieken, B. Merz, and G. Blöschl. A Probabilistic Modelling System for Assessing Flood Risks. *Nat. Hazards*, 38(1-2):79–100, May 2006. ISSN 0921-030X. doi: 10.1007/s11069-005-8603-7.

H. Apel, B. Merz, and A. H. Thieken. Quantification of uncertainties in flood risk assessments. *Int. J. River Basin Manag.*, 6(2):149–162, 2008.

M. E. Arias, T. a. Cochrane, M. Kummu, H. Lauri, G. W. Holtgrieve, J. Koponen, and T. Piman. Impacts of hydropower and climate change on drivers of ecological productivity of Southeast Asia's most important wetland. *Ecol. Modell.*, 272:252–263, Jan. 2014. ISSN 03043800. doi: 10.1016/j.ecolmodel.2013.10.015. URL `http://linkinghub.elsevier.com/retrieve/pii/S0304380013004821`.

N. E. M. Asselman and H. Middelkoop. Floodplain sedimentation: Quantities, patterns and processes. *Earth Surf. Process. Landforms*, 20(6):481–499, Sept. 1995. ISSN 01979337. doi: 10.1002/esp.3290200602.

M. Baborowski, O. Büttner, P. Morgenstern, F. Krüger, I. Lobe, H. Rupp, and W. V. Tümpling. Spatial and temporal variability of sediment deposition on artificial-lawn traps in a floodplain of the River Elbe. *Environ. Pollut.*, 148(3):770–8, Aug. 2007. ISSN 0269-7491. doi: 10.1016/j.envpol.2007.01.032.

E. Baran. Environmental assessment of hydropower on the Mekong mainstream Mekong fisheries and mainstream dams. *MRC*, (October):1–146, 2010.

E. Baran. Impact of sediment reduction on fish - State of knowledge. *Workshop*, (HCM city - Vietnam):7–8 OCT, 2013.

O. Büttner, K. Otte-Witte, F. Krüger, G. Meon, and M. Rode. Numerical modelling of floodplain hydraulics and suspended sediment transport and deposition at the event scale in the middle river Elbe, Germany. *Acta Hydrochim. Hydrobiol.*, 34(3):265–278, June 2006. ISSN 0323-4320. doi: 10.1002/aheh.200500626.

V. T. Chow. Open-channel hydraulics. *McGraw-Hill B. Co.*, page 728, 1959. doi: ISBN07-010776-9.

J. M. Delgado, H. Apel, and B. Merz. Flood trends and variability in the Mekong river. *Hydrol. Earth Syst. Sci.*, 14(3):407–418, Mar. 2010. ISSN 1607-7938. doi: 10.5194/hess-14-407-2010. URL `http://www.hydrol-earth-syst-sci.net/14/407/2010/`.

T. W. Doyle, R. H. Day, and T. C. Michot. Development of Sea Level Rise Scenarios for Climate Change Assessments of the Mekong Delta. *U.S. Geol. Surv.*, Open-File(1165):110, 2010. URL `http://pubs.usgs.gov/of/2010/1165/`.

N. V. Dung. Multi-objective automatic calibration of hydrodynamic models – development of the concept and an application in the Mekong Delta (PhD dissertation). *Univ. Stuttgart*, page 177, 2011b. URL `http://elib.uni-stuttgart.de/opus/volltexte/2012/6831/`.

N. V. Dung, B. Merz, A. Bárdossy, T. D. Thang, and H. Apel. Multi-objective automatic calibration of hydrodynamic models utilizing inundation maps and gauge data. *Hydrol. Earth Syst. Sci.*, 15(4):1339–1354, Apr. 2011a. ISSN 1607-7938. doi: 10.5194/hess-15-1339-2011.

J. Eastham, F. Mpelasoka, C. Ticehurst, P. Dyce, R. Ali, and M. Kirby. Mekong River Basin Water Resources Assessment : Impacts of Climate Change. *CSIRO Water a Heal. Ctry. Natl. Res. Flagsh.*, page 153, 2008. URL `http://wacc.edu.vn/vi/wp-content/uploads/2013/06/wfhc-MekongWaterResourcesAssessment.pdf`.

J. Ericson, C. Vorosmarty, S. Dingman, L. Ward, and M. Meybeck. Effective sea-level rise and deltas: Causes of change and human dimension implications. *Glob. Planet. Change*, 50(1-2):63–82, Feb. 2006. ISSN 09218181. doi: 10.1016/j.gloplacha.2005.07.004.

K. Fu, D. He, and X. Lu. Sedimentation in the Manwan reservoir in the Upper Mekong and its downstream impacts. *Quat. Int.*, 186(1):91–99, Aug. 2007. ISSN 10406182. doi: 10.1016/j.quaint.2007.09.041.

K. D. Fu and D. M. He. Analysis and prediction of sediment trapping efficiencies of the reservoirs in the mainstream of the Lancang River. *Chinese Sci. Bull.*, 52(S2):134–140, Dec. 2007. ISSN 1001-6538. doi: 10.1007/s11434-007-7026-0.

GSO. General statistic office - Statistic Yearbook of Vietnam 2012. *Gen. Stat. Off. Vietnam*, page 150, 2012. URL `http://www.gso.gov.vn/default.aspx?tabid=512&idmid=5&ItemID=14153`.

A. Gupta. *Large rivers: geomorphology and management (Book)*. John Wiley & Sons, Ltd, The Atrium, Southern Gate, Chichester, West Sussex PO19 8SQ, England, 2008. ISBN 9780470849873.

H. Gupta, S.-J. Kao, and M. Dai. The role of mega dams in reducing sediment fluxes: A case study of large Asian rivers. *J. Hydrol.*, 464-465:447–458, Sept. 2012. ISSN 00221694. doi: 10.1016/j.jhydrol.2012.07.038.

T. Heege, V. Kiselev, M. Wettle, and N. N. Hung. Operational multi-sensor monitoring of turbidity for the entire Mekong Delta. *Int. J. Remote Sens.*, 35(8):2910–2926, 2014. doi: 10.1080/01431161.2014.890300.

C. Hoanh. Impacts of climate change and development on Mekong flow regimes First assessment - 2009. *MRC*, (29):104, 2010. URL `http://www.mrcmekong.org/assets/Publications/technical/tech-No29-impact-of-climate-change.pdf`.

N. N. Hung, J. M. Delgado, V. K. Tri, L. M. Hung, B. Merz, A. Bárdossy, and H. Apel. Floodplain hydrology of the Mekong Delta, Vietnam. *Hydrol. Process.*, 26(5):674–686, Feb. 2012. ISSN 08856087. doi: 10.1002/hyp.8183.

N. N. Hung, J. M. Delgado, A. Güntner, B. Merz, A. Bárdossy, and H. Apel. Sedimentation in the floodplains of the Mekong Delta, Vietnam. Part I: suspended sediment dynamics. *Hydrol. Process.*, 28(7):3132–3144, Mar. 2014a. ISSN 08856087. doi: 10.1002/hyp.9856.

N. N. Hung, J. M. Delgado, A. Güntner, B. Merz, A. Bárdossy, and H. Apel. Sedimentation in the floodplains of the Mekong Delta, Vietnam Part II: deposition and erosion. *Hydrol. Process.*, 28(7):3145–3160, Mar. 2014b. ISSN 08856087. doi: 10.1002/hyp.9855.

ICEM. Strategic environmental assessment of hydropower on the Mekong mainstream-Final report. *Mekong River Comm.*, (October):1–198, 2010. URL `http://www.mrcmekong.org/assets/Publications/Consultations/SEA-Hydropower/SEA-FR-summary-13oct.pdf(lastaccess4/5/2014)`.

IPCC. Climate Change 2007: The Physical Science Basis. *Intergov. Panel Clim. Chang.*, (Technical Summary):19–91, 2007.

IPCC. Climate Change 2013: The Physical Science Basis. *Intergov. Panel Clim. Chang.*, (Technical Summary):33–115, 2014.

N. Kabeya, T. Kubota, A. Shimizu, T. Nobuhiro, Y. Tsuboyama, S. Chann, and N. Tith. Isotopic investigation of river water mixing around the confluence of the Tonle Sap and Mekong rivers. *Hydrol. Process.*, 22:1351–1358, 2008. doi: 10.1002/hyp.6944.

S. Kameyama, H. Shimazaki, S. Nohara, T. Sato, Y. Fujii, and K. Kudo. Hydrological and Sediment Transport Simulation To Assess the Impact of Dam Construction in the Mekong River Main Channel. *Am. J. Environ. Sci.*, 9(3):247–258, Mar. 2013. ISSN 1553-345X. doi: 10.3844/ajessp.2013.247.258. URL `http://thescipub.com/abstract/10.3844/ajessp.2013.247.258`.

S. M. Kashefipour and R. a. Falconer. Longitudinal dispersion coefficients in natural channels. *Water Res.*, 36(6):1596–608, Mar. 2002. ISSN 0043-1354.

M. Keskinen, M. Kummu, M. Käkönen, and O. Varis. Mekong at the crossroads: next steps for impact assessment of large dams. *Ambio*, 41(3):319–24, May 2012. ISSN 0044-7447. doi: 10.1007/s13280-012-0261-x. URL `http://www.ncbi.nlm.nih.gov/pubmed/22528981`.

T. Q. Khuong, T. Thi, N. Huan, P. S. Tan, and R. Buresh. Effect of site specific nutrient management on grain yield, nutrient use efficiency and rice production profit in the Mekong Delta. *Omonrice*, 158:153–158, 2007.

D. G. Kingston, J. R. Thompson, and G. Kite. Uncertainty in climate change projections of discharge for the Mekong River Basin. *Hydrol. Earth Syst. Sci.*, 15(5):1459–1471, May 2011. ISSN 1607-7938. doi: 10.5194/hess-15-1459-2011. URL `http://www.hydrol-earth-syst-sci.net/15/1459/2011/`.

G. Kondolf, R. Z. K, and M. J.T. Dams on theMekong: Cumulative sediment starvation. *Water Resour. Res.*, 50:1–12, 2014. doi: 10.1002/2013WR014651.

R. Krone. Flume studies of the transport of sediment in estuarial shoaling process: Final report. *Univ. California, Berkeley, Calif.*, page 110, 1962. URL `http://babel.hathitrust.org/cgi/pt?id=uc1.31822020695276;view=1up;seq=9`.

C. Kuenzer, H. Guo, J. Huth, P. Leinenkugel, X. Li, and S. Dech. Flood Mapping and Flood Dynamics of the Mekong Delta: ENVISAT-ASAR-WSM Based Time Series Analyses. *Remote Sens.*, 5(2):687–715, Feb. 2013. ISSN 2072-4292. doi: 10.3390/rs5020687.

M. Kummu and O. Varis. Sediment-related impacts due to upstream reservoir trapping, the Lower Mekong River. *Geomorphology*, 85(3-4):275–293, Mar. 2007. ISSN 0169555X. doi: 10.1016/j.geomorph.2006.03.024.

M. Kummu, D. Penny, J. Sarkkula, and J. Koponen. Sediment: curse or blessing for Tonle Sap Lake? *Ambio*, 37(3):158–63, May 2008. ISSN 0044-7447. URL `http://www.ncbi.nlm.nih.gov/pubmed/18595269`.

M. Kummu, X. Lu, J. Wang, and O. Varis. Basin-wide sediment trapping efficiency of emerging reservoirs along the Mekong. *Geomorphology*, 119(3-4):181–197, July 2010. ISSN 0169555X. doi: 10.1016/j.geomorph.2010.03.018.

M. Kummu, S. Tes, S. Yin, P. Adamson, J. Józsa, J. Koponen, J. Richey, and J. Sarkkula. Water balance analysis for the Tonle Sap Lake-floodplain system. *Hydrol. Process.*, 28(4):1722–1733, Feb. 2014. ISSN 08856087. doi: 10.1002/hyp.9718.

D. Lamberts and J. Koponen. Flood pulse alterations and productivity of the Tonle Sap ecosystem: a model for impact assessment. *Ambio*, 37(3):178–84, May 2008. ISSN 0044-7447. URL `http://www.ncbi.nlm.nih.gov/pubmed/18595272`.

H. Lauri, H. de Moel, P. J. Ward, T. a. Räsänen, M. Keskinen, and M. Kummu. Future changes in Mekong River hydrology: impact of climate change and reservoir operation on discharge. *Hydrol. Earth Syst. Sci. Discuss.*, 9(5):6569–6614, May 2012. ISSN 1812-2116. doi: 10.5194/hessd-9-6569-2012. URL `http://www.hydrol-earth-syst-sci-discuss.net/9/6569/2012/`.

P. Leinenkugel, C. Kuenzer, N. Oppelt, and S. Dech. Characterisation of land surface phenology and land cover based on moderate resolution satellite data in cloud prone areas — A novel product for the Mekong Basin. *Remote Sens. Environ.*, 136:180–198, Sept. 2013. ISSN 00344257. doi: 10.1016/j.rse.2013.05.004.

C. Liu, Y. He, E. Walling, and J. Wang. Changes in the sediment load of the Lancang-Mekong River over the period 1965–2003. *Sci. China Technol. Sci.*, 56(4):843–852, Feb. 2013. ISSN 1674-7321. doi: 10.1007/s11431-013-5162-0.

X. Liu and D. He. A new assessment method for comprehensive impact of hydropower development on runoff and sediment changes. *J. Geogr. Sci.*, 22(6):1034–1044, Nov. 2012. ISSN 1009-637X. doi: 10.1007/s11442-012-0981-7.

X. Lu, M. Kummu, and C. Oeurng. Reappraisal of sediment dynamics in the Lower Mekong River, Cambodia. *Earth Surf. Process. Landforms*, pages n/a–n/a, Apr. 2014. ISSN 01979337. doi: 10.1002/esp.3573.

X. X. Lu and R. Y. Siew. Water discharge and sediment flux changes over the past decades in the Lower Mekong River: possible impacts of the Chinese dams. *Hydrol. Earth Syst. Sci.*, 10(2):181–195, Mar. 2006. ISSN 1607-7938. doi: 10.5194/hess-10-181-2006.

N. V. Manh, B. Merz, and H. Apel. Sedimentation monitoring including uncertainty analysis in complex floodplains: a case study in the Mekong Delta. *Hydrol. Earth Syst. Sci.*, 17(8): 3039–3057, Aug. 2013. ISSN 1607-7938. doi: 10.5194/hess-17-3039-2013.

N. V. Manh, N. V. Dung, N. N. Hung, B. Merz1, and H. Apel1. Large-scale suspended sediment transport and sediment deposition in the Mekong Delta. *Hydrol. Earth Syst. Sci. Discuss.*, 11(1):1–52, Jan. 2014. ISSN 1812-2116. doi: 10.5194/hessd-11-1-2014. URL `http://www.hydrol-earth-syst-sci-discuss.net/11/1/2014/`.

MARD. Water resources planning of the Vietnamese Mekong Delta adaptation with climate change and sea level rise. *Rep. - Vietnamese Minist. Agric. Rural Dev.*, 2012. URL `http://www.vncold.vn/Web/Content.aspx?distid=2927(lastaccess:2013April)`.

W. Mendenhall, R. J. Beaver, and B. M. Beaver. *Introduction to Probability and Statistics.* Brooks/Cole, Cengage Learning, 2009.

B. Merz and A. H. Thieken. Separating natural and epistemic uncertainty in flood frequency analysis. *J. Hydrol.*, 309(1-4):114–132, July 2005. ISSN 00221694. doi: 10.1016/j.jhydrol.2004.11.015.

H. Middelkoop. Floodplain Sedimentation - Methods, Patterns, and Processes, A Review with exambles from the lower Rhine, the Netherlands. *Encycl. Hydrol. Sci.*, 84:1242 –1282, 2005. doi: 10.1002/0470848944.hsa085.

J. D. Milliman and K. L. Farnsworth. *River Discharge to the Coastal Ocean: A Global Synthesis (book).* Cambridge University Press, Dec. 2011. ISBN 9780521879873. doi: 10.5670/oceanog.2011.108.

MONRE. Climate changes and sea level rise scenarios for Vietnam. *Minist. Nat. Resour. Environ.*, page 112, 2012.

MRC. Annual Mekong Flood Report 2006. *Mekong River Comm.*, pages 1–94, 2007. URL `http://www.mrcmekong.org/assets/Publications/basin-reports/Annual-Mekong-Flood-Report-2006.pdf(lastaccess:15/04/2014)`.

MRC. The Flow of the Mekong. *Mekong River Comm.*, (2):1–12, 2009. URL `http://www.mrcmekong.org/assets/Publications/report-management-develop/MRC-IM-No2-the-flow-of-the-mekong.pdf(lastaccess:15/04/2014)`.

MRC. Multi-functionality of Paddy Fields over the Lower Mekong Basin. *Tech. Pap. Mekong River Comm.*, (26), 2010a. URL `http://www.mrcmekong.org/assets/Publications/technical/tech-No26-multi-functionality-of-paddy-field.pdf(lastaccess:7April,2013)`.

MRC. Annual Mekong Flood Report 2009. *Mekong River Comm.*, pages 1–95, 2010b. URL http://www.mrcmekong.org/assets/Publications/basin-reports/Annual-Mekong-Flood-Report-2009.pdf(lastaccess:15/04/2014).

MRC. Annual Mekong Flood Report 2010. *Mekong River Comm.*, pages 1–76, 2011a. URL http://www.mrcmekong.org/assets/Publications/basin-reports/Annual-Mekong-Flood-Report-2010.pdf(lastaccess:15/04/2014).

MRC. Flood Situation Report 2011. *Tech. Pap. Mekong River Comm.*, (36), 2011b. URL http://www.mrcmekong.org/assets/Publications/technical/Tech-No36-Flood-Situation-Report2011.pdf(lastaccess:7May2013).

MRC. Basin Development Plan Programme, Phase 2: Assessment of Basin-wide Development Scenarios. *Mekong River Comm.*, 1(Main report):254, 2011c. URL http://www.mrcmekong.org/assets/Publications/basin-reports/BDP-Assessment-of-Basin-wide-Dev-Scenarios-2011.pdf.

MRC/DMS. Origin, fate and impacts of the Mekong sediments. *Mekong River Comm.*, page 53, 2009. URL http://www.mpowernetwork.org/Knowledge_Bank/Key_Reports/PDF/Research_Reports/DMS_Sediment_Report.pdf(lastaccess:15/04/2014).

MRCS/WUP-FIN. Research findings and recommendations. *Mekong River Comm.*, 2007. URL http://wacc.edu.vn/vi/wp-content/uploads/2013/06/wup-fin2_final-report_part2.pdf(lastaccess:15/04/2014).

O. Navratil, M. Esteves, C. Legout, N. Gratiot, J. Nemery, S. Willmore, and T. Grangeon. Global uncertainty analysis of suspended sediment monitoring using turbidimeter in a small mountainous river catchment. *J. Hydrol.*, 398(3-4):246–259, Feb. 2011. ISSN 00221694. doi: 10.1016/j.jhydrol.2010.12.025.

F. Pappenberger and K. J. Beven. Ignorance is bliss: Or seven reasons not to use uncertainty analysis. *Water Resour. Res.*, 42(5):n/a–n/a, May 2006. ISSN 00431397. doi: 10.1029/2005WR004820.

D. T. K. Phuong and D. V. Xe. Assessment for efficiency finance of rice monoculture and rice – upland crops systems at Cai Lay district, Tien Giang province. *J. Sci. -CTU*, 18a: 220–227, 2011.

T. Piman, T. Lennaerts, and P. Southalack. Assessment of hydrological changes in the lower Mekong Basin from Basin-Wide development scenarios. *Hydrol. Process.*, 27(15):2115–2125, July 2013. ISSN 08856087. doi: 10.1002/hyp.9764. URL http://doi.wiley.com/10.1002/hyp.9764.

C. Prudhomme, R. Wilby, S. Crooks, a.L. Kay, and N. Reynard. Scenario-neutral approach to climate change impact studies: Application to flood risk. *J. Hydrol.*, 390(3-4):198–209, Sept. 2010. ISSN 00221694. doi: 10.1016/j.jhydrol.2010.06.043. URL http://linkinghub.elsevier.com/retrieve/pii/S0022169410004117.

T. a. Räsänen, J. Koponen, H. Lauri, and M. Kummu. Downstream Hydrological Impacts of Hydropower Development in the Upper Mekong Basin. *Water Resour. Manag.*, 26(12): 3495–3513, June 2012. ISSN 0920-4741. doi: 10.1007/s11269-012-0087-0. URL http://link.springer.com/10.1007/s11269-012-0087-0.

T. R. Roberts. Downstream ecological implications of China ' s Lancang Hydropower and Mekong Navigation project. *Int. Rivers Netw.*, pages 1–14, 2001.

J. D. Salas and H.-S. Shin. Uncertainty analysis of reservoir sedimentation. *J. Hydraul. Eng.*, 125(April):339–350, 1999. doi: ISSN0733-9429/99/0004-03390350.

S. Shamsudin, A. Rashid, M. Darom, I. N. Mohamad, A. A. Rahman, I. Campus, and K. Lumpur. Detention Pond Sediment Accumulation Prediction using Monte Carlo Simulation. *Am. J. Environ. Sci. 8*, 8(1):25–34, 2012. doi: ISSN1553-345X.

J. Steiger, A. M. Gurnell, P. Ergenzinger, D. Snelder, and F. Universita. Sedimentation in the riparian zone of an incising river. *Earth Surf. Process. Landforms*, 108:91–108, 2001.

J. Steiger, a. M. Gurnell, and J. M. Goodson. Quantifying and characterizing contemporary riparian sedimentation. *River Res. Appl.*, 19(4):335–352, July 2003. ISSN 1535-1459. doi: 10.1002/rra.708.

J. Syvitski and S. Higgins. Going under: The world's sinking deltas. *New Sci.*, 2012.

J. P. Syvitski and Y. Saito. Morphodynamics of deltas under the influence of humans. *Glob. Planet. Change*, 57(3-4):261–282, June 2007. ISSN 09218181. doi: 10.1016/j.gloplacha.2006.12.001.

J. P. M. Syvitski. Deltas at risk. *Sustain. Sci.*, 3(1):23–32, Feb. 2008. ISSN 1862-4065. doi: 10.1007/s11625-008-0043-3. URL `http://link.springer.com/10.1007/s11625-008-0043-3`.

J. P. M. Syvitski, A. J. Kettner, I. Overeem, E. W. H. Hutton, M. T. Hannon, G. R. Brakenridge, J. Day, C. Vörösmarty, Y. Saito, L. Giosan, and R. J. Nicholls. Sinking deltas due to human activities. *Nat. Geosci.*, 2:681 – 686, 2009. doi: 10.1038/ngeo629.

T. Tamura, K. Horaguchi, Y. Saito, V. L. Nguyen, M. Tateishi, T. K. O. Ta, F. Nanayama, and K. Watanabe. Monsoon-influenced variations in morphology and sediment of a mesotidal beach on the Mekong River delta coast. *Geomorphology*, 116(1-2):11–23, Mar. 2010. ISSN 0169555X. doi: 10.1016/j.geomorph.2009.10.003. URL `http://linkinghub.elsevier.com/retrieve/pii/S0169555X09004280`.

P. L. Thong, H. T. D. Xuan, and T. T. T. Duyen. Economic efficiency of Summer-Autumn and Autumn-spring rice crop in the Mekong River Delta. *J. Sci. -CTU*, 18a:267–276, 2011.

L. X. Thuyen, H. N. Tran, B. D. Tuan, and N. T. Bay. Transportation and deposition of fine sediment during flood season in Long Xuyen Quadrangle - Technical Report (Vietnamese). *Minist. Sci. Technol.*, pages 1–70, 2000.

J. Valbo-Jørgensen, D. Coates, and K. Hortle. Fish Diversity in the Mekong River Basin in: The Mekong : biophysical environment of an international river basin. *Acad. Press. San Diego*, pages 161–196, 2009.

K. Västilä, M. Kummu, C. Sangmanee, and S. Chinvanno. Modelling climate change impacts on the flood pulse in the Lower Mekong floodplains. *J. Water Clim. Chang.*, 01(1):67, Mar. 2010. ISSN 2040-2244. doi: 10.2166/wcc.2010.008. URL `http://www.iwaponline.com/jwc/001/jwc0010067.htm`.

N. B. Ve. Assessment of sustainability of 3 rice crops in the Vietnamese Mekong Delta (Vietnamese). *Three rice Crop. Work. - An Giang - Vietnam*, pages 1–8, 2009.

D. M. Vien, V. V. Binh, H. T. Huong, and V. T. Guong. The impact of flood sediments on rice yield and soil fertility in the Mekong River Delta (Vietnamese). *J. Sci. -CTU*, pages 1–11, 2011.

D. E. Walling. Evaluation and analysis of sediment data from the lower Mekong River (Technical Report). Technical report, 2005. URL `http://portal.mrcmekong.org/master-catalogue/search?giai=9506000003825_00011452E0100jdi(lastaccess:15/04/2014)`.

D. E. Walling. The changing sediment load of the Mekong River. *Ambio*, 37(3):150–7, May 2008. ISSN 0044-7447.

H. Wang, Y. Saito, Y. Zhang, N. Bi, X. Sun, and Z. Yang. Recent changes of sediment flux to the western Pacific Ocean from major rivers in East and Southeast Asia. *Earth-Science Rev.*, Volume 108(Issues 1–2):80–100, 2011.

J. E. M. Watson, T. Iwamura, and N. Butt. Mapping vulnerability and conservation adaptation strategies under climate change. *Nat. Clim. Chang.*, 3(11):989–994, Sept. 2013. ISSN 1758-678X. doi: 10.1038/nclimate2007. URL `http://www.nature.com/doifinder/10.1038/nclimate2007`.

E. Wolanski, N. N. Huan, L. T. Dao, N. H. Nhan, and N. N. Thuy. Fine-sediment Dynamics in the Mekong River Estuary, Vietnam. *Estuar. Coast. Shelf Sci.*, 43(5):565–582, Nov. 1996. ISSN 02727714. doi: 10.1006/ecss.1996.0088.

Z. Xue, J. P. Liu, D. DeMaster, L. Van Nguyen, and T. K. O. Ta. Late Holocene Evolution of the Mekong Subaqueous Delta, Southern Vietnam. *Mar. Geol.*, 269(1-2):46–60, Feb. 2010. ISSN 00253227. doi: 10.1016/j.margeo.2009.12.005.

C. Yoshimura, M. Zhou, A. S. Kiem, K. Fukami, H. H. a. Prasantha, H. Ishidaira, and K. Takeuchi. 2020s scenario analysis of nutrient load in the Mekong River Basin using a distributed hydrological model. *Sci. Total Environ.*, 407(20):5356–66, Oct. 2009. ISSN 1879-1026. doi: 10.1016/j.scitotenv.2009.06.026.

G. Ziv, E. Baran, S. Nam, I. Rodríguez-Iturbe, and S. a. Levin. Trading-off fish biodiversity, food security, and hydropower in the Mekong River Basin. *Proc. Natl. Acad. Sci. U. S. A.*, 109(15):5609–14, Apr. 2012. ISSN 1091-6490. doi: 10.1073/pnas.1201423109. URL `http://www.pubmedcentral.nih.gov/articlerender.fcgi?artid=3326487&tool=pmcentrez&rendertype=abstract`.